

# **A Study of Mesons and Glueballs**



**Tapashi Das**

Department of Physics

Gauhati University

This thesis is submitted to

Gauhati University as requirement for the degree of

*Doctor of Philosophy*

Faculty of Science


July 2017

## Certificate

This is to certify that the thesis titled "A Study of Mesons and Glueballs" is the result of research work of Tapashi Das, carried under our supervision, submitted to Gauhati University for the award of the degree of Doctor of Philosophy in Physics.

This thesis conforms to the standard of PhD Thesis under Gauhati University including the standard related to plagiarism and has a similarity index not more than 20% (twenty percent), excluding the bibliography.

  
Dr. Dilip Kumar Choudhury, Supervisor

  
18.07.17  
Dr. Dipali Das, Co-Supervisor

July 2017

## Declaration

I hereby declare that this thesis is the result of my own research work which has been carried out under the guidance of Dr. Dilip Kumar Choudhury of Gauhati University, Guwahati and Dr. Dipali Das of Pandu College, Guwahati. I further declare that this thesis as a whole or any part thereof has not been submitted to any university (or institute) for the award of any degree or diploma.

This thesis contains less than 90,000 (ninety thousand) words excluding bibliography and captions.

  
Tapashi Das

July 2017

## Acknowledgements

It is a great opportunity for me to acknowledge those people without whom the thesis would have been impossible. My sincere gratitude goes first to my supervisor, Prof. D. K. Choudhury, Gauhati University for his incredible guidance, help and support during the entire period of my work. His intense enthusiasm for Physics kept me committed to my research, and his ever inspiring behavior helped making my PhD research period delightful.

I would like to acknowledge my co-supervisor Dr. Dipali Das, Pandu College, Guwahati for her continuous encouragement throughout the research period.

My special thanks goes to Prof. M. P. Bora, Head of the Department of Physics for providing me with all the necessary infrastructure facilities.

I am thankful to all the faculty members of the department for their sincere encouragement. I would like to specially thank Dr. Kalpana Bora for her encouragement and valuable suggestions during the seminars I have presented at the department.

My special thanks goes to Dr. Namita Sharma Bordoloi, Cotton College, Guwahati and Dr. Krishna K. Pathak, Arya Vidyapeeth College, Guwahati for their support and guidance during the entire research period. Their motivation had widen my research from various perspectives.

My thanks also goes to all the faculty members of Pandu College, Guwahati for helping me in various aspects during my research period.

I whole-heartedly thank Prof. N. D. Hari Dass, Visiting Professor, TIFR, Hyderabad for his valuable suggestions and comments in my research work.

I thank all the research scholars of Gauhati University, High Energy Physics, Gayatri, Baishali, Luxmi, Jugal, Neelakshi, Neelakshi N. K. Bora, Dr. Subhankar Roy and especially K. Shashikanta who helped me with every technical problem concerning my laptop.

I also admiringly acknowledge the fund received towards my PhD from the University Grants Commission regarding Fellowship under UGC-BSR scheme.

Last but not the least, I express my deepest gratitude to my parents, my two brothers and my dearest friend Kaustuv who always stood beside me in all the difficulties during the period of my research.

*Tapashi Das.*  
(Tapashi Das)

## Abstract

The main work of the thesis is devoted to the study of heavy flavored mesons using a QCD potential model. **Chapter 1** deals with the brief introduction of the theory of Quantum Chromodynamics (QCD), potential models and the use of perturbation theory. In **Chapter 2**, the improved potential model is introduced and the solution of the non-relativistic Schrödinger's equation for a Coulomb-plus-linear potential,  $V(r) = -\frac{4\alpha_s}{3r} + br + c$ , Cornell potential has been conducted. The first-order wave functions are obtained using Dalgarno's method. We explicitly consider two quantum mechanical aspects in our improved model: (a) the scale factor 'c' in the potential should not affect the wave function of the system even while applying the perturbation theory and (b) the choice of perturbative piece of the Hamiltonian (confinement or linear) should determine the effective radial separation between the quarks and antiquarks. Therefore for the validation of the quantum mechanical idea, the constant factor 'c' is considered to be zero and a cut-off  $r^P$  is obtained from the theory. The model is then tested to calculate the masses, form factors, charge radii, RMS radii of mesons. In **Chapter 3**, the Isgur-Wise function and its derivatives of semileptonic decays of heavy-light mesons in both HQET limit ( $m_Q \rightarrow \infty$ ) and finite mass limit are calculated. In **Chapter 4**, the leptonic decay constants of various  $D$  and  $B$  mesons are studied both in coordinate and momentum space. The graphical variations of the meson wave functions are compared with that of the hydrogen atom distributions. The calculated results of Chapters 3 and 4 are

compared with available experimental data and also with the predictions of other models. In **Chapter 5**, we outline the method how group theoretical tool of Young Tableau of  $SU(3)_c$  is used to find the maximum number of constituent gluons in an experimentally observed scalar glueball. In **Chapter 6**, we have summarized our work including its limitations and the plausible renovation of the model for future study.

The thesis then ends with a detailed list of References consulted during the work and with the Appendices where calculations are shown.

# Table of contents

<b>List of figures</b>	<b>xiii</b>
<b>List of tables</b>	<b>xv</b>
<b>1 Introduction</b>	<b>1</b>
1.1 Phenomenological models . . . . .	2
1.2 Potential models . . . . .	3
1.3 Weak decay of mesons . . . . .	7
1.3.1 Leptonic decay of mesons . . . . .	9
1.3.2 Semileptonic decay of mesons . . . . .	12
1.4 Heavy Quark Symmetry and Isgur-Wise function . . . . .	15
1.5 Glueballs: an overview . . . . .	17
1.5.1 Potential for two-gluon glueball . . . . .	18
1.5.2 Potential for three-gluon glueball . . . . .	19
1.5.3 Experimental status of glueballs . . . . .	20
1.6 The work of this thesis . . . . .	22
<b>2 The improved potential model and some properties of heavy flavored mesons</b>	<b>27</b>
2.1 Introduction . . . . .	27



2.2	Formalism . . . . .	29
2.2.1	Construction of wave function in the model . . . . .	29
2.2.2	Ground state masses of mesons . . . . .	35
2.2.3	Form factor and charge radii . . . . .	36
2.2.4	RMS radii of heavy flavored mesons . . . . .	39
2.2.5	Relation between RMS and charge radius . . . . .	40
2.3	Calculation and results . . . . .	41
2.3.1	Values of $r^P$ . . . . .	41
2.3.2	Ground state masses of mesons . . . . .	42
2.3.3	Form factors . . . . .	43
2.3.4	Charge radii . . . . .	46
2.3.5	RMS radii . . . . .	49
2.4	Conclusion . . . . .	49
<b>3</b>	<b>Isgur-Wise function of heavy-light mesons in the potential model</b>	<b>52</b>
3.1	Introduction . . . . .	52
3.2	Formalism . . . . .	53
3.2.1	Slope and curvature of Isgur-Wise function . . . . .	53
3.3	Calculation and results . . . . .	56
3.4	Conclusion . . . . .	59
<b>4</b>	<b>Leptonic decay constants of heavy-light mesons in the potential model</b>	<b>60</b>
4.1	Introduction . . . . .	60
4.2	Formalism . . . . .	61
4.2.1	Definition of decay constant in coordinate space . . . . .	61
4.2.2	Definition of decay constant in momentum space . . . . .	63
4.2.3	Wave functions in momentum space . . . . .	64

4.2.4 Determination of cut-off $p^P$ in the model . . . . .	64
4.3 Calculation and results . . . . .	66
4.4 Conclusion . . . . .	75
<b>5 Constituent gluons in scalar glueballs: a group theoretical analysis</b>	<b>77</b>
5.1 Introduction . . . . .	77
5.2 Formalism . . . . .	79
5.3 Results . . . . .	82
5.4 Conclusion . . . . .	84
<b>6 Summary, limitation and future outlook</b>	<b>86</b>
<b>References</b>	<b>91</b>
<b>Appendix A Wave function for Coulomb potential <math>(-\frac{4\alpha_s}{3r})</math> as parent and linear potential <math>(br)</math> as perturbation</b>	<b>97</b>
<b>Appendix B Wave function for linear potential <math>(br)</math> as parent and Coulomb potential <math>(-\frac{4\alpha_s}{3r})</math> as perturbation</b>	<b>105</b>
<b>Appendix C Continuity of the wave functions <math>\psi_I(r)</math> and <math>\psi_{II}(r)</math> at <math>r^P</math></b>	<b>112</b>
<b>Appendix D Mass of <math>D(c\bar{u}/c\bar{d})</math> meson using formula (2.37) considering various co-efficients of equation (B.27)</b>	<b>115</b>
<b>Appendix E Form factor <math>F(Q^2)_I</math> with wave function (2.21)</b>	<b>118</b>
<b>Appendix F Form factor <math>F(Q^2)_{II}</math> with wave function (2.35)</b>	<b>121</b>
<b>Appendix G Derivation of equation (4.1) from equation (4.9)</b>	<b>126</b>
<b>Appendix H The wave function (4.10) in momentum space</b>	<b>129</b>



# List of figures

1.1	Variation of potential (1.1) and its parts with inter-quark separation $r$ with $\alpha_s = 0.39$ , $b = 0.183\text{GeV}^2$ and $c = 0$ . . . . .	5
1.2	Variation of potential (1.1) and its parts with inter-quark separation $r$ with $\alpha_s = 0.39$ , $b = 0.183\text{GeV}^2$ and $c = 0.5\text{GeV}$ . . . . .	5
1.3	Annihilation of $D^+$ , a pure leptonic decay process. . . . .	9
1.4	Semileptonic decay process for $\bar{B}^0 \rightarrow D^{*+}l\nu$ . . . . .	12
1.5	Processes favoring glueball production. . . . .	21
2.1	Variation of form factor $F(Q^2)$ with $Q^2$ for charged mesons. . . . .	44
2.2	Variation of form factor $F(Q^2)$ with $Q^2$ for neutral mesons. . . . .	45
3.1	Variation of form factor with $Y$ in the Isgur-Wise limit. The blue and red graph correspond to the results of quark model in relativistic approach of ref. [113] and non-relativistic approach of ref. [110] respectively. . . . .	58
3.2	Variation of form factor with $Y$ with finite mass correction. The blue and red graph correspond to the results of quark model in relativistic approach of ref. [113] and non-relativistic approach of ref. [110] respectively. . . . .	59
4.1	The radial wave function $\psi_I(r)$ for $D(c\bar{u}/c\bar{d})$ meson. . . . .	69

4.2	The radial wave function $\psi_{II}(r)$ for $D(c\bar{u}/c\bar{d})$ meson. . . . .	70
4.3	The radial probability density $ r\psi_I(r) ^2$ for $D(c\bar{u}/c\bar{d})$ meson. . . . .	70
4.4	The radial probability density $ r\psi_{II}(r) ^2$ for $D(c\bar{u}/c\bar{d})$ meson. . . . .	71
4.5	The radial wave function $\psi_I(r)$ for $B(u\bar{b})$ meson. . . . .	71
4.6	The radial wave function $\psi_{II}(r)$ for $B(u\bar{b})$ meson. . . . .	72
4.7	The radial probability density $ r\psi_I(r) ^2$ for $B(u\bar{b})$ meson. . . . .	72
4.8	The radial probability density $ r\psi_{II}(r) ^2$ for $B(u\bar{b})$ meson. . . . .	73
4.9	Wave function $\psi_I(p)$ for $D(c\bar{u}/c\bar{d})$ meson. . . . .	73
4.10	Wave function $\psi_{II}(p)$ for $D(c\bar{u}/c\bar{d})$ meson. . . . .	74
4.11	Wave function $\psi_I(p)$ for $B(u\bar{b})$ meson. . . . .	74
4.12	Wave function $\psi_{II}(p)$ for $B(u\bar{b})$ meson. . . . .	75
C.1	The wave function $\psi_I(r)$ for $D(c\bar{u}/c\bar{d})$ meson. . . . .	113
C.2	The wave function $\psi_{II}(r)$ for $D(c\bar{u}/c\bar{d})$ meson. . . . .	113
C.3	The complete wave function $\psi_I(r) + \psi_{II}(r)$ for $D(c\bar{u}/c\bar{d})$ meson. . . . .	114
D.1	Normalization constant (D.1) with different $r_0$ . . . . .	117

## List of tables

1.1	Weak decay of mesons and their products. . . . .	9
2.1	$r^P$ in <i>Fermi</i> with $c = 0$ and $b = 0.183\text{GeV}^2$ . . . . .	41
2.2	Masses of heavy-light mesons in <i>GeV</i> . . . . .	42
2.3	Masses of heavy-light mesons in <i>GeV</i> from parent and total wave function. . . . .	43
2.4	The mean square charge radii of $D$ and $B$ mesons. . . . .	46
2.5	Mean square charge radii of $D$ and $B$ mesons. . . . .	48
2.6	RMS radii ( $r_{rms}$ ) in <i>Fermi</i> . . . . .	49
2.7	RMS radii ( $r_{rms}$ ) in <i>Fermi</i> from different model prediction. . . . .	49
3.1	Values of $\rho^2$ and $C$ in the present work and other works in the limit $m_Q \rightarrow \infty$ . . . . .	56
3.2	Reduced mass of heavy-light mesons in <i>GeV</i> . . . . .	57
3.3	Values of slope ( $\rho'^2$ ) and curvature ( $C'$ ) of the form factor of heavy meson decays in the present and earlier work with finite mass correction. . . . .	57
4.1	$p^P$ in <i>GeV</i> with $c = 0$ and $b = 0.183\text{GeV}^2$ . . . . .	67
4.2	Values of cut-off $r_c$ in $\text{GeV}^{-1}$ . . . . .	67

4.3	Decay constants of $D$ and $B$ mesons using Van-Royen-Weisskopf formula with regularized wave functions (4.6) and (4.7) and comparison with experimental data and other theoretical models. All values are in the unit of $GeV$ .	68
4.4	Decay constants of $D$ and $B$ mesons with cut-off $p^P$ and comparison with experimental data and other theoretical models. All values are in the unit of $GeV$ .	68
5.1	Number of color singlets corresponding to the maximum number of constituent gluons.	83
5.2	Possible number of constituent gluons corresponding to the number of scalar glueballs observed.	84
D.1	Mass of $D(c\bar{u}/c\bar{d})$ meson in $GeV$ with different order of the terms of wave function (B.27) and with the different values of upper cut-off $r_0$ .	116
D.2	Normalization constant with different upper cut-off $r_0$ .	116

# 1

## Introduction

Quantum Chromodynamics (QCD) is a modern theory of the strong force which describes the interaction between quarks and gluons. This non-abelian gauge field theory of symmetry group  $SU(3)$  has two essential characteristics: one is confinement, which means that the force between quarks does not vanish as they are separated i.e. quarks and gluons cannot be identified as isolated particles, they are present only in color-singlet bound hadron states such as protons. Another important fact is asymptotic freedom. At very high-energy scales or at the short distance, quarks and gluons interact very weakly i.e. as the energy of the interactions goes to infinity, the effective coupling between quarks and gluons vanishes. Thus without interactions at very high energy, the theory can be regarded as a free theory. The



theoretical physicists well understand the asymptotic behavior of QCD. The perturbation theory can be used to describe the small interactions between the quarks and gluons. But the theory fails for the interaction with soft particles where the coupling strength is large. Though the theory can explain asymptotic freedom, but fails for confinement phenomenon of quarks. Confinement is thus non-perturbative and requires a non-perturbative approach. Lattice gauge theory is a non-perturbative regularization of field theory. It was proposed by Wilson [1] in 1974 which provides a non-perturbative quantization of gauge fields by a lattice. Lattice QCD clarifies the comparison between the theory and the experimental data. The significant advantage of it is, in lattice QCD calculations (done on a computer) where lots of data can be obtained and can be treated as experimental data and then further used to test the other phenomenological models. One of such model is QCD potential model. At non-perturbative low energy regime of QCD, lattice QCD gives us the information about the structure and energy spectrum of mesons. The other way to proceed in the non-perturbative regime of QCD is the postulation of a QCD inspired quark model using non-relativistic Schrödinger equation for light and heavy flavored pseudoscalar mesons. The present work of the thesis is devoted to such a possible model.

## 1.1 Phenomenological models

The phenomenological model approach is a highly efficient tool to understand the properties of physical observables like hadrons (mesons and baryons) and glueballs (a bound state of pure gluons). A great variety of models e.g. the Constituent Quark Models (CQM) [2], light cone QCD [3] and various effective field theories such as Heavy Quark Effective Theory (HQET) [4] and Chiral Perturbation Theory (ChPT) [5] besides QCD Sum Rules [6, 7] have been developed during forty years of QCD.

In Constituent Quark Model (CQM), the strongly interacting particles, the hadrons (baryons( $qqq$ ) and mesons( $q\bar{q}$ )) are made up of fundamental particles called quarks and gluon fields. These six quarks ( $u, d, s, c, b, t$ ) are called flavors. Quark model describes the hadronic properties of the wave function of a hadron. Among CQM, the non-relativistic constituent quark models (NRCQM) [8] are successful in describing the mass spectrum of hadrons, where the constituent quarks are assumed to be non-relativistic and interact through QCD potential provided by gluons. However, one can introduce relativistic dynamics as well.

The present work of the thesis is dedicated to one of the successful phenomenological models called potential model.

## 1.2 Potential models

Depending on the concepts of ‘quark confinement’ and ‘asymptotic freedom’, to find the phenomenological form of the static potential, a lot of work has been done which are available in the literature [9–12] for modeling mesons. Among those, in the potential model we follow a non-relativistic potential of the type

$$V(r) = \frac{-4\alpha_s}{3r} + br + c, \quad (1.1)$$

where ‘ $r$ ’ is the inter-quark separation of the bound state,  $\alpha_s$  is the strong running coupling constant and the factor  $\frac{4}{3}$  arises from the  $SU(3)$  color factor

$$C_F = \frac{N_C^2 - 1}{2N_C}, \quad (1.2)$$

where  $N_C$  is the number of colors and  $C_F$  is the casimir operator  $\lambda^c \cdot \lambda^c = C_F$ ,  $\lambda^c$  is the generator of  $SU(N_C)$  group. For  $SU(3)$ ,  $N_C = 3$ , therefore,  $C_F = \frac{4}{3}$ .

The parameter ' $b$ ' is called confinement parameter. The phenomenological value of ' $b$ ' is considered to be  $\approx 0.183\text{GeV}^2$  [13, 14].

This Coulomb-plus-linear non-relativistic confinement potential, called Cornell potential [10] is an essential ingredient of QCD to study quarkonium physics. It has achieved a lot of consideration to describe the systems of quark and antiquark bound states in the context of meson spectroscopy.

In equation (1.1), the Coulomb part of  $V(r)$  represents the shorter-range part of the potential and is due to one gluon exchange contribution which is flavor independent. The second term of the potential associated with the longer-range part and is responsible for the confinement of the quarks in the model. In QCD, both the potentials play a decisive role in the quark dynamics, and their separation is not possible. The third term ' $c$ ' in the potential is a phenomenological constant required to be fitted on the spectrum. The term ' $c$ ' can be regarded as the free-parameter in the theory.

Fig. 1.1 and 1.2 show the graphical representation of potential (1.1) with  $\alpha_s = 0.39$ ,  $b = 0.183\text{GeV}^2$  [13, 14] and with  $c = 0$  and  $c = 0.5\text{GeV}$  respectively. In the same graph we have also shown the variation of Coulomb and linear potential separately with inter-quark separation  $r$  ( $\text{GeV}^{-1}$ ).

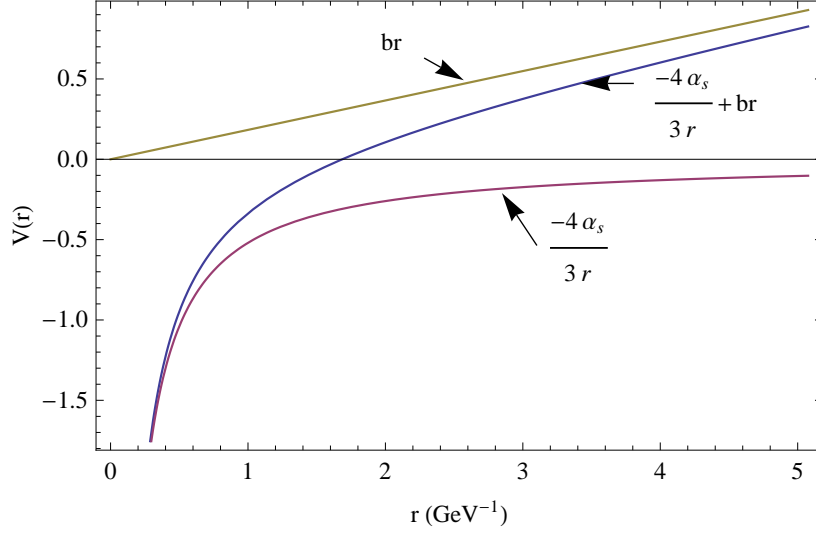


Fig. 1.1 Variation of potential (1.1) and its parts with inter-quark separation  $r$  with  $\alpha_s = 0.39$ ,  $b = 0.183\text{GeV}^2$  and  $c = 0$ .

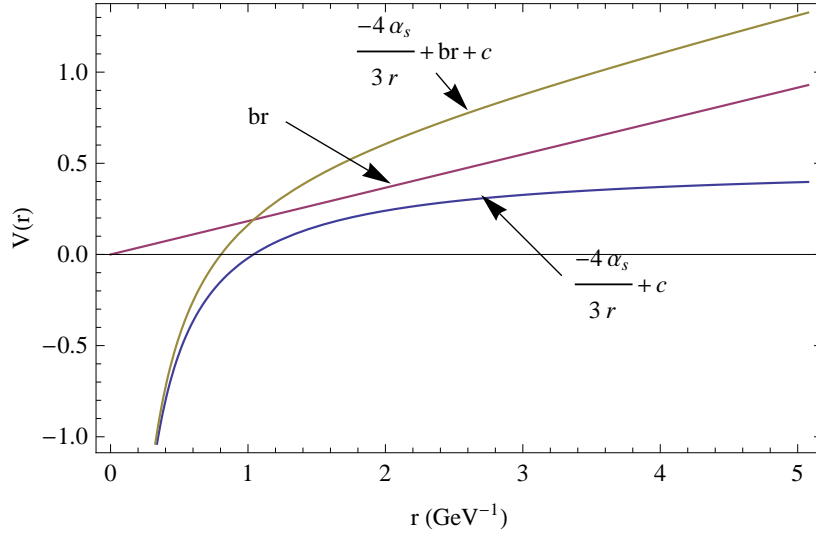


Fig. 1.2 Variation of potential (1.1) and its parts with inter-quark separation  $r$  with  $\alpha_s = 0.39$ ,  $b = 0.183\text{GeV}^2$  and  $c = 0.5\text{GeV}$ .

The energy of the potential can obtain by solving the corresponding Schrödinger's equation,

$$H\psi(r) = E\psi(r), \quad (1.3)$$

where the Hamiltonian operator  $H$  acts on the wave function  $\psi(r)$  of the bound system.

Hamiltonian,

$$H = -\frac{\hbar^2}{2\mu}\nabla^2 + V(r). \quad (1.4)$$

The exact solution of Schrödinger's equation is not possible mostly [15]. These exist only for a few idealized systems e.g. the harmonic oscillator, the hydrogen atom.

To solve real problems, one uses approximation methods. A variety of such methods are available in the literature which has its area of applicability, e.g. perturbation theory [16, 17], the variational method [16], and the WKB method [16]. In our present work, we have used the perturbation theory for our analysis.

For the potential of type (1.1), one of the significant advantages [10] based on the Coulomb and linear term of the potential is that it naturally leads to two choices for the parent Hamiltonian. Also, there are no appropriate small parameters so that one of the terms of the potential can be made perturbative within a perturbation theory.

In perturbation theory, we make small deformation to the Hamiltonian of the system,

$$H = H_0 + H', \quad (1.5)$$

where  $H_0$  is the Hamiltonian of the unperturbed system and  $H'$  is the perturbed Hamiltonian. The approximation method is most suitable when  $H$  is close to the unperturbed Hamiltonian  $H_0$ , i.e.  $H'$  is small.

The Schrödinger's equation corresponding to the unperturbed Hamiltonian is

$$H_0 \psi^{(0)}(r) = E_0 \psi^{(0)}(r). \quad (1.6)$$

In the method, it is assumed that the Schrödinger's equation can be solved for  $H_0$ , i.e., the unperturbed eigenfunction  $\psi^{(0)}$  and energy eigenvalue  $E_0$  are known to us. To obtain the perturbed eigen function  $\psi^{(1)}$  corresponding to Hamiltonian  $H'$ , one can apply the Dalgarno's method [18] of perturbation.

The wave functions obtained by using Dalgarno's method of perturbation are used to find the various properties of mesons. In this thesis, the study of meson properties include the masses, Isgur-Wise function of heavy-light mesons and their derivatives. Root Mean Square (RMS) radii, form factors, charge radii and decay constants are also studied here. The results are compared with available experimental data and also with the predictions of other models.

### 1.3 Weak decay of mesons

In the standard model of particle physics, the quark and antiquark of the mesons are bound together by the strong interaction. Mesons are classified according to their quark/anti-quark composite and in  $J^{PC}$  multiplets too, where  $J$  is total angular momentum, parity  $P$  is given by  $(-1)^{l+1}$ , where  $l$  is the orbital angular momentum,  $C$  is charge conjugation  $(-1)^{l+s}$ . The  $C$ -parity can also be generalized to the  $G$ -parity  $(-1)^{l+l+s}$  for the mesons made of quarks

and their own antiquarks, where  $I$  is the isospin quantum number.

The  $l = 0$  states give the pseudoscalar ( $0^{-+}$ ) and vector ( $1^{--}$ ) mesons.

According to the quark and antiquark combination of the mesons, they are classifying into three categories:

**Light-light mesons:** both the quark and antiquark are light ( $u, d$  or  $s$  only). e.g.  $\pi(u\bar{d}/d\bar{u})$  and  $K(u\bar{s}/d\bar{s})$  mesons.

**Heavy-light mesons:** one quark or antiquark is heavy ( $c, b$  or  $t$ ) and the other is light. e.g.  $D(c\bar{d}/c\bar{u})$  and  $B(u\bar{b}/d\bar{b})$  mesons.

**Heavy-heavy mesons:** both the quark and antiquark are heavy. e.g.  $\eta_c(c\bar{c})$ ,  $\eta_b(b\bar{b})$  mesons etc.

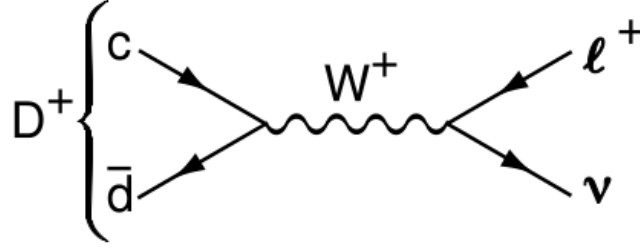
Mesons undergo weak transition via charged  $W^{\pm}$  boson. Depending on the decay products, there are three types of weak decays which are extensively studied in the literature. They are leptonic decays, semileptonic decays and non-leptonic decays. However, the thesis does not involve the non-leptonic decay. Leptonic and semileptonic decays are studied here only. In Table 1.1, we tabulate the three types of weak decays and their product particles.

Table 1.1 Weak decay of mesons and their products.

Type of weak decay	Products	Examples
Leptonic decay	Leptons only	$D^+ \longrightarrow l^+ \nu$ $\pi^\pm \longrightarrow l^\pm \nu$ $K^\pm \longrightarrow l^\pm \nu$ etc.
Semileptonic decay	Leptons and hadrons	$B^+ \longrightarrow D l^+ \nu$ $B^- \longrightarrow \pi^0 l^- \bar{\nu}$ $B_c \longrightarrow J/\psi l^+ \nu$ etc.
Non-leptonic decay	Hadrons only	$B^0 \longrightarrow D^- \pi^+$ $\bar{B}^0 \longrightarrow D^+ \rho^-$ $\bar{B} \longrightarrow \bar{K} J/\psi$ etc.

### 1.3.1 Leptonic decay of mesons

As an illustration in Fig. 1.3, we consider a pure leptonic decay process of  $D^+(c\bar{d})$  meson, which decays to a lepton-neutrino pair via a virtual  $W$  boson.

Fig. 1.3 Annihilation of  $D^+$ , a pure leptonic decay process.

Similar annihilation processes can also occur in  $\pi^+, K^+, D_s$  and  $B^+$  mesons.

For a pseudoscalar  $P$  meson, the lowest order decay width is [19]

$$\Gamma(P \rightarrow l\nu) = \frac{G_F^2}{8\pi} f_P^2 m_l^2 M_P \left(1 - \frac{m_l^2}{M_P^2}\right) |V_{q_1 q_2}|^2, \quad (1.7)$$

where  $M_P$  is the mass of  $P$  meson,  $m_l$  is the mass of lepton,  $|V_{q_1 q_2}|$  is the Cabibbo-Kobayashi-Maskawa (CKM) matrix element between the constituent quarks  $q_1$  and  $q_2$  in



meson  $P$ . The standard notation of  $3 \times 3$  CKM matrix in terms of quark flavor is

$$V_{CKM} = \begin{pmatrix} V_{ud} & V_{us} & V_{ub} \\ V_{cd} & V_{cs} & V_{cb} \\ V_{td} & V_{ts} & V_{tb} \end{pmatrix}.$$

From PDG2016 [2], we can express  $V_{CKM}$  as

$$V_{CKM} = \begin{pmatrix} 0.97417 \pm 0.00021 & 0.2248 \pm 0.0006 & (4.09 \pm 0.39) \times 10^{-3} \\ 0.220 \pm 0.005 & 0.995 \pm 0.016 & (40.5 \pm 1.5) \times 10^{-3} \\ (8.2 \pm 0.6) \times 10^{-3} & (40.0 \pm 2.7) \times 10^{-3} & 1.009 \pm 0.031 \end{pmatrix}.$$

In equation (1.7),  $G_F$  is the Fermi coupling constant ( $\approx 1.166 \times 10^{-5} GeV^{-2}$ ) [2]. The decay constant  $f_P$  is the “wave function overlap” of the quark and antiquark of the mesons (e.g. the overlap of the wave function of  $c$  and  $\bar{d}$  in  $D^+$  in Fig. 1.3) which is proportional to the matrix element of the axial current between the  $P$ -meson state and the vacuum:

$$\langle 0 | \bar{q}_1 \gamma_\mu \gamma_5 q_2 | P(p) \rangle = i p_\mu f_P. \quad (1.8)$$

Particle lifetime,  $\tau = \frac{1}{\Gamma}$  is one of the important characteristics of meson which depends on the available decay modes or channels, which are subjected to conservation laws for appropriate quantum numbers, coupling strength of the decay process and kinematic constraints.

For particles which are associated with multiple decay modes, the total decay rate ( $\Gamma_{total}$ ) will be the total value of the rates of the individual modes ( $\Gamma_i$ ),

$$\Gamma_{total} = \sum_{i=1}^n \Gamma_i. \quad (1.9)$$

When the mass of the elementary particle is measured, the total decay rate appears as the irreducible “width” of the distribution, hence called “decay width”.

Another interesting parameter in decay processes is their branching fraction ( $B_i$ ) which is the probability of the decay by distinct modes. Thus the branching fraction of mode ‘ $i$ ’ is

$$B_i = \frac{\Gamma_i}{\Gamma_{total}}. \quad (1.10)$$

Measurements of branching fraction and lifetime allow an experimental determination of the product  $|V_{q_1 q_2}| f_P$ . Once decay constant  $f_P$  is known to us, one can obtain the corresponding CKM element. On the other hand, taking the value of  $|V_{q_1 q_2}|$  assuming CKM unitarity, one can infer the experimental measurement of the decay constant which can later be compared with the theory.

Purely leptonic decay processes are considered to be the simplest and cleanest decay modes of the pseudoscalar charged mesons. The decay amplitude can be written as the product of the well-understood leptonic current for the system and a more complicated hadronic current for the quark transition. The hadronic current, however, cannot be so easily evaluated, since the quarks in the hadrons are not free and so non-perturbative strong interaction effects become important in describing the physical states.

Mathematically, the amplitude for a leptonic decay can be written as [20]

$$\mathcal{A}(P \rightarrow l\nu) = -i \frac{G_F}{\sqrt{2}} V_{q_1 q_2} L^\mu H_\mu, \quad (1.11)$$

where the leptonic current  $L^\mu$  can be defined in terms of the Dirac spinors  $u_l$  and  $v_\nu$  as

$$L^\mu = \bar{u}_l \gamma^\mu (1 - \gamma_5) \nu_l \quad (1.12)$$

and the hadronic current is

$$H^\mu = \langle 0 | \bar{q}_1 \gamma^\mu (1 - \gamma_5) q_2 | P \rangle = i f_P q^\mu, \quad (1.13)$$

which is simple, since the only four vector available to be constructed with the leptonic current is  $q^\mu$ . Here the momentum transfer  $q^2 = m^2$  is constant and hence the form factor which is a function of  $q^2$  becomes a constant  $f_P$ , the decay constant of the meson.

### 1.3.2 Semileptonic decay of mesons

As an illustration in Fig. 1.4, we consider a semileptonic decay process of  $\bar{B}^0(\bar{d}b)$  meson, which decays to a  $D^{*+}(c\bar{d})$  meson and a lepton-neutrino pair via a virtual  $W^-$  boson.

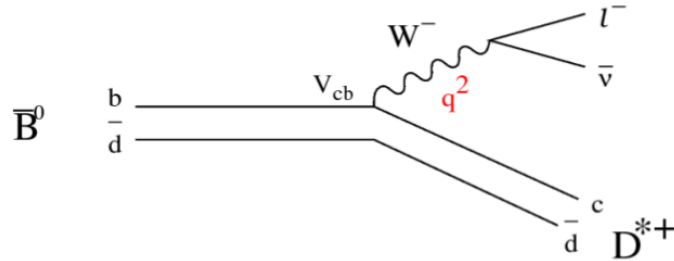


Fig. 1.4 Semileptonic decay process for  $\bar{B}^0 \rightarrow D^{*+} l \nu$ .

Historically, the semileptonic process of nuclear decay opened the era of weak interaction physics and presented the physicists with the mystery of the electron's undetected partner, the neutrino [21]. In leptonic decays ( $P \rightarrow l \nu$ ), the hadronic current describes the annihilation of the quark and antiquark in the initial state meson, whereas in semileptonic decays ( $P_1 \rightarrow P_2 l \nu$ ), it describes the evolution from the initial to final state hadrons. The decay,  $P \rightarrow l \nu$ , in the standard model proceeds via the axial-vector current  $\bar{q}_1 \gamma_\mu \gamma_5 q_2$ , whereas

semileptonic decays  $P_1 \rightarrow P_2 l \bar{\nu}$  proceed via the vector current  $\bar{q}_1 \gamma_\mu q_2$ . Thus the determination of the CKM matrix element  $|V_{q_1 q_2}|$  from leptonic and semileptonic decays tests the  $V - A$  structure of the standard model electroweak charged-current interaction [19].

For semileptonic decay of a meson  $P_1$  into a meson  $P_2$ , the amplitude takes the form [22, 23],

$$\mathcal{A}(P_1 \rightarrow P_2 l^- \bar{\nu}) = -i \frac{G_F}{\sqrt{2}} V_{q_1 q_2} L^\mu H_\mu, \quad (1.14)$$

where the hadronic current is

$$H^\mu = \langle P_2 | \bar{q}_1 \gamma^\mu (1 - \gamma_5) q_2 | P_1 \rangle. \quad (1.15)$$

This is not calculated in a simple manner as is done in leptonic decay since  $q^2$  is different from event to event. Thus  $H_\mu$  can be expressed in terms of different form factors, which isolate the effects of strong interactions on the amplitude.

As an illustration, for the pseudoscalar to pseudoscalar transition

$$\bar{B} \longrightarrow D l \bar{\nu}, \quad (1.16)$$

a set of form factors  $F_i(q^2)$  can be defined as [4]

$$\langle \tilde{D}(p') | \bar{c} \gamma^\mu b | \tilde{B}(p) \rangle = F_1(q^2) \left[ (p + p')^\mu - \frac{m_B^2 - m_D^2}{q^2} q^\mu \right] + F_0(q^2) \frac{m_B^2 - m_D^2}{q^2} q^\mu, \quad (1.17)$$

where  $p$  and  $p'$  are momentum of  $B$  and  $D$  mesons respectively and  $q = p - p'$ . The form factors  $F_0(q^2)$  and  $F_1(q^2)$  are subjected to the constraint that at  $q^2 = 0$ ,  $F_0(0) = F_1(0)$ .

Again, for the pseudoscalar to vector transition

$$\bar{B} \longrightarrow D^* l \bar{\nu}, \quad (1.18)$$

a set of form factors  $V(q^2), A_0(q^2), A_1(q^2)$  and  $A_2(q^2)$  can be defined as

$$\begin{aligned} \langle \tilde{D}^*(p', \epsilon) | \bar{c} \gamma^\mu (1 - \gamma_5) b | \tilde{B}(p) \rangle = & \frac{2i\epsilon^{\mu\nu\alpha\beta}}{m_B + m_{D^*}} \epsilon_\nu^* p'_\alpha p_\beta V(q^2) - \\ & \left[ (m_B + m_{D^*}) \epsilon^{*\mu} A_1(q^2) - \frac{\epsilon^* \cdot q}{m_B + m_{D^*}} (p + p')^\mu A_2(q^2) - 2m_{D^*} \frac{\epsilon^* \cdot q}{q^2} q^\mu A_3(q^2) \right] \\ & - 2m_{D^*} \frac{\epsilon^* \cdot q}{q^2} q^\mu A_0(q^2), \end{aligned} \quad (1.19)$$

where  $\epsilon$  is the polarization of the  $D^*$  meson.

The form factor  $A_3(q^2)$  is given by the linear combination of  $A_1(q^2)$  and  $A_2(q^2)$  as

$$A_3(q^2) = \frac{m_B + m_{D^*}}{2m_{D^*}} A_1(q^2) - \frac{m_B - m_{D^*}}{2m_{D^*}} A_2(q^2). \quad (1.20)$$

At  $q^2 = 0$ ,  $A_0(0) = A_3(0)$ .

In the infinite heavy quark mass limit,  $m_Q \rightarrow \infty$ , a new heavy flavor symmetry appears in the effective Lagrangian of the standard model which provides the model independent normalization of the weak form factors and the necessity of HQET (Heavy Quark Effective Theory) [4, 24] enters into the literature. In this heavy quark symmetry, the form factors (two for pseudoscalar to pseudoscalar transition and four for pseudoscalar to vector transition)

of heavy-light mesons in semileptonic decay can be expressed in terms a single form factor which is termed as Isgur-Wise function [4].

## 1.4 Heavy Quark Symmetry and Isgur-Wise function

The bound states containing heavy quarks ( $m_Q \gg \Lambda_{QCD}$ ) describing the strong interactions are easier to understand compared to states containing light quarks only, wherein the standard model  $u, d, s$  are light quarks ( $q$ ) and  $c, b, t$  are heavy quarks ( $Q$ ). For heavy quarks, the effective coupling constant ( $\alpha_s$ ) is small. The length scale  $\frac{1}{\Lambda_{QCD}} \sim 1 \text{ Fermi}$  determines the typical size of hadrons ( $R_{had}$ ). Systems containing both the heavy quarks ( $Q\bar{Q}$ , e.g.  $c\bar{c}$ -charmonium,  $b\bar{b}$ -bottomonium) have size  $\frac{\lambda_Q}{\alpha_s} \ll R_{had}$ , where  $\lambda_Q$  is the Compton wavelength. For systems which are composed of a heavy quark ( $Q$ ), where  $m_Q \gg \Lambda_{QCD}$ ,  $\lambda_Q \ll R_{had}$  and other light constituents, a new symmetry arises known as Heavy Quark Symmetry [25–31]. In the limit  $m_Q \rightarrow \infty$ , the heavy quark and the system which contains it have the same velocity and the systems which differ only by the quantum number of their constituent heavy quarks have the same configuration of the remaining light degrees of freedom. This means for two bound systems containing two different heavy quarks  $Q$  and  $Q'$ , when their masses  $m_Q, m_{Q'} \gg \Lambda_{QCD}$ , the configuration of the light degrees do not change if we replace  $Q \leftrightarrow Q'$ , where  $Q$  and  $Q'$  are moving with same velocities. In heavy quark effective theory limit, the heavy quark looks like a static color source for the light quarks, which is similar to the atomic system.

The concept of a new flavor symmetry for hadrons containing a heavy quark was first introduced by Shuryak in 1980 [32], who later studied many properties of heavy mesons and baryons with QCD sum rules [6]. But an explicit model independent formulation of the physical ideas of the spin-flavor symmetry was developed by Nussinov and Wetzel [27], Voloshin and Shifman [28, 29], Politzer and Wise [30, 31], Isgur and Wise [25, 26] and

Grinstein [33], until finally Georgi [24] reformulated the low energy effective Lagrangian for a heavy quark in a covariant way in a theory called Heavy Quark Effective Theory (HQET).

The heavy quark is covered by a most complicated, strongly interacting cloud of light quarks and antiquarks by the exchange of soft gluons. This cloud was sometimes called brown muck by Isgur, and the properties of such systems cannot be calculated from first principles in a perturbative way. The HQET applies to the hadron system containing only one heavy quark.

The inference of Heavy Quark Symmetry for the semi-leptonic decays of  $B$  mesons,  $\bar{B} \rightarrow D l \bar{\nu}$  and  $\bar{B} \rightarrow D^* l \bar{\nu}$  is that, if we consider that  $b$  and  $c$  quarks are heavy enough to satisfy the requirements of HQET, then the six real, independent form factors that define these decays are expressible in terms of Isgur-Wise function  $\xi(y)$ .

In the heavy quark infinite mass limit ( $m_Q \rightarrow \infty$ ), (1.17) and (1.19) leads to

$$\begin{aligned} F_1(q^2) \approx V(q^2) \approx A_0(q^2) \approx A_2(q^2) \approx \xi(y) \\ \text{and } F_0(q^2) \approx A_1(q^2) \approx 0. \end{aligned} \quad (1.21)$$

Thus, the HQET predicts that all the form factors that describe these decays are expressible in terms of the Isgur-Wise function,  $\xi(y)$ . This is an important application of the HQET in non-relativistic quark model (NRQM). In the NRQM, the initial meson is assumed to be at rest, and after the transition moves with velocity  $v'$ . The Isgur-Wise function measures the overlap of the wave functions of the light degrees of freedom in the initial and final meson state, where one of the quarks is moving relative to the other and it takes the form

$$\xi(y) = \int |\psi(r)|^2 e^{-imv'r} d^3r. \quad (1.22)$$

The Isgur-Wise functions are normalized to unity i.e.  $\xi(y=1) = 1$  at zero-recoil point ( $v = v'$ ), where  $y = v \cdot v'$ , Lorentz boost. The condition  $\xi(y=1) = 1$  is a resultant of the conservation of vector current and signify the complete overlap of the wave functions when  $v = v'$ .

The method of application of HQET in NRQM was initiated by Close and Wambach [34, 35].

Besides quark and antiquark systems, which are extensively studied in literature and experimentally configured, there are particles like glueballs, pentaquarks and hybrid which are also the prediction of QCD. The experimental status for these states is however not yet been confirmed as that of meson and baryon systems.

We will outline briefly the theoretical and experimental status of glueballs which is a part of our present work.

## 1.5 Glueballs: an overview

The non-abelian nature of  $SU(3)$ -color group allows the existence of purely gluonic bound states called glueballs. These glueballs are pure QCD bound states and are hadrons without valence quarks; they are bound state of gluons only. The experimental determination and understanding properties of these pure glueball states are challenging because these states can mix with nearby  $q\bar{q}$  resonances. Though the potential model, which is so successful to describe the bound states of quarks, is a bit controversial to use in case of a bound state of pure gluons. But from the ongoing efforts on gluon propagator, it has been confirmed that gluons may have a dynamically generated mass. In the early 80's, Cornwall arrived at such dynamical mass  $m_g = (500 \pm 200)MeV$  [36, 37] and the relativistic corrections are



expanded in the powers of  $\frac{1}{m_g^2}$  [38]. Because gluons have an effective mass, so there is a chance to use non-relativistic Schrödinger's equation and hence the potential model to study the bound state of gluons [37–39]. Theoretically, various models have been constructed to study the properties and masses of glueballs [40]. In 1976, the MIT bag model was first used to examine glueball properties, where it was assumed that the gluons are confined inside the bag [41].

### 1.5.1 Potential for two-gluon glueball

Here the gluons are described as massive spin-1 particle interacting through one-gluon exchange and breakable string [37, 39]. At the short distance, the effective coupling between gluon-gluon becomes weak, and the interaction can be treated perturbatively. The short distance potential is approximated by one-gluon exchange potential and at long distance, gluons are confined non-perturbatively via a string potential [37],

$$V_{str}(r) = 2m_g \left(1 - e^{-\frac{r}{r_0}}\right), \quad (1.23)$$

where  $m_g$  is the mass of gluon,  $r_0 = 0.6 \text{Fermi}$  [37] and ' $r$ ' is the gluon-gluon separation.

The gluon-gluon potential for two-gluon glueball is [39]

$$V_{2g}(r) = -\lambda \left[ \left\{ \frac{1}{4} + \frac{1}{3} \mathbf{S}^2 + \frac{1}{2m_g^2} (\mathbf{L} \cdot \mathbf{S}) \frac{1}{r} \frac{\partial}{\partial r} - \frac{1}{2m_g^2} \left( (\mathbf{S} \cdot \nabla)^2 - \frac{1}{3} \mathbf{S}^2 \nabla^2 \right) \right\} \frac{e^{-mr}}{r} + \left( 1 - \frac{5}{6} \mathbf{S}^2 \right) \frac{\pi}{m^2} \delta^3(r) \right] + V_{str}(r), \quad (1.24)$$

where

$$\lambda = \frac{3g^2}{4\pi} \quad (1.25)$$

is the adjoint strong coupling constant and  $\mathbf{S} = \mathbf{S}_1 + \mathbf{S}_2$  is the total spin of the two-gluon glueball.

The Hamiltonian for two-gluon glueball is

$$H = 2m_g - \frac{1}{m_g} \nabla^2 + V_{2g}. \quad (1.26)$$

Another simplest way of modeling a two-gluon glueball is the use of spinless two-body Salpeter Hamiltonian (semirelativistic) [38],

$$H_0 = 2\sqrt{p^2} + a_g r - 3\frac{\alpha_s}{r}, \quad (1.27)$$

where, the kinematic part is the kinetic energy of two spinless valence gluons. The potential includes a Coulomb plus linear form, Cornell shape. The linear term can be treated as the static energy of flux tube linking the two gluons, where  $a_g$  is the string tension. The Coulomb term represents the lowest order approximation of the one-gluon exchange between two gluons.  $\alpha_s$  is the effective strong coupling constant ( $\alpha_s < 1$ ). The factor 3 is the color factor associated with a gluon pair in a color singlet. A relativistic correction can also be introduced to the Hamiltonian of the system.

### 1.5.2 Potential for three-gluon glueball

For three-gluon glueball the potential is [42]

$$V_{3g} = \sum_{i < j} [V_{OGE}(r_{ij}) + \frac{1}{2} V_{str}(r_{ij})], \quad (1.28)$$

which is obtained by summing over pairs of two-body potentials, where  $V_{OGE}$  is the one-gluon exchange potential and  $V_{str}$  is the string potential.

### 1.5.3 Experimental status of glueballs

In lattice QCD, it appears that the lowest lying glueballs are  $C = +$  ones. Also, the bound state of two-gluon glueball has  $C = +1$  [43]. Therefore, it is natural to assume that the two-gluon glueballs are the lightest. Increasing the number of constituent gluons increases the mass of glueballs. The production reactions which are associated with glueball production are glue rich and glue poor reactions. The glue rich reactions include  $J/\psi$  decays, Pomeron-Pomeron exchange reactions and  $p - \bar{p}$  annihilation. The latter include 2-photon production and photo production.

The first of glue rich process is radiative  $J/\psi$  decay,  $J/\psi \longrightarrow \gamma G$  (Fig. 1.5(a)). In  $J/\psi$  decay, the  $c\bar{c}$  pair decays via annihilation and the intermediate state must have gluons in it. The gluons interact and must form glueballs. The similar argument can also be used for  $p - \bar{p}$  annihilation (Fig. 1.5(b)) and  $\gamma$  decays, where quark-antiquark pairs annihilate into gluons, they interact and may form glueballs. Another glue rich process for glueball production is central production. In central production, two hadrons pass by each other ‘nearly untouched’ and are scattered diffractively in the forward direction. The valence quarks are exchanged. The process is often called Pomeron-Pomeron scattering (Fig. 1.5(c)). The absence of valence quarks in the production process makes the central production a good place to search for glueballs [44].

The mass of  $0^{++}$  scalar glueball in bag model [41], for  $(TE)^2$  gluons is  $0.96 \text{ GeV}/C^2$  and for  $(TM)^2$  is  $1.59 \text{ GeV}/C^2$ . Flux-tube model was carried out by Isgur and Paton [45, 46] to calculate the mass of glueball, where the glueball is treated as a closed flux tube. The mass of lightest scalar glueball  $0^{++}$  was found to be  $1.52 \text{ GeV}/c^2$  in the model. Besides that QCD sum rule predicts the lightest scalar glueball with a mass in the range of 0.3 to  $0.6 \text{ GeV}/c^2$  [47]. Lattice calculations using a larger lattice and smaller lattice parameters

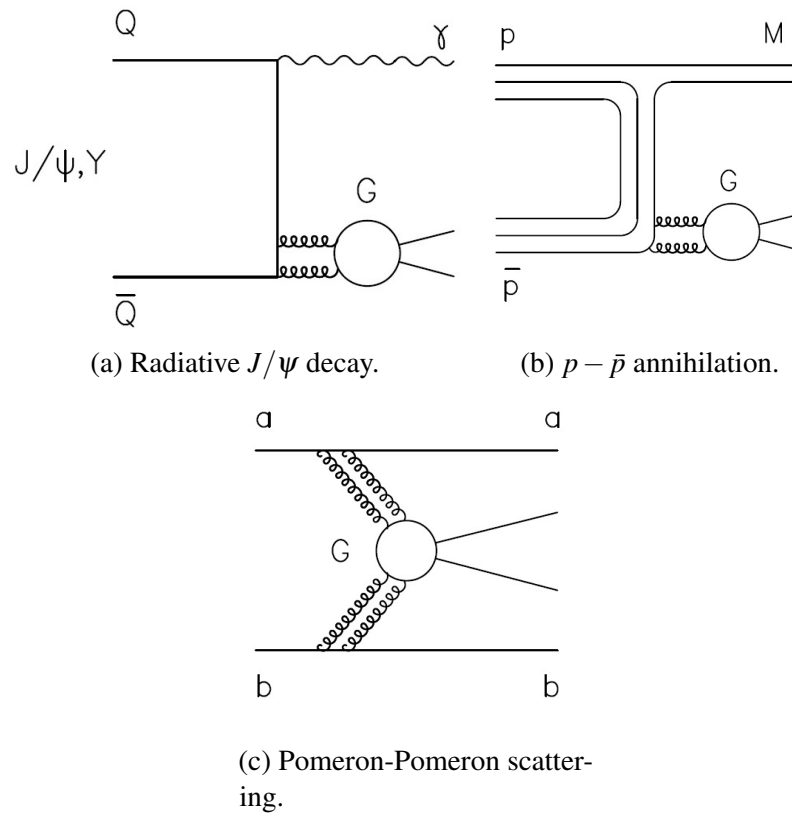


Fig. 1.5 Processes favoring glueball production.

yields the mass of scalar glueball to be  $1.625 \pm 0.094 \text{ GeV}/c^2$  [48, 49]. The total decay width of the scalar glueball was also calculated by authors in the process of decay of scalar glueball to pairs of pseudoscalar mesons and was found to be under  $0.2 \text{ GeV}/c^2$ . The Particle Data Group (PDG) data suggest existence of five scalar glueball candidates:  $f_0(500)$  or  $\sigma$ ,  $f_0(980)$ ,  $f_0(1370)$ ,  $f_0(1500)$  and  $f_0(1710)$  with  $IJ^{PC} = 00^{++}$  in the energy region up to  $1.8 \text{ GeV}$  [50]. Among them,  $f_0(1500)$  and  $f_0(1710)$  appears to be the strongest candidates for scalar glueballs since they are produced in radiative  $J/\psi$  decay and not seen on  $\gamma\gamma$  collisions. The state  $f_0(1500)$  has a mass of  $1.505 \text{ GeV}/c^2$  and a width of  $0.110 \text{ GeV}/c^2$  [51]. In 2004, BES II Collaboration [52], suggest the existence of the new resonance  $f_0(1790)$ . There are several other resonances which are possible candidates of glueballs:  $\sigma(750)$ ,  $i(1440)$ ,  $G(1550)$ ,  $\theta(1710)$ ,  $\xi(2220)$ ,  $g_T(2050)$ ,  $g_T(2300)$  and  $g_T(2350)$  [53]. But no definite conclusions can be obtained concerning the nature of these states. All lattice simulations and experiments agree that the lightest scalar glueballs have mass in the range  $1500\text{-}1750 \text{ MeV}$ , while the tensor and pseudoscalar glueballs have mass in the range  $2000\text{-}2400 \text{ MeV}$  [48, 54–57].

There are many new experiments planned, e.g. the PANDA Experiment at GSI in Germany [58], BES III at BEPC II in Beijing [59], the GlueX Experiment at Jefferson Laboratory in the USA [60], ALICE at CERN [61, 62], which will provide us more data on this.

## 1.6 The work of this thesis

The primary motivation of the thesis is to study meson properties in a non-relativistic quark model. Certain modifications are suggested to the model which expands its area of applicability.

In the model, the wave functions are obtained with Coulomb-plus-linear, Cornell potential (1.1) using Dalgarno's method of perturbation and relativistic correction is incorporated in a free Dirac way. The wave function was obtained initially in ref. [63, 64] by considering the Coulomb potential as the parent and the linear potential as the perturbation. The obtained wave function was then used to study various static and dynamical properties of heavy and light flavored mesons such as form factors, decay constants and charge radii, where a negligible confinement effect ( $b \sim 0$ ) and a large value of coupling constant  $\alpha_s$  ( $\alpha_s \sim 0.65$ ) could be incorporated.

Further in ref. [65, 66], the slope and curvature of Isgur-Wise function were studied by using two loop V-scheme [67, 68]. However, application of V-Scheme was found to be successful in studying the Isgur-Wise function of  $D$  and  $D_s$  mesons but was not so successful in studying the  $B$ ,  $B_s$  and  $B_c$  mesons.

The wave functions are also obtained using a different perturbative approach, known as Variationally Improved Perturbation Theory (VIPT) in ref. [69], where acquired wave functions are used to find properties of heavy-light mesons, and the results for charge radii are found to be very small for the Coulomb part of the potential as parent compared to the linear part of the Cornell potential.

Overall it is to mention that in ref. [65, 66, 70], the properties of the mesons were studied considering the Coulombic part of the Cornell potential dominant over the linear part. On the other hand, in ref. [71], the Schrödinger equation is solved by considering the linear part to be dominant over the Coulombic part of the potential.

However, it is well known that at short distance Coulomb potential plays a more dominant role than the linear confinement because while the former is inversely proportional to ' $r$ ', the latter is linear. Similarly, for the large distance the confinement takes over the Coulomb effect. Therefore if the inter-quark separation ' $r$ ' can be roughly divided into two regions  $0 < r < r^P$  for short distance and  $r^P < r < r_0$  for long distance effectively, where  $r^P$  is the point where one of the potentials will dominate over the other. Therefore in the present work of the thesis we tried to incorporate both the short range and long range effect of the potential in the construction of total wave function.

Also, it is already mentioned that the constant term ' $c$ ' in the potential (1.1) is a phenomenological constant, which is needed to reproduce correct results for mesons. This constant term is found to have a variety of numerical values including +ve [14] and -ve[72–76]. Though this constant term is believed to behave like an energy scale parameter, it seems that this term plays a crucial role in the analysis of meson properties. We would like to criticize this here with few points:

Firstly, for hydrogen atom problem, if such a ' $c$ ' is added along with the Coulombic potential ( $-\frac{4\alpha_s}{3r}$ ), it results only in a shift in energy scale and does not have an effect on the wave function. However, in the case of Cornell potential, if ' $c$ ' is considered to be in the perturbative term along with the linear confinement term (with the Coulombic term in parent Hamiltonian), it has been found to have a significant effect on the total wave function [65, 66]. If instead of perturbation, ' $c$ ' is added to parent Hamiltonian along with the Coulombic potential (confinement term in perturbed Hamiltonian), the term also shows its effect.

Secondly, if we consider the linear potential ( $br$ ) with a constant term ' $c$ ', the wave function is not affected, only there is an energy shift. But adding this constant term to the Cornell potential either in the perturbed Hamiltonian along with the Coulomb potential (confinement term in parent Hamiltonian) [71] or in the parent Hamiltonian along with the confinement term (Coulomb term in the perturbed Hamiltonian), the whole wave function is disturbed.

But in general, it is expected that a constant term ' $c$ ' in the potential should not affect the wave function of the system while applying the perturbation theory. This means a Hamiltonian  $H$  with such a constant and another  $H'$  without it should give rise to the same wave functions, but only the energy eigenvalues are shifted by the constant. Since it is seen that whether the term ' $c$ ' is in the parent or perturbed part of the Hamiltonian, it always appears in the total wave function of the bound state. Thus the scaling factor ' $c$ ' plays a crucial role in the analysis of meson properties while applying the Dalgarno's method of perturbation. Therefore for the validation of the quantum mechanical idea while using perturbation theory like Dalgarno's method in the present work of thesis, we have considered the scaling factor  $c = 0$  in the potential (1.1).

Considering these two facts, we further improve the wave functions and revisited the model and various properties of mesons are studied in chapter 2, 3 and 4.

In **Chapter 2**, we reported the use of Dalgarno's method considering both Coulomb potential as the parent (linear potential as perturbation) and linear potential as the parent (Coulomb potential as perturbation) and obtained the wave functions with  $c = 0$ . From the wave functions, we compute the ground state masses of various heavy-light mesons ( $D, D_s, B, B_s$  and  $B_c$ ) introducing a cut-off parameter  $r^P$ . The results for charge radii of heavy



flavored mesons ( $D^+, D^0, D_s$  and  $B^+, B^0, B_s$ ) are reported. The analytical expressions for form factors in terms of momentum transfer ( $Q^2$ ) are also obtained and studied graphically. The root-mean-square (RMS) radii of mesons including  $c\bar{c}$  and  $b\bar{b}$  mesons are found.

In **Chapter 3**, we study the Isgur-Wise function and its derivatives for heavy-light mesons using both infinite mass limit (HQET) and finite mass limit consideration.

In **Chapter 4**, the decay constant of mesons are studied in both coordinate and momentum space. To study decay constant in momentum space, we transform the wave function from coordinate to momentum space by using Fourier transformation. Here we introduce a new cut-off  $p^P$  in momentum space. The variation of the wave functions in both coordinate and momentum space are studied graphically.

In **Chapter 5**, as a part of glueball physics, we outline the group theoretical method of Young Tableau of  $SU(3)_c$  to find the maximum number of constituent gluons in an experimentally observed scalar glueball.

In **Chapter 6**, we summarize the work in the thesis, presenting our concluding remarks and the future outlook. We also critically analyze limitations of the work in the chapter.

# 2

## The improved potential model and some properties of heavy flavored mesons

### 2.1 Introduction

As mentioned in Chapter 1, the QCD potential model [77] is considered to be very successful in explaining the static and dynamical properties of heavy-light mesons. Various heavy-light mesons include in the study are  $D, D_s, B, B_s$  and  $B_c$  mesons. Some of the important features of the mesons contain their masses, form factors, charge radii and RMS radii. In this chapter,

we obtain the analytic expressions of the Schrödinger wave functions for the Cornell potential (1.1) with  $c = 0$ . The first-order perturbed wave functions are obtained using Dalgarno's method [16, 18] of perturbation. The wave functions obtained are then used to study the results for the masses, form factors, charge radii and RMS radii of the heavy-light mesons ( $q\bar{Q}$  or  $\bar{q}Q$ ), where  $Q/\bar{Q} = c, b$  are the heavy quarks and  $q/\bar{q} = u, d, s$  are the light quarks.

In this chapter, we have suggested improvements to the perturbative procedure of ref. [63–66, 69–71] by dividing the inter-quark separation  $r$  at a point  $r^P$ , where in the region  $r < r^P$  (short distance), the Coulomb potential is dominant and linear is small and in the region  $r > r^P$  (long distance), linear potential is dominant and Coulomb is small.

The exact magnitude of  $r^P$  has explicit dependence on strong coupling constant  $\alpha_s$ , the confinement parameter ' $b$ ' of the Cornell potential.

In ref.[69], the charge radii of various heavy and light mesons were found to be very small for the Coulombic potential as parent compared to the linear parent potential, where Variationally Improved Perturbation Theory (VIPT) [10] was used. In ref.[78], charge radii of mesons were obtained, where the results for light mesons were found to agree well with the experimental values, but for heavy flavored  $B$  mesons, the results were large compared to other theoretical models. Similarly, the confinement parameter ' $b$ ' could not be incorporated in ref.[63, 78]. In this chapter, we take into account these limitations in the study of bound states  $D^+, D^0, D_s^+, B^+, B^0, B_s^0$  in perturbative approach and revisit the charge radii.

The RMS radii of various  $D$  and  $B$  mesons including  $c\bar{c}$  and  $b\bar{b}$  mesons are also studied in the chapter, while the results for only charmonium and bottomonium are available in the literature [79, 80]. RMS radii of mesons are of great interest for understanding the property

concerning the average size of the bound state of the mesons. The relation between charge radii and RMS radii of mesons are also shown in the chapter.

The obtained results are compared with the available experimental data and with the other theoretical models.

## 2.2 Formalism

### 2.2.1 Construction of wave function in the model

The modeling of meson wave function is a challenge since the exact wave function is not available in QCD mostly. The non-relativistic quark model which has been highly successful for both the meson states containing heavy and light quarks starting from the origin of de Rujula, Georgi and Glashow [81] has been improved in different manners. In the model, series solution of the two-body Schrödinger's equation for the Cornell potential is obtained using Dalgarno's method of perturbation. Though the model is non-relativistic in nature, the relativistic effect is incorporated in a free Dirac way [82, 83] due to light quarks involved. In QCD potential model approach, the general form of Fermi-Breit Hamiltonian [84] is

$$H(r) = H^{conf}(r) + H^{hyp}(r) + H^{S.O.}(r), \quad (2.1)$$

where

$$H^{conf}(r) = \left( -\frac{\alpha_s(r)}{r} + \frac{3}{4}br + \frac{3}{4}c \right) (\bar{F}_i \cdot \bar{F}_j), \quad (2.2)$$

$$H^{hyp}(r) = \frac{\alpha_s(r)}{m_i m_j} \left[ \frac{8\pi}{3} \bar{S}_i \cdot \bar{S}_j \delta^3(r) + \frac{1}{r^3} \left\{ \frac{3}{r^2} (\bar{S}_i \cdot \bar{r})(\bar{S}_j \cdot \bar{r}) - \bar{S}_i \cdot \bar{S}_j \right\} \right] (\bar{F}_i \cdot \bar{F}_j), \quad (2.3)$$

$$H^{S.O}(r) = H^{S.O(cm)}(r) + H^{S.O(t.p)}(r), \quad (2.4)$$

where

$$H^{S.O(cm)}(r) = \frac{\alpha_s(r)}{r^3} \left( \frac{1}{m_i} + \frac{1}{m_j} \right) \left( \frac{\bar{S}_i}{m_i} + \frac{\bar{S}_j}{m_j} \right) \bar{L}(\bar{F}_i \cdot \bar{F}_j), \quad (2.5)$$

$$H^{S.O(t.p)}(r) = -\frac{1}{2r} \frac{\partial H^{conf}}{\partial r} \left( \frac{\bar{S}_i}{m_i^2} + \frac{\bar{S}_j}{m_j^2} \right) \bar{L}. \quad (2.6)$$

Here  $\bar{S}_i$  and  $\bar{S}_j$  are the spins of the  $i^{th}$  and  $j^{th}$  quarks/antiquarks separated by a distance  $r$ .

However, for the ground state ( $l = 0$ ), only the contact term proportional to  $\delta^3(r)$  contributes and the Hamiltonian takes the simpler form

$$H = \frac{4\alpha_s}{3} \left[ -\frac{1}{|r|} - \frac{8\pi}{3} \frac{\bar{S}_i \cdot \bar{S}_j}{m_i m_j} \delta^3(r) \right] + br + c. \quad (2.7)$$

Now for the validation of the quantum mechanical idea as mentioned in Chapter 1, with  $c = 0$ , the spin independent Fermi-Breit Hamiltonian with confinement has the simple form as equation (1.1),

$$V(r) = -\frac{4\alpha_s}{3r} + br. \quad (2.8)$$

This Coulomb-plus-linear potential, called Cornell potential is the basis of the present model under study. It is established on the two kinds of asymptotic behaviors: ultraviolet at short distance (Coulomb like) and infrared at large distance (linear confinement term).

The Schrödinger equation is solved perturbatively, where the non-relativistic two body Schrödinger equation (1.3) of Chapter 1 takes the form

$$H|\psi\rangle = (H_0 + H')|\psi\rangle = E|\psi\rangle, \quad (2.9)$$

so that the first-order perturbed eigenfunction  $\psi^{(1)}$  and eigen energy  $W^{(1)}$  can be obtained using the relation

$$H_0\psi^{(1)} + H'\psi^{(0)} = W^{(0)}\psi^{(1)} + W^{(1)}\psi^{(0)}, \quad (2.10)$$

where  $H_0$  is the free Hamiltonian for two quarks/antiquarks and is defined as

$$H_0 = -\frac{\nabla^2}{2\mu} + V(r) \quad (2.11)$$

and

$$W^{(0)} = \langle \psi^{(0)} | H_0 | \psi^{(0)} \rangle, \quad (2.12)$$

$$W^{(1)} = \langle \psi^{(0)} | H' | \psi^{(0)} \rangle. \quad (2.13)$$

As already mentioned in Chapter 1 that based on the Coulomb part and the linear part of the potential (2.8), we can make two choices of ‘parent’ Hamiltonian (choice-I and II), which can be usefully compared [10]:

choice-I:  $H_0 = -\frac{\nabla^2}{2\mu} - \frac{4\alpha_s}{3r}$  as parent and  $H' = br$  as perturbation and

choice-II:  $H_0 = -\frac{\nabla^2}{2\mu} + br$  as parent and  $H' = -\frac{4\alpha_s}{3r}$  as perturbation.

From choice-I and II, we can find the bounds on  $r$  upto which both the choices are valid.

From choice-I,

$$\left| -\frac{4\alpha_s}{3r} \right| > |br| \quad (2.14)$$

and from choice-II,

$$|br| > \left| -\frac{4\alpha_s}{3r} \right|. \quad (2.15)$$

Inequality (2.14) and (2.15) will correspond to a particular point  $r$ , say  $r^P$ , where  $r^P = \sqrt{\frac{4\alpha_s}{3b}}$  such that for the short distance, i.e.  $r < r^P$  Coulomb part is dominant over the linear confinement term and for long distance, i.e.  $r > r^P$  linear part is dominant over the Coulombic term. Thus the point  $r^P$  measures the distance at which the potential changes from being dominantly Coulombic ( $r < r^P$ ) to dominantly linear ( $r > r^P$ ). At potential level, the continuity at a particular point of  $r$  is quite clear as is evident from Fig.1 of ref.[10].

The first-order perturbed wave function for the perturbed potential ( $br$ ) of choice-I is (Appendix A)

$$\psi_I^{(1)}(r) = -\frac{1}{2\sqrt{\pi}a_0^3} \mu b a_0 r^2 e^{-\frac{r}{a_0}} \left( \frac{r}{a_0} \right)^{-\varepsilon}, \quad (2.16)$$

where  $\mu$  is the reduced mass of the meson defined as

$$\mu = \frac{m_q m_Q}{m_q + m_Q}, \quad (2.17)$$

$m_q$  and  $m_Q$  are the masses of the light and heavy quark/antiquark respectively and

$$a_0 = \left( \frac{4}{3} \mu \alpha_s \right)^{-1}. \quad (2.18)$$

$\varepsilon$  is the correction for relativistic effect [82, 83] due to Dirac modification factor,

$$\varepsilon = 1 - \sqrt{1 - \left( \frac{4}{3} \alpha_s \right)^2}. \quad (2.19)$$

The corresponding eigen function  $\psi^{(0)}(r)$  for the unperturbed potential  $\frac{-4\alpha_s}{3r}$  with relativistic correction is

$$\psi_I^{(0)}(r) = \frac{1}{\sqrt{\pi a_0^3}} \left( \frac{r}{a_0} \right)^{-\varepsilon} e^{-\frac{r}{a_0}}. \quad (2.20)$$

Thus the normalized wave function for choice-I is

$$\psi_I^{total}(r) = \psi_I^{(0)}(r) + \psi_I^{(1)}(r) = \frac{N}{\sqrt{\pi a_0^3}} \left[ 1 - \frac{1}{2} \mu b a_0 r^2 \right] \left( \frac{r}{a_0} \right)^{-\varepsilon} e^{-\frac{r}{a_0}}, \quad (2.21)$$

where the normalization constant is

$$N = \frac{1}{\left[ \int_0^{r^p} \frac{4r^2}{a_0^3} \left[ 1 - \frac{1}{2} \mu b a_0 r^2 \right]^2 \left( \frac{r}{a_0} \right)^{-2\varepsilon} e^{-\frac{2r}{a_0}} dr \right]^{\frac{1}{2}}}. \quad (2.22)$$

Similarly, considering upto  $O(r^4)$ , the perturbed wave function (Appendix B) for the perturbed potential  $\left( -\frac{4\alpha_s}{3r} \right)$  of choice-II is

$$\psi_{II}^{(1)}(r) = \frac{1}{r} [A_0 r^0 + A_1(r)r + A_2(r)r^2 + A_3(r)r^3 + A_4(r)r^4] A_i[\rho_1 r + \rho_0] \left( \frac{r}{a_0} \right)^{-\varepsilon},$$

where  $A_i[r]$  is the Airy function [85, 86] and the co-efficients  $A_0, A_1, A_2, \dots$  etc. are appearing from the series solution as occurred in Dalgarno's method of perturbation, which are functions of  $\alpha_s, \mu$ , and  $b$ :

$$A_0 = 0, \quad (2.23)$$



$$A_1 = \frac{-2\mu \frac{4\alpha_s}{3}}{2\rho_1 k_1 + \rho_1^2 k_2}, \quad (2.24)$$

$$A_2 = \frac{-2\mu W^1}{2 + 4\rho_1 k_1 + \rho_1^2 k_2}, \quad (2.25)$$

$$A_3 = \frac{-2\mu W^0 A_1}{6 + 6\rho_1 k_1 + \rho_1^2 k_2}, \quad (2.26)$$

$$A_4 = \frac{-2\mu W^0 A_2 + 2\mu b A_1}{12 + 8\rho_1 k_1 + \rho_1^2 k_2}. \quad (2.27)$$

The parameters:

$$\rho_1 = (2\mu b)^{\frac{1}{3}} \quad (2.28)$$

and

$$\rho_0 = - \left[ \frac{3\pi(4n-1)}{8} \right]^{\frac{2}{3}}. \quad (2.29)$$

$\rho_0$  is defined as the zero of the Airy function, such that  $Ai[\rho_0] = 0$ . In our case  $n = 1$  for ground state of meson and

$$k = \frac{a_1 - b_1 \rho_0}{b_1 \rho_1}, \quad (2.30)$$

where  $a_1 = 0.355$  and  $b_1 = 0.258$  are the values at the origin for homogeneous Airy functions [86] and

$$k_1 = 1 + \frac{k}{r}, \quad (2.31)$$

$$k_2 = \frac{k^2}{r^2}. \quad (2.32)$$

The corresponding unperturbed wave function  $\psi_{II}^{(0)}$  for choice-II with relativistic correction is

$$\psi_{II}^{(0)}(r) = \frac{1}{r} Ai[\rho_1 r + \rho_0] \left( \frac{r}{a_0} \right)^{-\varepsilon}. \quad (2.33)$$

Thus the total normalized wave function for linear potential as parent and Coulomb potential as perturbation, considering upto  $O(r^4)$  with the Dirac modification factor for relativistic effect is

$$\psi_{II}^{total}(r) = \psi_{II}^{(0)}(r) + \psi_{II}^{(1)}(r) \quad (2.34)$$

$$= \frac{N'}{r} [1 + A_0 r^0 + A_1 r^1 + A_2 r^2 + A_3 r^3 + A_4 r^4] Ai[\rho_1 r + \rho_0] \left( \frac{r}{a_0} \right)^{-\varepsilon}, \quad (2.35)$$

where the normalization constant  $N'$  is

$$N' = \frac{1}{\left[ \int_{r^P}^{r_0} 4\pi [1 + A_0 r^0 + A_1(r)r + A_2(r)r^2 + A_3(r)r^3 + A_4(r)r^4]^2 (Ai[\rho_1 r + \rho_0])^2 \left( \frac{r}{a_0} \right)^{-2\varepsilon} dr \right]^{\frac{1}{2}}}. \quad (2.36)$$

Even though the Airy's function vanishes exponentially as  $r \rightarrow \infty$  [85] and is normalizable too, the additional cut-off  $r_0$  is used in the integration basically due to the polynomial approximation of the series expansion used in the Dalgarno's method of perturbation. And this is independent of the property of the Airy function. The continuity of the wave functions at the point  $r^P$  is checked in Appendix C and the sensitivity of the cut-off  $r_0$  and the normalizability of the wave function (2.35) are discussed in Appendix D.

### 2.2.2 Ground state masses of mesons

The pseudoscalar meson mass ( $M_P$ ) in the ground state [87] can be defined as:

$$M_P = m_{q/Q} + m_{\bar{q}/\bar{Q}} + \langle H \rangle \quad (2.37)$$

where  $m_{q/Q}$  is mass of light (or heavy) quark and  $m_{\bar{q}/\bar{Q}}$  is mass of light (or heavy) anti-quark constituting the meson bound state.

The expression (2.37) shows that to calculate the masses of mesons one needs to find  $\langle H \rangle$ , so that

$$\langle H \rangle = \left\langle \frac{p^2}{2\mu} \right\rangle + \langle V(r) \rangle \quad (2.38)$$

$$= 4\pi \int_0^\infty r^2 \psi^*(r) H \psi(r) dr \quad (2.39)$$

$$= 4\pi \int_0^\infty r^2 \left( \frac{p^2}{2\mu} + V(r) \right) |\psi(r)|^2 dr. \quad (2.40)$$

In the modified approach we redefine the above equation with the cut-off  $r^P$  as

$$\langle H \rangle = 4\pi \left[ \int_0^{r^P} r^2 \left( \frac{p^2}{2\mu} + V(r) \right) |\psi_I(r)|^2 dr + \int_{r^P}^{r_0} r^2 \left( \frac{p^2}{2\mu} + V(r) \right) |\psi_{II}(r)|^2 dr \right], \quad (2.41)$$

where  $\psi_I(r)$  and  $\psi_{II}(r)$  are the total wave functions as defined in equations (2.21) and (2.35) respectively.

### 2.2.3 Form factor and charge radii

The elastic charge form factor for a charged system of point quarks has the  $Q^2$  dependent form [88]

$$F(Q^2) = \sum_{i=1}^2 \frac{e_i}{Q_i} \int_0^\infty 4\pi r |\psi(r)|^2 \sin(Q_i r) dr, \quad (2.42)$$

where  $Q^2$  is the four momentum transfer square and  $e_i$  is the charge of the  $i^{th}$  quark/antiquark and

$$Q_i = \frac{\sum_{j \neq i} m_j Q}{\sum_{i=1}^2 m_i}, \quad (2.43)$$

where  $Q_i$  describes how the virtuality  $Q^2$  is shared between the quark and antiquark pair of the meson and  $m_i$  and  $m_j$  are the masses of the  $i^{th}$  and  $j^{th}$  quark/antiquark respectively.

With the improved version of the model, we redefine equation (2.42) as

$$\begin{aligned} F(Q^2) &= \sum_{i=1}^2 \frac{e_i}{Q_i} \int_0^{r^P} 4\pi r |\psi_I(r)|^2 \sin(Q_i r) dr \\ &+ \sum_{i=1}^2 \frac{e_i}{Q_i} \int_{r^P}^{r_0} 4\pi r |\psi_{II}(r)|^2 \sin(Q_i r) dr, \end{aligned} \quad (2.44)$$

$$F(Q^2) = F(Q^2)|_I + F(Q^2)|_{II}. \quad (2.45)$$

To check the behavior of the form factor with momentum transfer square  $Q^2$  we obtain the analytic expressions for form factors considering the Airy function upto order  $r^1$  as shown in Appendix E and F.

### With Dirac modification factor:

The 1<sup>st</sup> part of the integration (2.44),  $F(Q^2) |_I$  is solved using  $\psi_I(r)$ , the Coulomb potential as parent and linear as perturbation wave function (2.21) (as shown in Appendix E) with relativistic correction which gives

$$F(Q^2) |_I = N^2 \sum_{i=1}^2 e_i \left[ \frac{1}{2^{1-2\varepsilon}} \gamma(2-2\varepsilon, r^P) (2-2\varepsilon) \frac{1}{(1 + \frac{a_0^2 Q_i^2}{4})^{\frac{3}{2}-\varepsilon}} - \frac{\mu b a_0^3}{2^{3-2\varepsilon}} \gamma(4-2\varepsilon, r^P) (4-2\varepsilon) \frac{1}{(1 + \frac{a_0^2 Q_i^2}{4})^{\frac{5}{2}-\varepsilon}} + \frac{\mu^2 b^2 a_0^6}{2^{7-2\varepsilon}} \gamma(6-2\varepsilon, r^P) (6-2\varepsilon) \frac{1}{(1 + \frac{a_0^2 Q_i^2}{4})^{\frac{7}{2}-\varepsilon}} \right], \quad (2.46)$$

where the Incomplete Gamma function  $\gamma(s, r^P)$  is defined as

$$\int_0^{r^P} t^{s-1} e^{-t} dt = \gamma(s, r^P). \quad (2.47)$$

From the reality condition of equation (2.19), as we get  $0 < \varepsilon < 1$ , hence the form factor falls with the increasing value of  $Q^2$ .

Similarly, the 2<sup>nd</sup> part of integration (2.44),  $F(Q^2) |_II$  is solved using wave function (2.35) (as shown in Appendix F), which gives

$$F(Q^2) |_II = 4\pi N'^2 a_0^{2\varepsilon} \sum_{i=1}^2 e_i \left[ \sum_{k=1}^{11} F_k \frac{1}{(Q_i^2)^{\frac{k-2\varepsilon}{2}}} \right], \quad (2.48)$$

where  $F_k$ 's are defined in equation (F.5) of Appendix F.

The constraint on equation (2.48) is that for the term with  $k = 1$ ,  $\varepsilon < 1$ .

### Without Dirac modification factor:

The 1<sup>st</sup> part of the integration (2.44)  $F(Q^2) |_I$  with  $\varepsilon = 0$  gives

$$F(Q^2) |_I = N^2 \sum_{i=1}^2 e_i \left[ \gamma(2, r^P) \frac{1}{(1 + \frac{a_0^2 Q_i^2}{4})^{\frac{3}{2}}} - \frac{\mu b a_0^3}{2} \gamma(4, r^P) \frac{1}{(1 + \frac{a_0^2 Q_i^2}{4})^{\frac{5}{2}}} + \frac{3\mu^2 b^2 a_0^6}{2^6} \gamma(6, r^P) \frac{1}{(1 + \frac{a_0^2 Q_i^2}{4})^{\frac{7}{2}}} \right]. \quad (2.49)$$

Similarly, with  $\varepsilon = 0$ ,  $F(Q^2) |_{II}$  is

$$F(Q^2) |_{II} = 4\pi N'^2 \sum_{i=1}^2 e_i \left[ \sum_{k=2}^{11} F'_k \frac{1}{(Q_i^2)^{\frac{k}{2}}} \right], \quad (2.50)$$

where  $F'_k$ 's are defined in equation (F.8) of Appendix F.

Including equations (2.46) and (2.48), equations (2.49) and (2.50) are also showing us the  $\frac{1}{Q^2}$  behavior of form factors, which means at large  $Q^2$  form factor falls. Thus we conclude that the parameter  $\varepsilon$  doesn't change the qualitative asymptotic behavior of the form factors.

The average charge radii square for the mesons is extracted from the form factors at their low  $Q^2$  behavior using the relation [89],

$$\langle r^2 \rangle = -6 \frac{d^2}{dQ^2} F(Q^2) |_{Q^2=0}. \quad (2.51)$$

#### 2.2.4 RMS radii of heavy flavored mesons

The RMS radius [90, 91] of the bound state of quark and antiquark like meson is defined as

$$\langle r_{rms}^2 \rangle = \int_0^\infty r^2 |\psi(r)|^2 dr \quad (2.52)$$

having radial wave function  $\psi(r)$ .

With the cut-off parameters  $r^P$  and  $r_0$ , we modify the equation (2.52) to

$$\langle r_{rms}^2 \rangle = \int_0^{r^P} r^2 |\psi_I(r)|^2 dr + \int_{r^P}^{r_0} r^2 |\psi_{II}(r)|^2 dr. \quad (2.53)$$

### 2.2.5 Relation between RMS and charge radius

The charge radii can be measured using the electromagnetic probe, but not the RMS radii defined as in equation (2.52). The RMS radius is nearly the average  $\langle r^2 \rangle$  of the quark wave function, which presumably may be determined in Quark Gluon Plasma (QGP) experiments presently studied at LHC [92]. However, a simple approximate relationship between the two can be found from the following equation

$$r_E^2 = \sum_i e_i \left[ \langle r_i^2 \rangle + \frac{3}{4m_i^2} \int d^3p |\Phi(p)|^2 \left( \frac{m_i}{E_i} \right)^{2f} \right] \quad (2.54)$$

derived by Godfrey and Isgur [93].

Here  $r_E^2$  is the charge radius,  $\langle r_i^2 \rangle$  is the RMS radius,  $e_i$  is the charge of the  $i^{th}$  quark/antiquark,  $r_1$  and  $r_2$  are the distances of the two quarks/antiquarks measured from the centre of mass,  $m$  is the mass of the quark and  $E = \sqrt{p^2 + m^2}$ .  $\Phi(p)$  is the quark momentum distribution. The exponent ' $f$ ' can be determined in a semi-empirical way.

From equation (2.54) we obtain the inequality

$$r_E^2 > \sum_i e_i \langle r_i^2 \rangle. \quad (2.55)$$

Making the transformation of the coordinates, we choose one of the quarks/antiquarks located at the origin. It results in

$$r_E^2 > e < r^2 > \quad (2.56)$$

where  $< r^2 >$  can be interpreted as the standard RMS as defined in equation (2.52) and  $e = \sum e_i$ .

## 2.3 Calculation and results

### 2.3.1 Values of $r^P$

In Table 2.1, we have recorded the numerical values of the quantities to be calculated (in *Fermi*) at charmonium and bottomonium scale.

Table 2.1  $r^P$  in *Fermi* with  $c = 0$  and  $b = 0.183 GeV^2$

$\alpha_s$ -value	$r^P$ ( <i>Fermi</i> )
0.39 (for charmonium scale)	0.332
0.22 (for bottomonium scale)	0.249



### 2.3.2 Ground state masses of mesons

To calculate the results we have used Mathematica version 7.0.0. The input parameters in the numerical calculations are  $m_u = 0.336\text{GeV}$ ,  $m_d = 0.336\text{GeV}$ ,  $m_s = 0.483\text{GeV}$ ,  $m_c = 1.55\text{GeV}$ ,  $m_b = 4.95\text{GeV}$  and  $b = 0.183\text{GeV}^2$  and  $\alpha_s$  values 0.39 and 0.22 for charmonium and bottomonium scale respectively [94].

With these values, we calculate the masses of various heavy-light mesons using equation (2.37). The results obtained are then compared with the experimental data [2] and is shown in Table 2.2. For our calculations, we set the cut-off ( $r_0$ ) in the range of 1 *Fermi* ( $5.076\text{ GeV}^{-1}$ ) [95] in getting the results with the wave function  $\psi_{II}(r)$ .

Table 2.2 Masses of heavy-light mesons in  $\text{GeV}$ .

$\alpha_s$	Meson	$r^P (\text{GeV}^{-1})$	Mass ( $M_P$ ) ( $\text{GeV}$ )	Experimental Mass ( $\text{GeV}$ ) [2]
0.39	$D(c\bar{u}/c\bar{d})$	1.68	2.378	$1.869 \pm 0.00009$
	$D_s(c\bar{s})$		2.500	$1.968 \pm 0.0001$
0.22	$B(ub/db)$	1.26	5.798	$5.279 \pm 0.00015$
	$B_s(s\bar{b})$		5.902	$5.366 \pm 0.00022$
	$B_c(\bar{b}c)$		6.810	$6.275 \pm 0.001$

From Table 2.2, it is clear that our mass predictions are off by more than 500  $\text{MeV}$  for both the open bottom and open charm mesons.

We have also tested the perturbative stability of the results for masses in the present model in Table 2.3, where it is clearly seen that the contribution of the perturbed wave function is less than that of the parent wave function.

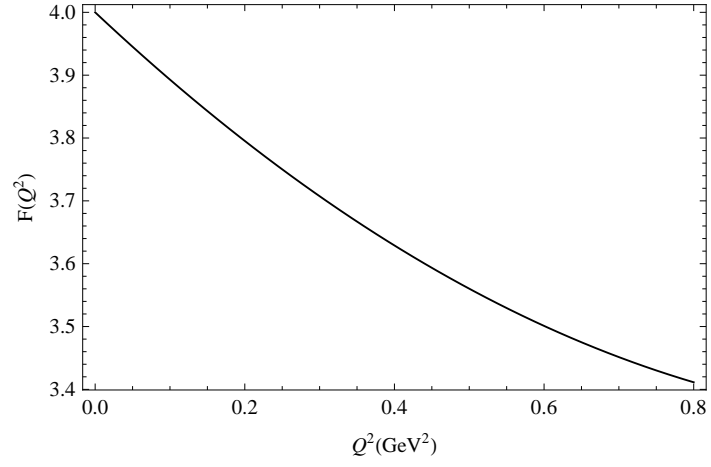
Table 2.3 Masses of heavy-light mesons in  $GeV$  from parent and total wave function.

Meson	Mass ( $M_P$ ) ( $GeV$ )	
	With parent wave function	With total wave function
$D(c\bar{u}/c\bar{d})$	2.250	2.378
$D_s(c\bar{s})$	2.348	2.500
$B(u\bar{b}/d\bar{b})$	5.681	5.798
$B_s(s\bar{b})$	5.780	5.902
$B_c(\bar{b}c)$	6.713	6.810

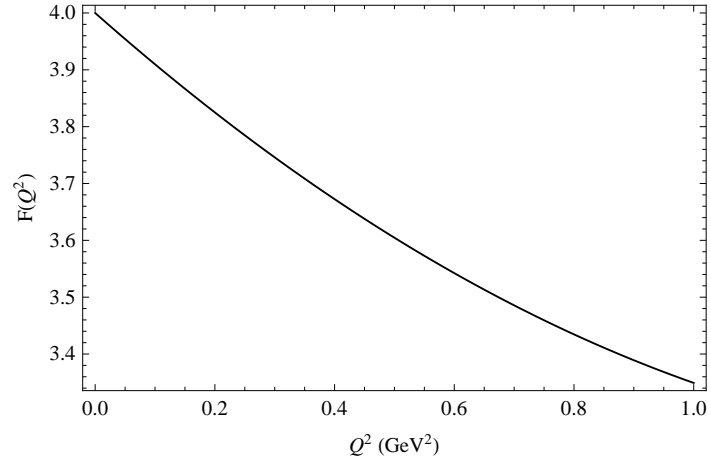
### 2.3.3 Form factors

In Fig. 2.1 we study the variation of form factor  $F(Q^2)$  with  $Q^2$  for charged mesons ( $D^+(c\bar{d})$ ,  $D^+(c\bar{s})$  and  $B^+(u\bar{b})$ ) and in Fig. 2.2 we display the variation of form factor for neutral mesons ( $D^0(c\bar{u})$ ,  $B^0(d\bar{b})$  and  $B_s^0(s\bar{b})$ ) respectively, using equation (2.44) with Dirac modification factor.

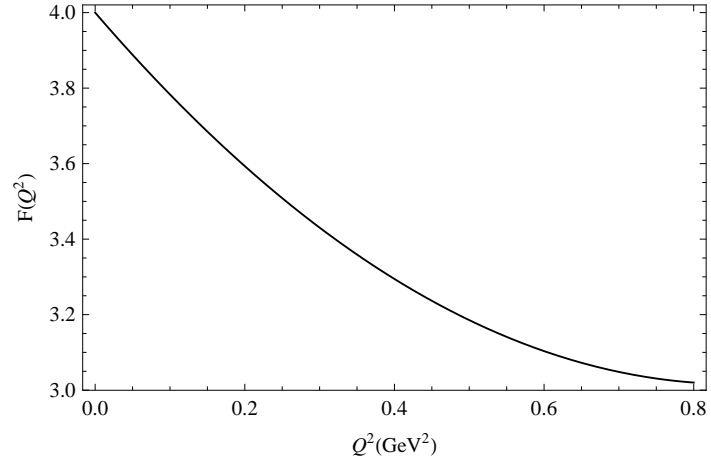
Fig. 2.1 shows the form factor  $F(Q^2)$  decreases with the increase of  $Q^2$  as it should.



(a) Variation of form factor  $F(Q^2)$  with  $Q^2$  for  $D^+(c\bar{d})$  meson

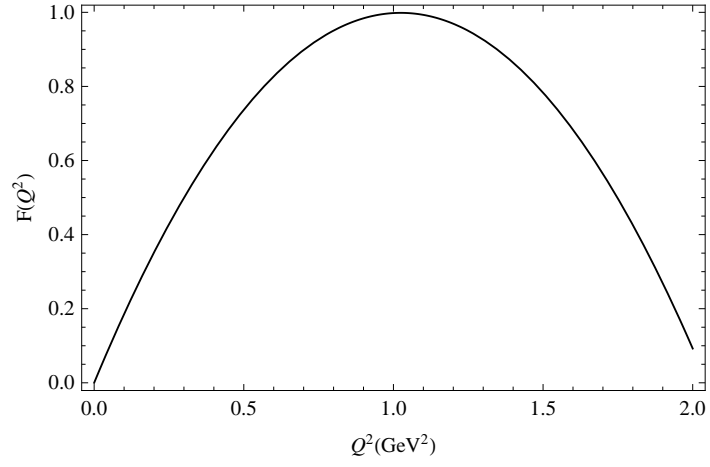


(b) Variation of form factor  $F(Q^2)$  with  $Q^2$  for  $D^+(c\bar{s})$  meson.

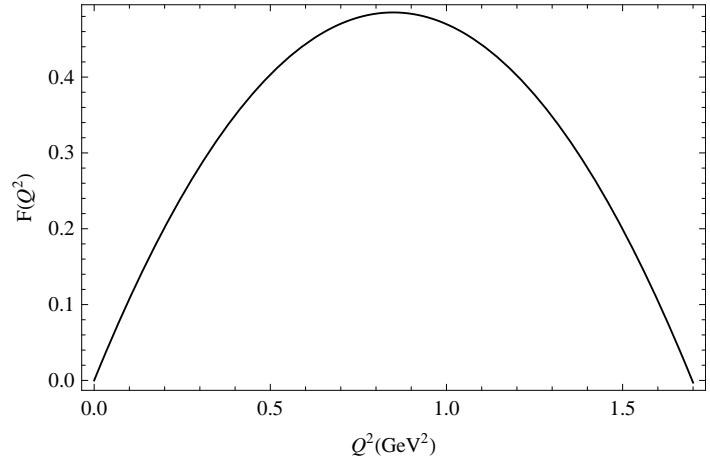


(c) Variation of form factor  $F(Q^2)$  with  $Q^2$  for  $B^+(u\bar{b})$  meson.

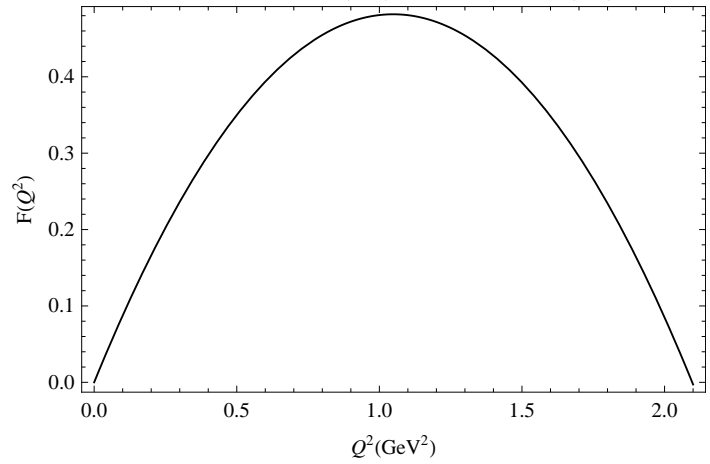
Fig. 2.1 Variation of form factor  $F(Q^2)$  with  $Q^2$  for charged mesons.



(a) Variation of form factor  $F(Q^2)$  with  $Q^2$  for  $D^0(c\bar{u})$  meson.



(b) Variation of form factor  $F(Q^2)$  with  $Q^2$  for  $B^0(d\bar{b})$  meson.



(c) Variation of form factor  $F(Q^2)$  with  $Q^2$  for  $B_s^0(s\bar{b})$  meson.

Fig. 2.2 Variation of form factor  $F(Q^2)$  with  $Q^2$  for neutral mesons.

However, it is seen that while the form factor of the charged mesons decreases with the increasing value of  $Q^2$ , but for neutral mesons form factor first increases for slight  $Q^2$  than decreases with the increasing value of momentum transfer square. A similar behavior for neutral pseudoscalar Kaon is also suggested in ref.[96]. Our study also shows a temporary rise in form factor does exist for heavy flavored neutral mesons near  $Q^2 \approx 1\text{GeV}^2$  (Fig. 2.2). This is presumably due to the non-dominant behavior of small  $Q^2$  over the other parameters involved. From the graphs, it is evident that the range of validity of the model is not beyond  $\sim 2.1\text{GeV}^2$ .

### 2.3.4 Charge radii

In Table 2.4, we present the results obtained for the charge radii using equation (2.51) for various  $D$  and  $B$  mesons in Table 2.4 and compare them with the results of ref. [69, 78] and with the prediction of other models [89, 97].

Table 2.4 The mean square charge radii of  $D$  and  $B$  mesons.

Meson	$\langle r^2 \rangle \text{ (Fermi}^2\text{)}$					
	Present work		Previous work[78]	Previous work [69]	[89]	[97]
	with Dirac modification factor	without Dirac modification factor				
$D^+(c\bar{d})$	0.260	0.265	0.134	0.011	0.184	0.219
$D^0(c\bar{u})$	-0.453	-0.463	-0.234	-0.013	-0.304	-0.403
$D_s^+(c\bar{s})$	0.216	0.222	0.126	0.010	0.124	-
$B^+(u\bar{b})$	0.536	0.538	2.96	0.060	0.378	-
$B^0(d\bar{b})$	-0.266	-0.267	-1.47	-0.030	-0.187	-
$B_s^0(s\bar{b})$	-0.214	-0.215	-1.37	-0.025	-0.119	-

From Table 2.4 we can see that our predicted results for  $D^+(c\bar{d})$  and  $D^0(c\bar{u})$  mesons are in good agreement with those of ref. [97]. The present results for  $B$  mesons are found to be very much improved than earlier analysis of ref. [69]. It is observed that the introduction of

the Dirac modification factor doesn't change the results significantly.

From Table 2.4 it is interesting to see that for all the neutral mesons the mean square charge radius is negative. A well explanation for negative charge radius square of the neutral meson can be found in ref. [98]. Here let us explain this for neutral  $D^0(c\bar{u})$  meson.

We define a center of mass coordinate for the quark antiquark ( $Q\bar{q}$ ) bound state of meson,

$$R = \frac{m_Q r_Q + m_{\bar{q}} r_{\bar{q}}}{m_Q + m_{\bar{q}}}, \quad (2.57)$$

where  $r_Q$  and  $r_{\bar{q}}$  are the heavy ( $Q$ ) and light anti-quark ( $\bar{q}$ ) coordinates respectively.

The mean square charge radius of the meson can be written as the deviation from the center of mass coordinate squared weighted by the quark and antiquark constituents of the meson, which has the simplified form,

$$\langle r^2 \rangle_{D^0} = \frac{(Q_Q m_{\bar{q}}^2 + Q_{\bar{q}} m_Q^2) \langle \delta^2 \rangle_{D^0}}{(m_Q + m_{\bar{q}})^2}, \quad (2.58)$$

where  $Q_Q$  and  $Q_{\bar{q}}$  are charge of the quark and anti-quark respectively.

$\delta = r_Q - r_{\bar{q}}$  is the relative coordinate.

For  $D^0(c\bar{u})$  meson,  $m_{\bar{q}} = m_u = m = 0.336 \text{ GeV}$

and  $m_Q = m_c = 1.55 \text{ GeV} = \gamma m$ ;  $\gamma = 4.61$ .

Thus from equation (2.58),

$$\langle r^2 \rangle_{D^0} = \frac{2 - 2\gamma^2}{3 + 3\gamma^2} \langle \delta^2 \rangle_{D^0}. \quad (2.59)$$

Since  $\gamma = 4.61$  and  $\langle \delta^2 \rangle_{D^0} > 0$ , from equation (2.59), it is clear that  $D^0(c\bar{u})$  has a negative square charge radius.

In  $D^0(c\bar{u})$  meson, a negatively charged light  $u$ -antiquark is orbiting around a heavier positively charged  $c$ -quark. Since the mass of  $c$ -quark is very large compared to the  $u$ -antiquark, when we probe lightly into the charge distribution, we will see the charge of the light objects which are in the tail of the distribution orbiting out at large distances.

The same explanation is valid for  $B^0(d\bar{b})$  and  $B_s^0(s\bar{b})$  mesons also, where a light  $d$ -quark is orbiting around a heavier  $b$ -antiquark and a light  $s$ -quark is orbiting around a heavier  $b$ -antiquark respectively.

The perturbative stability of our results is also checked in the present model as shown in Table 2.5.

Table 2.5 Mean square charge radii of  $D$  and  $B$  mesons.

Meson	$\langle r^2 \rangle$ (Fermi <sup>2</sup> )	
	With Parent wave function	With Total wave function
$D^+(c\bar{d})$	0.233	0.260
$D^0(c\bar{u})$	-0.406	-0.453
$D_s^+(c\bar{s})$	0.205	0.216
$B^+(u\bar{b})$	0.490	0.536
$B^0(d\bar{b})$	-0.242	-0.266
$B_s^0(s\bar{b})$	-0.207	-0.214

### 2.3.5 RMS radii

We obtain the RMS radii of various mesons using equation (2.53) as shown in Table 2.6.

Table 2.6 RMS radii ( $r_{rms}$ ) in *Fermi*.

$\alpha_s$	Meson	$r_{rms}$ in <i>Fermi</i> with Dirac modification factor	$r_{rms}$ in <i>Fermi</i> without Dirac modification factor
0.39	$\pi^+(u\bar{d})$	0.989	0.948
	$K(u\bar{s}/d\bar{s})$	0.992	0.950
	$D(c\bar{u}/c\bar{d})$	0.998	0.955
	$D_s^+(c\bar{s})$	1.007	0.961
	$c\bar{c}$	1.046	0.990
0.22	$B_c^+(\bar{b}c)$	1.082	1.061
	$b\bar{b}$	1.141	1.116

In Table 2.7, we give the different model predictions of rms radii for heavy flavored mesons available in literature [79, 80] for  $c\bar{c}$  and  $b\bar{b}$ .

Table 2.7 RMS radii ( $r_{rms}$ ) in *Fermi* from different model prediction.

Meson	$r_{rms}(Fermi)$	
	Ref.[79]	Ref.[80]
$c\bar{c}$	0.4490	0.4530
$b\bar{b}$	0.2245	0.2260

From Table 2.6, we see that our values of rms radii for  $c\bar{c}$  and  $b\bar{b}$  are higher than those of Table 2.7.

## 2.4 Conclusion

In this chapter, we have used a cut-off  $r^P$  which is obtained from the theory to predict the results for masses, charge radii and RMS radii of various heavy flavored mesons. The results for masses of  $D$  mesons are higher than those of experimental results. However, it is to be mentioned that by changing cut-off parameters  $r^P$  and  $r_0$  the exact value of experimental



masses could be obtained. To modify the values of  $r^P$  we need to change the values of the strong coupling constant ( $\alpha_s$ ). From the Table 2.3 it is seen that the results based on the unperturbed wave functions are better than those of the total ones. However, it is needed to be mentioned that these tabulated values are shown to check the perturbative stability of the results, such that the contribution from the parent part is more than the perturbed term.

We have also studied the graphical behavior of the form factors. Graphs for form factors of the mesons are shown displaying the variation with momentum transfer square ( $Q^2$ ). From the graphs, it is seen that the form factors for charged mesons decrease with increasing values of  $Q^2$ , but for neutral mesons, a temporary rise in form factor is observed, a feature not uncommon even for light neutral Kaon [96] also. At the lower scale,  $Q^2$  itself ceases to play the dominant factor of the overall behavior in this particular model.

The mean square charge radii of heavy pseudoscalar mesons have not been measured experimentally yet. In earlier cases in ref.[78], the model did not show good results for the charge radii of  $B$  mesons, though the model was quite successful in the prediction of results for light mesons and heavy flavored  $D$  mesons. We have improved the results of ref.[69, 78] by introducing two cut-off parameters  $r^P$  and  $r_0$ . In ref.[78], the confinement parameter ' $b$ ' was taken to be zero due to perturbative constraints. However, with the improved version of the present work, we overcome such limitation by incorporating the value of confinement parameter to be  $b = 0.183 GeV^2$ .

Also by changing the values of strong coupling constant for charmonium and bottomonium scale, the results for RMS radii for  $b\bar{b}$  and  $c\bar{c}$  can be improved.

---

The values of cut-off parameters  $r^P$ ,  $r_0$  and masses of quarks which are input parameters are kept fixed for the next chapters of the thesis.

# 3

## Isgur-Wise function of heavy-light mesons in the potential model

### 3.1 Introduction

The heavy hadron spectroscopy played a significant role in the foundation of QCD. In last few years, it has sparked a renewed interest in the subject due to various data available from the B factories[99], CLEO [100], LHCb [101] and the Tevatron [102]. In more recent times the discovery of X-Y states [103] as possible charmonium and bottomonium hybrids have

extended such study of the exotic heavy hadron spectroscopy. The most recent discoveries of the charmonium pentaquarks [104] have further increased its importance. The simplest systems of this area are the heavy-light and heavy-heavy hadrons.

In the last few years, the experimental study of heavy-light and heavy-heavy mesons have renewed the theoretical interest towards HQET (Heavy Quark Effective Theory) and Isgur-Wise function [105–107].

In this chapter, we will report a study of such heavy flavored mesons in QCD potential model [77].

## 3.2 Formalism

### 3.2.1 Slope and curvature of Isgur-Wise function

Isgur, Wise, Georgi [25, 108] and others[4] showed that in weak semi-leptonic decays of heavy-light mesons (e.g.  $B$  mesons to  $D$  or  $D^*$  mesons), in the limit  $m_Q \rightarrow \infty$  all the form factors that describe these decays are expressible in terms of a single universal function of velocity transfer. This function is known as the Isgur-Wise function, which is normalized to unity at zero-recoil. It measures the overlap of the wave functions of the light degrees of freedom in the initial and final mesons moving with velocities  $v$  and  $v'$  respectively.

The Isgur-Wise function is denoted by  $\xi(Y)$ , where  $Y = v \cdot v'$  and  $\xi(Y)|_{Y=1} = 1$  is the normalization condition at the zero-recoil point ( $v = v'$ ) [34].

The calculation of Isgur-Wise function is non-perturbative in principle and is performed earlier [66, 71] for different phenomenological wave functions for mesons. This function

depends upon the meson wave function and some kinematic factor as

$$\xi(Y) = \int_0^\infty 4\pi r^2 |\psi(r)|^2 \cos(pr) dr, \quad (3.1)$$

where  $\psi(r)$  is the wave function for light quark only and

$$\cos(pr) = 1 - \frac{p^2 r^2}{2} + \frac{p^4 r^4}{24} + \dots \quad (3.2)$$

with  $p^2 = 2\mu^2(Y - 1)$ .

Taking  $\cos(pr)$  upto  $O(r^4)$  we get,

$$\begin{aligned} \xi(Y) = \int_0^\infty 4\pi r^2 |\psi(r)|^2 dr - \left[ 4\pi\mu^2 \int_0^\infty r^4 |\psi(r)|^2 dr \right] (Y - 1) + \\ \left[ \frac{2}{3}\pi\mu^4 \int_0^\infty r^6 |\psi(r)|^2 dr \right] (Y - 1)^2. \end{aligned} \quad (3.3)$$

In an explicit form, the Isgur-Wise function can be written as [4, 25]

$$\xi(Y) = 1 - \rho^2(Y - 1) + C(Y - 1)^2, \quad (3.4)$$

where  $\rho^2 > 0$ .

The quantity  $\rho^2$  is the slope of the Isgur-Wise function which determines the behavior of Isgur-Wise function close to zero recoil point ( $Y = 1$ ) is known as the charge radius:

$$\rho^2 = -\frac{\partial \xi}{\partial Y} \Big|_{Y=1}. \quad (3.5)$$

The second order derivative is the curvature of the Isgur-Wise function known as convexity parameter:

$$C = \frac{1}{2} \left( \frac{\partial^2 \xi}{\partial Y^2} \right) \bigg|_{Y=1}. \quad (3.6)$$

Now from equations (3.3) and (3.4),

$$\rho^2 = 4\pi\mu^2 \int_0^\infty r^4 |\psi(r)|^2 dr, \quad (3.7)$$

$$C = \frac{2}{3}\pi\mu^4 \int_0^\infty r^6 |\psi(r)|^2 dr \quad (3.8)$$

and

$$\int_0^\infty 4\pi r^2 |\psi(r)|^2 dr = 1. \quad (3.9)$$

In the present work, we improve the equations for  $\rho^2$  and  $C$  to

$$\rho^2 = 4\pi\mu^2 \left[ \int_0^{r^P} r^4 |\psi_I(r)|^2 dr + \int_{r^P}^{r_0} r^4 |\psi_{II}(r)|^2 dr \right] \quad (3.10)$$

and

$$C = \frac{2}{3}\pi\mu^4 \left[ \int_0^{r^P} r^6 |\psi_I(r)|^2 dr + \int_{r^P}^{r_0} r^6 |\psi_{II}(r)|^2 dr \right]. \quad (3.11)$$

Using these modified expressions for slope and curvature of Isgur-Wise function in equation (3.4), we have computed the results. In equations (3.10) and (3.11),  $\psi_I(r)$  and  $\psi_{II}(r)$  are the wave functions as defined in equations (2.21) and (2.35) of Chapter 2 respectively.

### 3.3 Calculation and results

In Table 3.1 and 3.3, we find the slope ( $\rho^2$  and  $\rho'^2$ ) and the curvature ( $C$  and  $C'$ ) using modified equations (3.10) and (3.11) respectively. The input parameters in the numerical calculations are  $m_u = 0.336\text{GeV}$ ,  $m_d = 0.336\text{GeV}$ ,  $m_s = 0.483\text{GeV}$ ,  $m_c = 1.55\text{GeV}$ ,  $m_b = 4.95\text{GeV}$  and  $b = 0.183\text{GeV}^2$  and  $\alpha_s$  values 0.39 and 0.22 for charmonium and bottomonium scale respectively, which are same with the previous chapter.

The numerical results for  $\rho^2$  and  $C$  in the Isgur-Wise limit is shown in Table 3.1, where we consider the mass of active quark/antiquark (in this case  $b$ -quark) to be infinitely heavy ( $m_Q/m_{\bar{Q}} \rightarrow \infty$ ). In this infinite heavy quark mass limit, reduced mass  $\mu$  becomes that of the light quark/antiquark ( $m_q/\bar{m}_q$ ) (in this case  $u$ -quark), i.e.

$$\lim_{m_Q \rightarrow \infty} \mu = \lim_{m_Q \rightarrow \infty} \frac{m_q m_Q}{m_q + m_Q} = m_q. \quad (3.12)$$

We have also compared our results with the predictions of other models [109–116].

Table 3.1 Values of  $\rho^2$  and  $C$  in the present work and other works in the limit  $m_Q \rightarrow \infty$ .

	$\rho^2$	$C$
Present work	1.176	0.180
Other work		
Le Yaouanc et al. [109]	$\geq 0.75$	0.47
Rosner [110]	1.66	2.76
Mannel [111]	0.98	0.98
Pole Ansatz [112]	1.42	2.71
Ebert et al. [113]	1.04	1.36
QCD sum rule [114]	0.65	0.47
UKQCD Collaboration [115]	$0.83^{+15+24}_{-11-22}$	-
CLEO Collaboration [116]	$0.76 \pm 0.16 \pm 0.08$	-

However, in a generalized way we can also check the flavor dependence of the form factor in heavy meson decays. We calculate the slope ( $\rho'^2$ ) and curvature ( $C'$ ) of the form

factor of semi-leptonic decays in finite mass limit with the flavor dependent correction. In Table 3.3, we compare our present results with ref. [65, 66], where the reduced masses of the mesons are obtained in Table 3.2 using equation (2.17). The results in the present work clearly show an improvement over the ref. [65, 66].

Table 3.2 Reduced mass of heavy-light mesons in  $GeV$ .

Meson	Reduced mass ( $\mu$ ) ( $GeV$ )
$D(c\bar{u}/c\bar{d})$	0.276
$D_s(c\bar{s})$	0.368
$B(u\bar{b}/d\bar{b})$	0.314
$B_s(s\bar{b})$	0.440
$B_c(\bar{b}c)$	1.180

Table 3.3 Values of slope ( $\rho'^2$ ) and curvature ( $C'$ ) of the form factor of heavy meson decays in the present and earlier work with finite mass correction.

	Meson	$\rho'^2$	$C'$
Present work	$D(c\bar{u}/c\bar{d})$	0.911	0.106
	$D_s(c\bar{s})$	1.318	0.228
	$B(u\bar{b}/d\bar{b})$	1.110	0.260
	$B_s(s\bar{b})$	1.722	0.721
	$B_c(\bar{b}c)$	4.646	6.074
Ref.[65, 66]	$D(c\bar{u}/c\bar{d})$	1.136	5.377
	$D_s(c\bar{s})$	1.083	3.583
	$B(u\bar{b}/d\bar{b})$	128.28	5212
	$B_s(s\bar{b})$	112.759	4841
Ref.[117]	$B_c(\bar{b}c)$	5.45	31.39

From Table 3.3, a large variations for the values of  $\rho'^2$  and  $C'$  are observed with respect to Table 3.1. This disparity is also seen from the predictions of ref. [65, 66] specially for  $B(u\bar{b}/d\bar{b})$  and  $B_s(s\bar{b})$  mesons. This is because in Table 3.1, the slope ( $\rho^2$ ) and curvature ( $C$ ) of Isgur-Wise function are obtained in infinite heavy quark mass limit ( $m_Q \rightarrow \infty$ ). But in Table 3.3, the values slope ( $\rho'^2$ ) and curvature ( $C'$ ) of form factors are obtained in finite mass limit. Also in the present work we have considered the scale factor,  $c = 0$ . So, the scale



parameter doesn't have any affect in the wave functions of the system, while in ref. [65, 66] the values were obtained for a non-zero value of ' $c$ '.

The graphical variation of Isgur-Wise function  $\xi(Y)$  with  $Y$  in the Isgur-Wise limit is shown in Fig.3.1 (using Table 3.1), where the mass of the  $b$ -quark is considered to be infinitely heavy and the reduced mass  $\mu$  is  $0.336\text{GeV}$  (mass of  $u$  or  $d$ -quark/antiquark). In a similar way, we draw Fig.3.2 (using Table 3.3) for finite mass and flavor dependent correction. For comparison the results of ref. [110] and [113] are plotted in the same graphs.

To draw the graphs, we have used equations (3.10) and (3.11) in (3.4).  $\xi(Y)$  is found to have the expected fall with  $Y = v.v'$ . It is seen from the figure that the computed results are well within the values of the model [110, 113].

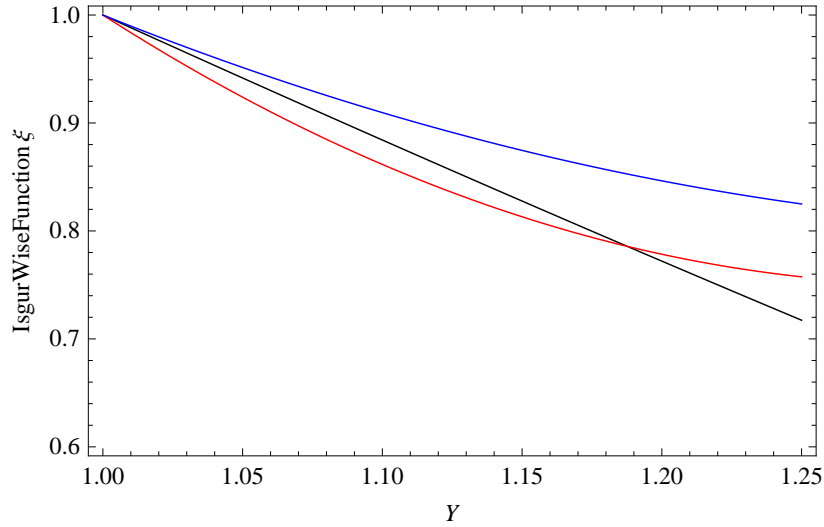


Fig. 3.1 Variation of form factor with  $Y$  in the Isgur-Wise limit. The blue and red graph correspond to the results of quark model in relativistic approach of ref. [113] and non-relativistic approach of ref. [110] respectively.

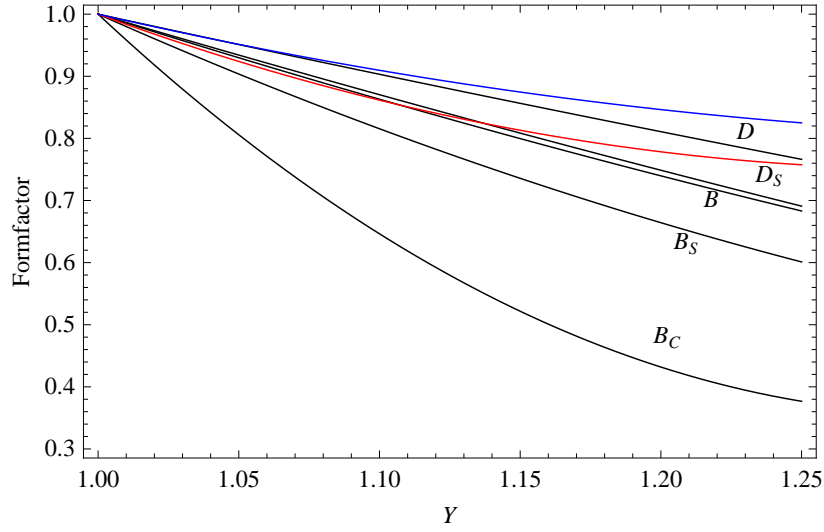


Fig. 3.2 Variation of form factor with  $Y$  with finite mass correction. The blue and red graph correspond to the results of quark model in relativistic approach of ref. [113] and non-relativistic approach of ref. [110] respectively.

### 3.4 Conclusion

In this chapter, we have calculated the slope and the convexity parameter of the Isgur-Wise function considering the scaling factor ‘ $c$ ’ to be zero by giving equal fitting to both the Coulomb and linear part of the Cornell potential unlike in the ref. [63, 65, 70, 71, 117–119]. The values of slope and curvature of the Isgur-Wise function calculated in this chapter are well within the limit of other model values (Table 3.1). Also our calculations provide a measure of the slope and curvature of the form factors with finite mass corrections. From our results, we can say that the modifications induced by mass effect are not so significant for  $D(c\bar{u}/c\bar{d})$ ,  $D_s(c\bar{s})$ ,  $B(u\bar{b}/d\bar{b})$ ,  $B_s(s\bar{b})$  mesons. However, for the mesons where light quark/antiquark is not so light compared to the heavy quark/antiquark, the finite mass limit do show a very strong dependence on the spectator quark mass, as for  $B_c(c\bar{b})$  meson (Table 3.3). It presumably suggests that the finite mass correction approach is not effective for mesons where the constituent light quark/antiquark is not so light compared to the other heavy quark/antiquark constituent.

# 4

## Leptonic decay constants of heavy-light mesons in the potential model

### 4.1 Introduction

The strong interactions between the quark and the antiquark in a meson lead to the determination of the wave function of the bound state. The study of the wave functions of heavy-flavored mesons like  $D$  and  $B$  are important not only for studying the properties of strong interactions between heavy and light quarks but also for investigating the mechanism

of heavy meson decays. The wave function determines the momentum distributions of the quark and antiquark in mesons, which is a significant quantity for calculating the amplitude, form factors and decay constants of heavy meson decays [73, 120–123].

In this chapter, the modified wave functions using a short distance scale  $r_c$  in analogy to hydrogen atom are obtained in coordinate space. The decay constants  $f_D, f_{D_s}, f_B, f_{B_s}$  and  $f_{B_c}$  are computed in both coordinate and momentum space and compared with the available experimental data and other theoretical models. Here we introduce a new cut-off parameter,  $p^P$  in momentum space, in addition to  $r^P$ . We also study the variation of the wave functions with inter-quark distance  $r$  and momentum  $p$ .

## 4.2 Formalism

### 4.2.1 Definition of decay constant in coordinate space

In the non-relativistic limit, the pseudoscalar decay constant  $f_P$  and the ground state wave function at the origin  $\psi(0)$  are related by the Van-Royen-Weisskopf formula [124],

$$f_P = \sqrt{\frac{12}{M_P} |\psi(0)|^2}. \quad (4.1)$$

With QCD correction factor the decay constant can be written as [125]

$$f_{P_c} = \sqrt{\frac{12}{M_P} |\psi(0)|^2 \bar{C}^2}, \quad (4.2)$$

where

$$\bar{C}^2 = 1 - \frac{\alpha_s}{\pi} \left[ 2 - \frac{m_i - m_j}{m_i + m_j} \ln \frac{m_i}{m_j} \right], \quad (4.3)$$

where  $M_P$  is the pseudoscalar meson mass obtained in Chapter 2 (Table 2.2).

Equations (4.1) and (4.2) show that we need to obtain wave function at the origin to find decay constant. But with the Dirac modification factor  $\left(\frac{r}{a_0}\right)^{-\varepsilon}$ , the wave functions (2.21) and (2.35) at  $r = 0$  develop a singularity. Again with  $\varepsilon = 0$ , though the wave function at the origin for (2.21) survives, but for (2.35) the singularity remains. In this case, one has to regularize the wave function at the origin [126] which has a quantum mechanical origin in QED. It is well known that the relativistic wave function of the hydrogen atom has such singularities too. However, such an effect is noticeable only for a tiny region [83],

$$2mz\alpha r \leq e^{-\left(\frac{1}{1-\gamma}\right)} \leq e^{-\frac{2}{z^2\alpha^2}} \sim 10^{-\frac{16300}{z^2}}, \quad (4.4)$$

where  $z$  and  $m$  are the atomic number and reduced mass of the hydrogen atom respectively,  $\alpha$  is the electromagnetic coupling constant and  $\gamma = \sqrt{1 - z^2\alpha^2}$ . In QCD, one replaces  $m$ ,  $\alpha$  and  $1 - \gamma$ , the hydrogen-like properties by  $\mu$ ,  $\frac{4}{3}\alpha_s$  and  $\varepsilon$  respectively. Here  $\alpha_s$  is the strong coupling constant,  $\varepsilon$  is as defined by equation (2.19) and  $(2mz\alpha r)^{(\gamma-1)}$  changes to  $\left(\frac{r}{a_0}\right)^{-\varepsilon}$ , which leads to a cut of parameter  $r_c$  up to which the model can be extrapolated ( $r \geq r_c$ ). Using the typical length scale for the relativistic correction term  $\left(\frac{r}{a_0}\right)^{-\varepsilon} \leq \frac{1}{e}$ , one obtains

$$r_c \sim a_0 e^{-\frac{1}{\varepsilon}}. \quad (4.5)$$

With this cut-off  $r_c$ , the normalized and regularized wave function corresponding to wave function (2.21) is

$$\psi_I^{total}(r') = \frac{N}{\sqrt{\pi a_0^3}} \left[ 1 - \frac{1}{2} \mu b a_0 (r')^2 \right] \left( \frac{r'}{a_0} \right)^{-\varepsilon} e^{-\frac{r'}{a_0}}. \quad (4.6)$$

Similarly, for (2.35), the corresponding regularized wave function is

$$\psi_{II}^{total}(r') = \frac{N'}{r} [1 + A_1 r' + A_2 (r')^2 + A_3 (r')^3 + A_4 (r')^4] Ai[\rho_1 r' + \rho_0] \left( \frac{r'}{a_0} \right)^{-\varepsilon}, \quad (4.7)$$

with

$$r' = r + r_c. \quad (4.8)$$

### 4.2.2 Definition of decay constant in momentum space

The decay constant in the momentum space [127] can be expressed through the meson wave function  $\psi(p)$  as

$$f_P = \sqrt{\frac{12}{M_P}} \int \frac{d^3 p}{(2\pi)^{\frac{3}{2}}} \left( \frac{E_i + m_i}{2E_i} \right)^{\frac{1}{2}} \left( \frac{E_j + m_j}{2E_j} \right)^{\frac{1}{2}} \left( 1 + \lambda_P \frac{p^2}{[E_i + m_i][E_j + m_j]} \right) \psi(p) \quad (4.9)$$

with

$$\lambda_P = -1$$

and

$$E_i = \sqrt{p^2 + m_i^2},$$

$$E_j = \sqrt{p^2 + m_j^2}.$$

In the non-relativistic limit  $\frac{p^2}{m^2} \ll 1.0$ , the expression (4.9) reduces to the Van-Royen-Weisskopf formula (4.1) as shown in Appendix G.

### 4.2.3 Wave functions in momentum space

The Fourier Transformation of the wave function (2.21) is

$$\psi_I(p)^{total} = \sqrt{\frac{2}{\pi p^2}} \int_0^{r^P} r \sin(pr) \psi_I(r) dr, \quad (4.10)$$

where the wave function  $\psi_I(r)$  is as defined in equations (2.21).

Similarly, the corresponding wave function in momentum space for (2.35) is

$$\psi_{II}(p)^{total} = \sqrt{\frac{2}{\pi p^2}} \int_{r^P}^{r_0} r \sin(pr) \psi_{II}(r) dr, \quad (4.11)$$

where the wave function  $\psi_{II}(r)$  is as defined in equation (2.35).

The analytical form of the wave functions (4.10) and (4.11) taking Airy function up to  $O(r^1)$  are shown in Appendix H and I respectively.

Now just as we have used a cut-off  $r^P$  in  $r$ -space as mentioned in Chapter 2, here too we introduce a cut-off parameter  $p^P$  in  $p$ -space. This is done, since in the short range ( $p < p^S$ ), linear potential is perturbatively compatible while for the long range ( $p^P < p$ ), the Coulomb potential is.

### 4.2.4 Determination of cut-off $p^P$ in the model

The Fourier Transformation of the Coulomb part of the potential  $-\frac{4\alpha_s}{3r}$  [128] is

$$\int d^3r \left( -\frac{4\alpha_s}{3r} \right) e^{ipr}$$

$$= -\frac{16\pi\alpha_s}{3p^2}. \quad (4.12)$$

On the other hand, the Fourier Transformation of the linear part  $br$  cannot be obtained directly. One introduces a parameter  $\varepsilon$  by defining a screened potential [128] and follows the limit  $\varepsilon \rightarrow 0$  as

$$bre^{-\varepsilon r}$$

$$= b \frac{\partial^2}{\partial \varepsilon^2} \frac{e^{-\varepsilon r}}{r}. \quad (4.13)$$

The Fourier Transformation of the above is

$$\begin{aligned} & b \frac{\partial^2}{\partial \varepsilon^2} \int d^3r e^{ipr} \frac{e^{-\varepsilon r}}{r} \\ &= -\frac{8\pi b}{(p^2 + \varepsilon^2)^2} + \frac{32\pi b \varepsilon^2}{(p^2 + \varepsilon^2)^3}. \end{aligned} \quad (4.14)$$

In the limit  $\varepsilon \rightarrow 0$ , equation (4.14) reduces to

$$= -\frac{8\pi b}{p^4}. \quad (4.15)$$

From perturbation conditions, we write:

for choice-I: (Coulomb potential as parent and linear potential as perturbation)

$$\left| -\frac{16\pi\alpha_s}{3p^2} \right| > \left| -\frac{8\pi b}{p^4} \right| \quad (4.16)$$

and for choice-II: (linear potential as parent and Coulomb potential as perturbation)



$$\left| -\frac{8\pi b}{p^4} \right| > \left| -\frac{16\pi\alpha_s}{3p^2} \right|. \quad (4.17)$$

Inequality (4.16) and (4.17) will correspond to a particular point of  $p$ , say  $p^P$ , where  $p^P = \sqrt{\frac{3b}{2\alpha_s}}$ , such that for  $p < p^P$  Coulomb part is dominant over the linear confinement term and for  $p > p^P$  linear part is dominant over the Coulombic term.

Now with the cut-off parameter  $p^P$ , equation (4.9) will be modified to

$$f_P = \sqrt{\frac{12}{M_P}} \int_0^{p^P} \frac{d^3 p}{(2\pi)^{\frac{3}{2}}} \left( \frac{E_q + m_q}{2E_q} \right)^{\frac{1}{2}} \left( \frac{E_{\bar{q}} + m_{\bar{q}}}{2E_{\bar{q}}} \right)^{\frac{1}{2}} \left( 1 + \lambda_P \frac{p^2}{[E_q + m_q][E_{\bar{q}} + m_{\bar{q}}]} \right) \psi_I(p) +$$

$$\sqrt{\frac{12}{M_P}} \int_{p^P}^{p_0} \frac{d^3 p}{(2\pi)^{\frac{3}{2}}} \left( \frac{E_q + m_q}{2E_q} \right)^{\frac{1}{2}} \left( \frac{E_{\bar{q}} + m_{\bar{q}}}{2E_{\bar{q}}} \right)^{\frac{1}{2}} \left( 1 + \lambda_P \frac{p^2}{[E_q + m_q][E_{\bar{q}} + m_{\bar{q}}]} \right) \psi_{II}(p) \quad (4.18)$$

where  $\psi_I(p)$  and  $\psi_{II}(p)$  are the wave functions in momentum space as defined in equations (4.10) and (4.11) respectively.

### 4.3 Calculation and results

The input parameters in the numerical calculations are  $m_u = 0.336\text{GeV}$ ,  $m_d = 0.336\text{GeV}$ ,  $m_s = 0.483\text{GeV}$ ,  $m_c = 1.55\text{GeV}$ ,  $m_b = 4.95\text{GeV}$  and  $b = 0.183\text{GeV}^2$  and  $\alpha_s$  values 0.39 and 0.22 for charmonium and bottomonium scale respectively.

#### Values of $p^P$ :

In Table 4.1, we have recorded the numerical values of the quantities to be calculated at charmonium and bottomonium scale.

Table 4.1  $p^P$  in  $GeV$  with  $c = 0$  and  $b = 0.183GeV^2$ 

$\alpha_s$ -value	$p^P$ ( $GeV$ )
0.39 (for charmonium scale)	0.838
0.22 (for bottomonium scale)	1.117

**Values of  $r_c$ :**

In Table 4.2, we compute the numerical values of small scale  $r_c$  using (4.5) for various  $B$  and  $D$  mesons.

Table 4.2 Values of cut-off  $r_c$  in  $GeV^{-1}$ 

Meson	$r_c$ ( $GeV^{-1}$ )
$D(c\bar{u}/c\bar{d})$	0.0073
$D_s(c\bar{s})$	0.0055
$B(\bar{b}u/\bar{b}d)$	$1.452 \times 10^{-9}$
$B_s(\bar{b}s)$	$1.038 \times 10^{-9}$
$B_c(\bar{b}c)$	$3.872 \times 10^{-10}$

**Decay constants in coordinate space:**

We calculate the decay constants of various  $D$  and  $B$  mesons using equations (4.1) and (4.2) as shown in Table 4.3 with the regularized wave functions (4.6) and (4.7).

Table 4.3 Decay constants of  $D$  and  $B$  mesons using Van-Royen-Weisskopf formula with regularized wave functions (4.6) and (4.7) and comparison with experimental data and other theoretical models. All values are in the unit of  $GeV$ .

Meson	(this work) $f_P$	(this work) $f_{P_c}$	Experimental value & Other work
$D(c\bar{u}/c\bar{d})$	0.293	0.274	$0.205 \pm 0.085 \pm 0.025$ [129, 130] (Exp.)
$D_s(c\bar{s})$	0.368	0.335	$0.254 \pm 0.059$ [129, 130] (Exp.)
$B(\bar{b}u/\bar{b}d)$	0.206	0.203	$0.207 \pm 0.014$ [73] 0.189 [131]
$B_s(\bar{b}s)$	0.239	0.236	$0.237 \pm 0.017$ [73] 0.218 [131]
$B_c(\bar{b}c)$	0.410	0.389	0.433 (Rel), 0.562 (NR) [132] 0.470 [87]

### Decay constants in momentum space:

The formula given by Godfrey as defined in equation (4.9) is sufficient to incorporate relativistic effect for decay constant. Therefore, to obtain the results we have considered  $\varepsilon = 0$  in the wave functions (4.10) and (4.11). With cut-offs  $p^P$  and  $p_0$ , the results in the momentum space are as recorded in Table 4.4.

Table 4.4 Decay constants of  $D$  and  $B$  mesons with cut-off  $p^P$  and comparison with experimental data and other theoretical models. All values are in the unit of  $GeV$ .

Meson	(this work) $f_P$	Experimental value & Other work
$D(c\bar{u}/c\bar{d})$	0.107	$0.205 \pm 0.085 \pm 0.025$ [129, 130] (Exp.)
$D_s(c\bar{s})$	0.147	$0.254 \pm 0.059$ [129, 130] (Exp.)
$B(\bar{b}u/\bar{b}d)$	0.068	$0.198 \pm 0.014$ [73] 0.189 [131]
$B_s(\bar{b}s)$	0.076	$0.237 \pm 0.017$ [73] 0.218 [131]
$B_c(\bar{b}c)$	0.101	0.433(Rel), 0.562 (NR)[132] 0.470 [87]

The maximum value of  $p_0$  in equation (4.18) in obtaining the results of Table 4.4 can be considered  $\sim 1.2GeV$  demanding the positivity of the decay constant.

Table 4.3 and 4.4 show that the decay constant of mesons in coordinate space using equation (4.2) agree well with the data than for the decay constants in the momentum space using equation (4.18). In momentum space, the results are found to be smaller than those of experimental data and theoretical values.

Fig. 4.1 and 4.2 show the graphical variation of wave functions  $\psi_I(r)$  (equation (2.21)) and  $\psi_{II}(r)$  (equation (2.35)) with  $r$  respectively.

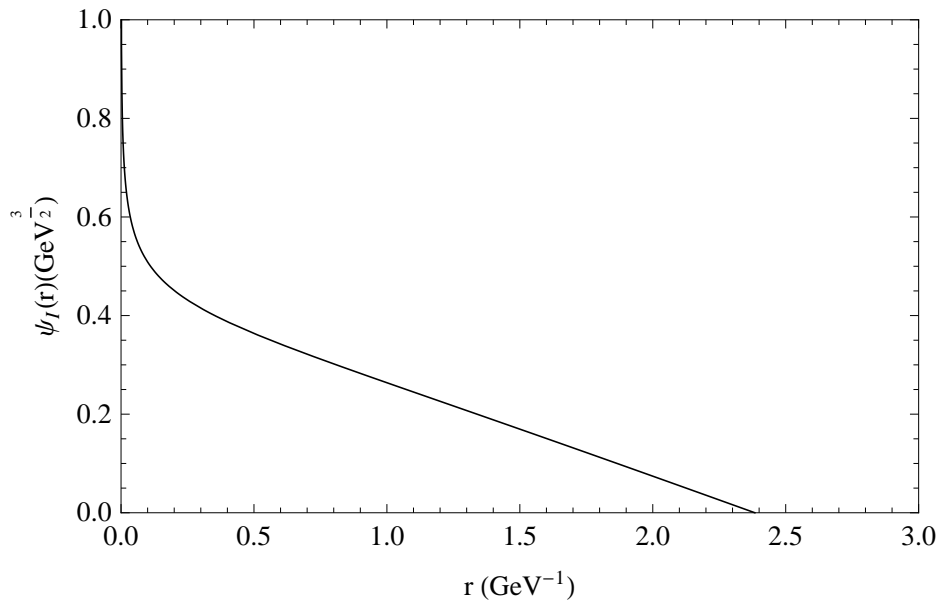


Fig. 4.1 The radial wave function  $\psi_I(r)$  for  $D(c\bar{u}/c\bar{d})$  meson.

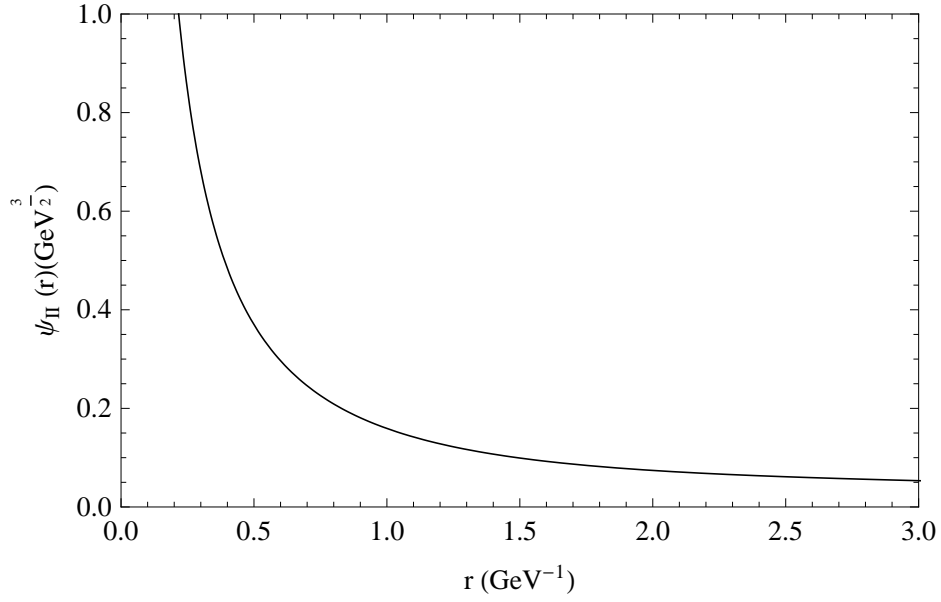


Fig. 4.2 The radial wave function  $\psi_{II}(r)$  for  $D(c\bar{u}/c\bar{d})$  meson.

The variation of probability density  $|r\psi_I(r)|^2$  and  $|r\psi_{II}(r)|^2$  with  $r$  for  $D(c\bar{u}/c\bar{d})$  meson are shown in fig. 4.3 and 4.4 respectively.

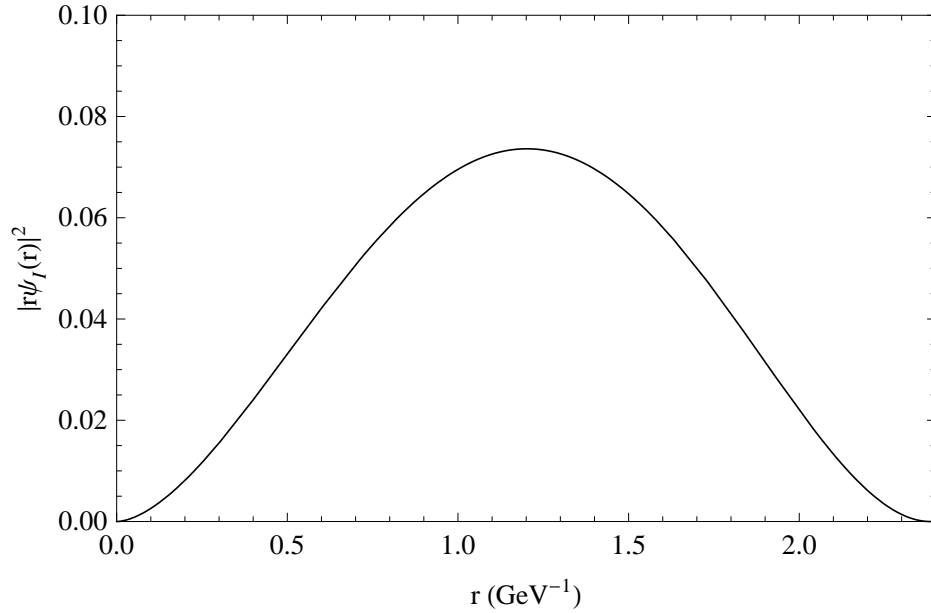


Fig. 4.3 The radial probability density  $|r\psi_I(r)|^2$  for  $D(c\bar{u}/c\bar{d})$  meson.

Fig. 4.5 and 4.6 show the graphical variation of wave functions  $\psi_I(r)$  (equation (2.21)) and  $\psi_{II}(r)$  (equation (2.35)) with  $r$  for  $B(u\bar{b})$  meson respectively.

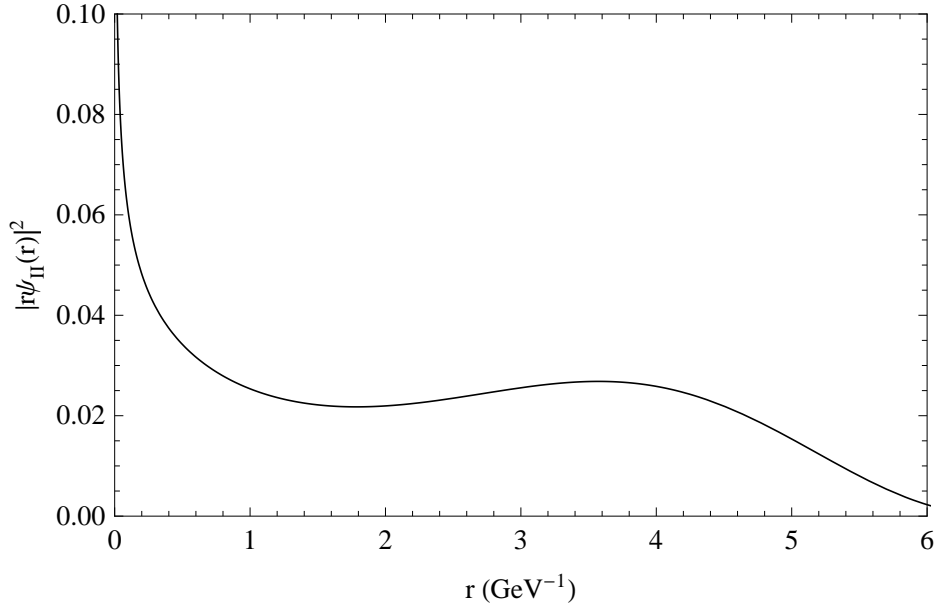


Fig. 4.4 The radial probability density  $|r\psi_{II}(r)|^2$  for  $D(c\bar{u}/c\bar{d})$  meson.

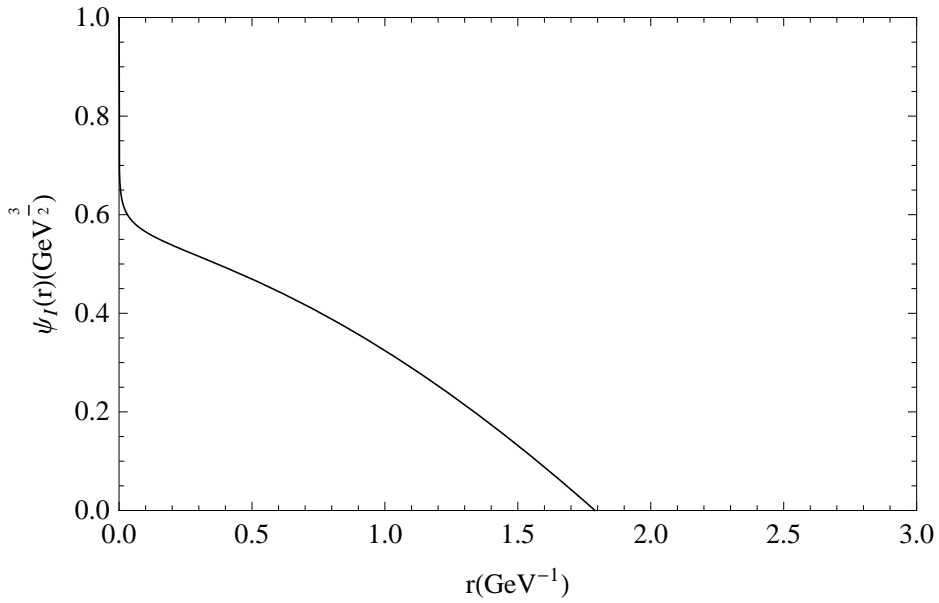


Fig. 4.5 The radial wave function  $\psi_I(r)$  for  $B(u\bar{b})$  meson.

The variation of probability density  $|r\psi_I(r)|^2$  and  $|r\psi_{II}(r)|^2$  with  $r$  for  $B(u\bar{b})$  meson are shown in fig. 4.7 and 4.8 respectively.

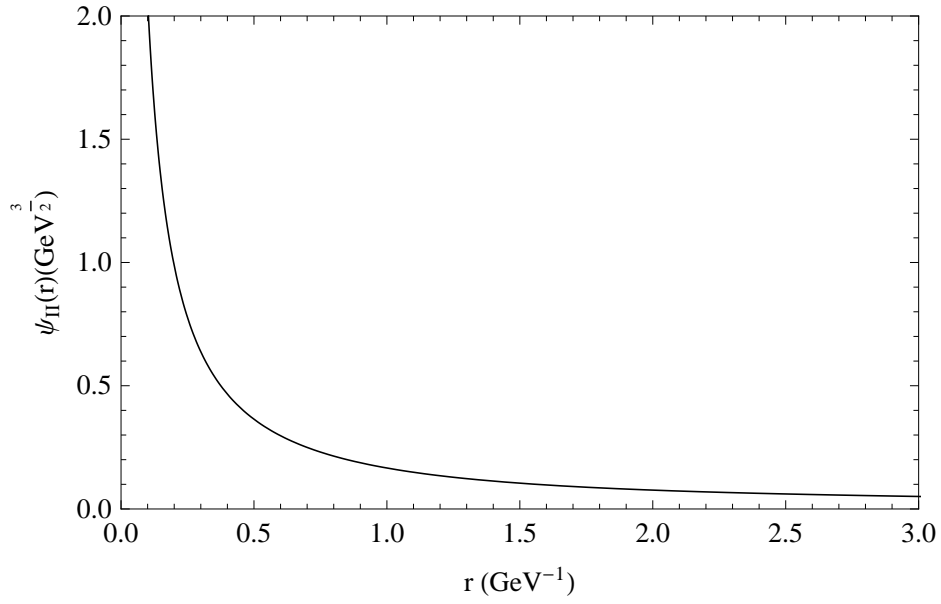


Fig. 4.6 The radial wave function  $\psi_{II}(r)$  for  $B(u\bar{b})$  meson.

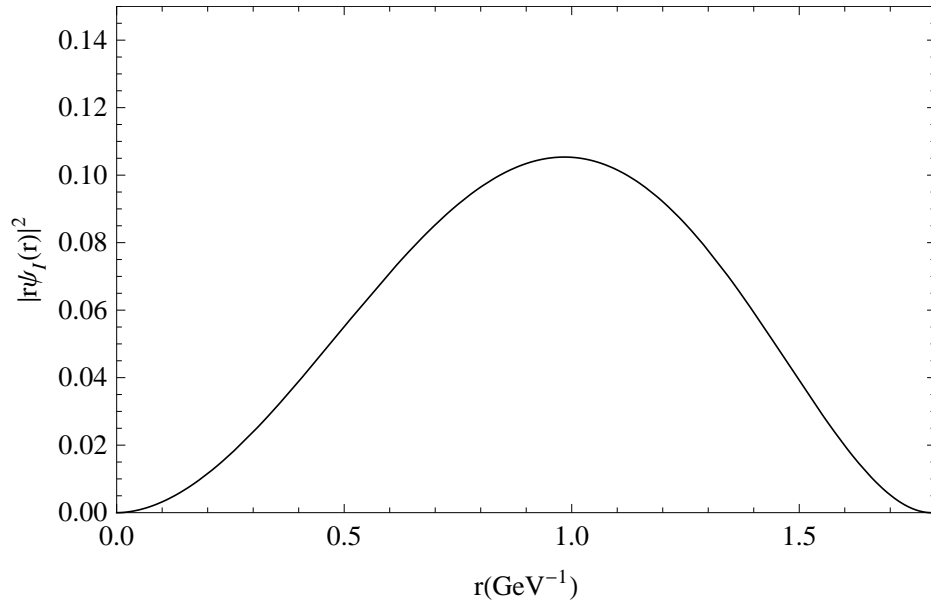


Fig. 4.7 The radial probability density  $|r\psi_I(r)|^2$  for  $B(u\bar{b})$  meson.

The graphical representation of the wave functions as well as the radial probability density with  $r$  show similar variation as that of hydrogen atom [133] except that the scaling factors- ‘ $m$ ’ the reduced mass of hydrogen atom, ‘ $a$ ’ the atomic Bohr’s radius, ‘ $\alpha$ ’ the fine structure constant is replaced by ‘ $\mu$ ’ the reduced mass of the meson, ‘ $a_0$ ’ the QCD analog of Bohr’s

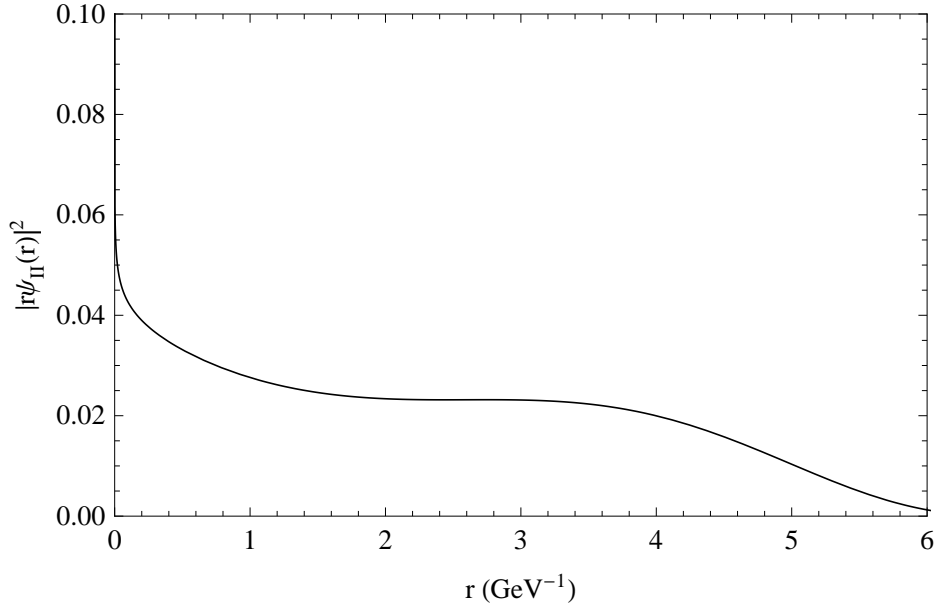


Fig. 4.8 The radial probability density  $|r\psi_{II}(r)|^2$  for  $B(u\bar{b})$  meson.

radius and ' $\alpha_s$ ' the strong coupling constant respectively.

Respectively in Fig. 4.9 and 4.10, we show the graphical variation of wave functions  $\psi_I(p)$  (equation(4.10)) and  $\psi_{II}(p)$  (equation (4.11)) in momentum space with  $p$  for  $D(c\bar{u}/c\bar{d})$ .

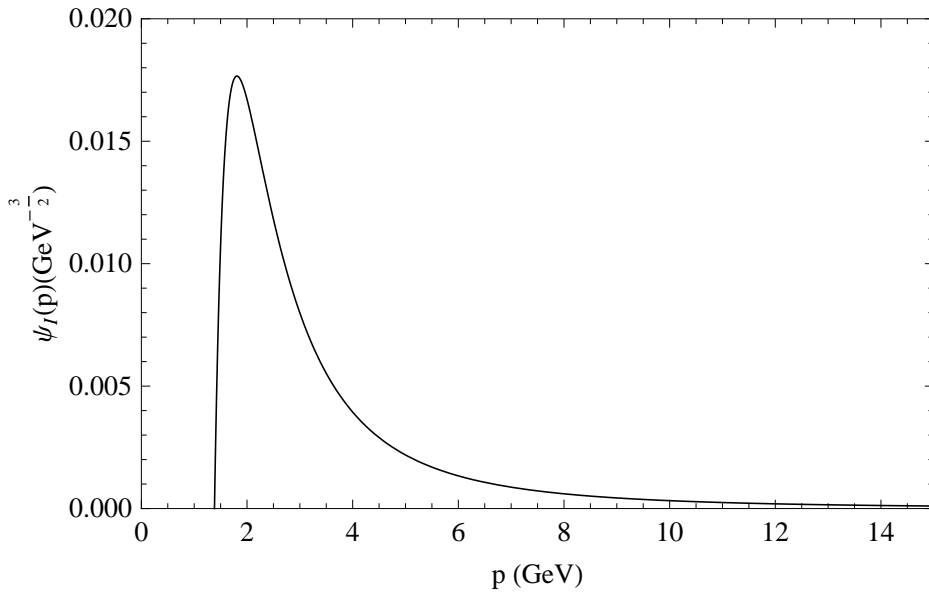


Fig. 4.9 Wave function  $\psi_I(p)$  for  $D(c\bar{u}/c\bar{d})$  meson.



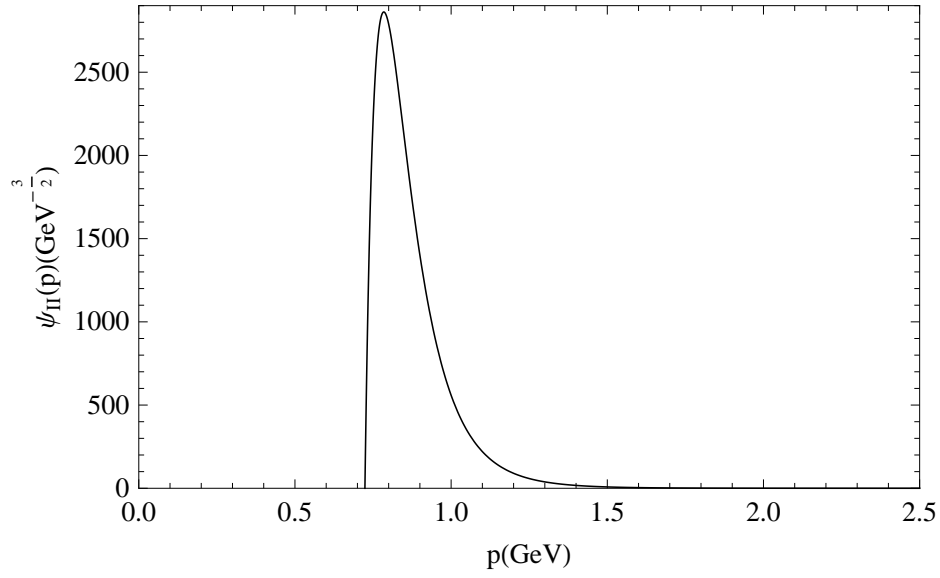


Fig. 4.10 Wave function  $\psi_{II}(p)$  for  $D(c\bar{u}/c\bar{d})$  meson.

Similarly, in Fig. 4.11 and 4.12 we show the graphical variation of wave functions  $\psi_I(p)$  (equation(4.10)) and  $\psi_{II}(p)$  (equation (4.11)) with  $p$  for  $B(u\bar{b})$  mesons in momentum space respectively.

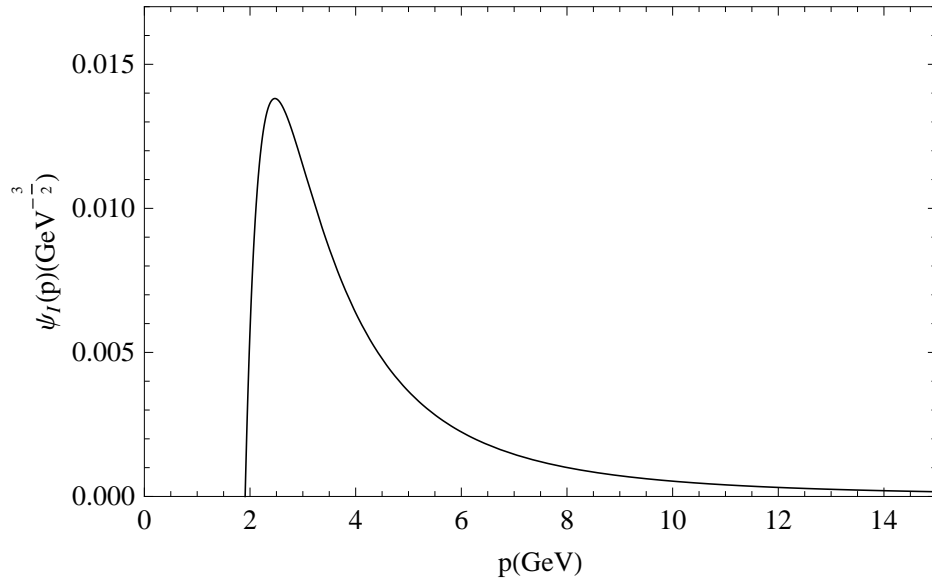


Fig. 4.11 Wave function  $\psi_I(p)$  for  $B(u\bar{b})$  meson.

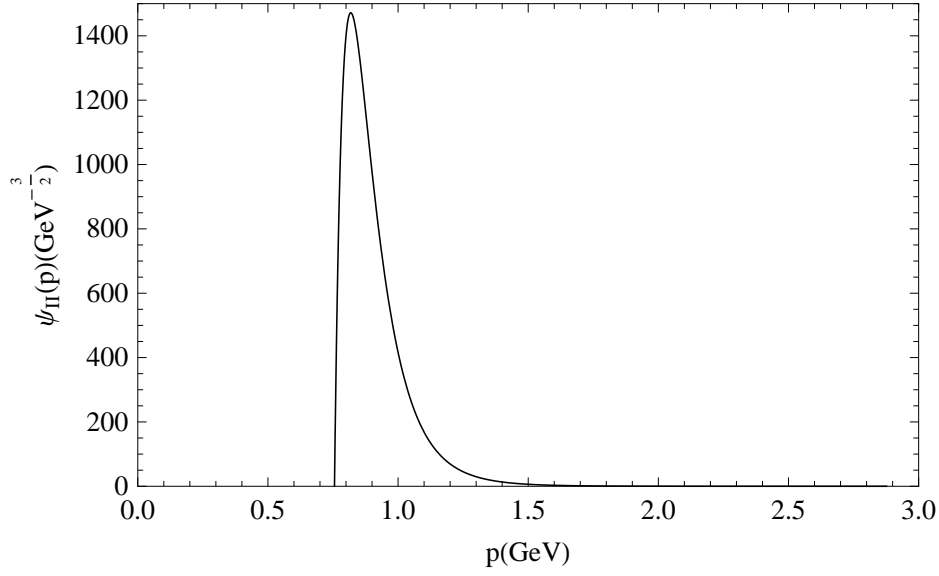


Fig. 4.12 Wave function  $\psi_{II}(p)$  for  $B(u\bar{b})$  meson.

The qualitative features of the heavy flavored meson wave functions (Fig. 4.9 to 4.12) are similar to those of the model of ref. [73]. One can also study the corresponding probability density in momentum space.

## 4.4 Conclusion

In this chapter, the results for decay constants of mesons found using equations (4.1) and (4.2) are well consistent with those of experimental data and other theoretical models. Whereas the decay constants of mesons obtained using (4.18) are lower than that of using Van-Royen-Weisskopf formula, also the values are smaller compared to experimental values and other theoretical models. Then the addition of the Dirac modification factor to the wave function will further reduces the results. However, it is seen that the equation (4.9) takes into account the relativistic effect up to any order of  $(\frac{v}{c})$  or  $(\frac{p}{m})$  and additional effects are unwarranted. Thus at phenomenological level it is observed that the equation (4.9) is not appropriate in the present model to compare with the data. This is done to test the predictive power of the

model in momentum space ( $p$ -space).

Decay constants of heavy-light mesons (e.g.  $D$ ,  $D_s$  mesons) are still not measured with high accuracy compared to light mesons (e.g.  $\pi$ ,  $K$  mesons). However, the discrepancies are reduced to a certain extent by updates from experiments [130, 134–138]. Reliable experimental data for decay constants of  $D$  and  $D_s$  mesons have been obtained for measurements done in CLEO [130, 134, 135], Belle [136], BABAR [137], BES III [138] collaborations, etc. Again, the decay constant  $f_{B_s}$  for  $B_s$  meson cannot be measured experimentally due to its charge neutrality. Hence it has to be determined from theory. For experimentalists, it has now become a great challenge to extract the value of decay constant  $f_B$  of  $B$  meson.

# 5

## Constituent gluons in scalar glueballs: a group theoretical analysis

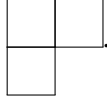
### 5.1 Introduction

A glueball is a theoretical compound particle. It is composed entirely of gluons, without valence quarks. Gluons carry color charge and experience the strong interactions. Therefore glueballs are viable in QCD. Such states have not been an easy subject to study due to the lack of phenomenological support and therefore much controversy has been associated with

their properties. Also glueballs are tough to identify in particle accelerators because they mix with normal meson states. Glueball is mainly produced in radiative  $J/\psi$  decay and  $p - \bar{p}$  annihilation processes as mentioned in Chapter 1. Theoretical calculations based on non-perturbative methods like lattice QCD and QCD sum rules concur that the lightest glueball should be a scalar resonance ( $J^{pc} = 0^{++}$ ) with a mass range  $1600 \pm 150 \text{ MeV}$  followed by a tensor ( $2^{++}$ ) and a pseudoscalar ( $0^{-+}$ ) glueball in the 2000-2500  $\text{MeV}$  mass region [139, 140]. But unfortunately, no definite answer to the question whether a glueball has been observed or not can be given yet. It is to be mentioned that although gluons are color octets, glueballs are color singlets. So a single gluon cannot be a glueball, but a gluelump [141]. The forthcoming experiment FAIR with PANDA as detector [142] is specifically designed to detect glueballs and hybrid mesons in charmonium spectroscopy. Theoretical calculations predict that glueballs should occur at energy ranges available with current collider technology. But due to the difficulties as mentioned, they have so far not been observed and established with certainty. But still, it is a worthwhile theoretical pursuit.

In this chapter, we report the results for scalar glueballs using Young Tableau which is used to determine the number of constituent gluons in low-lying scalar glueballs. In Mathematics [144], a Young tableau is a helpful combination tool in representation theory. In 1900, Alfred Young, a mathematician at Cambridge University, introduced Young tableau [143]. By taking the direct product of irreducible representations, the representations of higher dimensions are obtained. These representations are however reducible. Young tableau gives an explicit way of reducing it to the direct sum of various irreducible representations [144, 145]. In quark model, the three quarks: up( $u$ ), down( $d$ ) and strange ( $s$ ) belong to the fundamental representation 3, corresponding to the Young Tableau representation  $\square$  of flavor  $SU(3)$  and the corresponding antiquarks ( $\bar{u}, \bar{d}, \bar{s}$ ) belong to the conjugate representation

$\bar{3}$ , the corresponding Young Tableau configuration being .

Similarly, the gluons are color octets and their fundamental representation in  $SU(3)_c$  is 8 and the corresponding Young Tableau configuration is .

The group theoretical tool can only be used for low-lying scalar  $C = +1$  glueballs, since only for the scalar glueball  $l = 0$  and  $s = 0$ ;  $J = 0$ . Similarly, in case of scalar glueball there will not be any additional angular momentum multiplicity.

## 5.2 Formalism

Here we outline the method how group theoretical tool of Young Tableau of  $SU(3)_c$  can be used to find the maximum number of constituent gluons in an experimentally observed scalar glueball.

We show the product result for  $(8_c \times 8_c)$  in  $SU(3)_c$ :

For that we put  $a$ 's in the  $1^{st}$  row and  $b$ 's in the  $2^{nd}$  row as

$$\begin{array}{|c|c|} \hline & \\ \hline & \\ \hline \end{array} \otimes \begin{array}{|c|c|} \hline a & a \\ \hline b & \\ \hline \end{array} = \left( \begin{array}{|c|c|c|} \hline & & a \\ \hline & & \\ \hline \end{array} \oplus \begin{array}{|c|c|} \hline & \\ \hline & a \\ \hline \end{array} \oplus \begin{array}{|c|c|} \hline & \\ \hline & \\ \hline a \\ \hline \end{array} \right) \oplus \begin{array}{|c|} \hline a \\ \hline b \\ \hline \end{array} \quad (5.1)$$

$$\begin{aligned}
= & \left( \begin{array}{|c|c|c|c|} \hline & & a & a \\ \hline & & & \\ \hline \end{array} \oplus \begin{array}{|c|c|c|} \hline & & a \\ \hline & & a \\ \hline \end{array} \oplus \begin{array}{|c|c|c|} \hline & & a \\ \hline & & \\ \hline & & a \\ \hline \end{array} \right. \\
& \left. \oplus \begin{array}{|c|c|c|} \hline & & a \\ \hline & & a \\ \hline & & \\ \hline & & a \\ \hline \end{array} \oplus \begin{array}{|c|c|c|} \hline & & \\ \hline & & a \\ \hline & & \\ \hline & & a \\ \hline \end{array} \oplus \begin{array}{|c|c|c|} \hline & & a \\ \hline & & \\ \hline & & \\ \hline & & a \\ \hline \end{array} \right) \otimes \begin{array}{|c|} \hline b \\ \hline \end{array}
\end{aligned}
\tag{5.2}$$

From (5.2), we can get rid of the last one containing two  $a$ 's in the same column, and there are also four rows which are forbidden for  $SU(3)$  [146, 147]. At this stage, we also combine any non-distinct diagrams of (5.2) yielding,

$$= \left( \begin{array}{|c|c|c|c|} \hline & & a & a \\ \hline & & & \\ \hline \end{array} \oplus \begin{array}{|c|c|c|} \hline & & a \\ \hline & & a \\ \hline \end{array} \oplus \begin{array}{|c|c|c|} \hline & & a \\ \hline & & \\ \hline & & a \\ \hline \end{array} \oplus \begin{array}{|c|c|c|} \hline & & \\ \hline & & a \\ \hline & & \\ \hline & & a \\ \hline \end{array} \right) \otimes \begin{array}{|c|} \hline b \\ \hline \end{array}
\tag{5.3}$$

$$\begin{aligned}
= & \begin{array}{|c|c|c|c|c|} \hline & & a & a & b \\ \hline & & & & \\ \hline \end{array} \oplus \begin{array}{|c|c|c|c|} \hline & & a & a \\ \hline & & b & \\ \hline \end{array} \oplus \begin{array}{|c|c|c|c|} \hline & & a & a \\ \hline & & & \\ \hline & & & b \\ \hline \end{array} \\
& \oplus \begin{array}{|c|c|c|c|} \hline & & a & b \\ \hline & & a & \\ \hline \end{array} \oplus \begin{array}{|c|c|c|c|} \hline & & a & \\ \hline & & a & b \\ \hline \end{array} \oplus \begin{array}{|c|c|c|c|} \hline & & a & \\ \hline & & a & \\ \hline & & & b \\ \hline \end{array} \\
& \oplus \begin{array}{|c|c|c|c|} \hline & & a & b \\ \hline & & & \\ \hline & & & a \\ \hline \end{array} \oplus \begin{array}{|c|c|c|c|} \hline & & a & \\ \hline & & b & \\ \hline & & a & \\ \hline \end{array} \oplus \begin{array}{|c|c|c|c|} \hline & & a & \\ \hline & & & \\ \hline & & a & \\ \hline & & & b \\ \hline \end{array} \\
& \oplus \begin{array}{|c|c|c|c|} \hline & & & b \\ \hline & & a & \\ \hline & & a & \\ \hline \end{array} \oplus \begin{array}{|c|c|c|c|} \hline & & & \\ \hline & & a & \\ \hline & & a & b \\ \hline \end{array} \oplus \begin{array}{|c|c|c|c|} \hline & & & \\ \hline & & a & \\ \hline & & a & b \\ \hline \end{array}.
\end{aligned} \tag{5.4}$$

Now dropping the Young Tableaux diagram which have 4 rows,

$$\begin{aligned}
\begin{array}{|c|c|} \hline & \\ \hline & \\ \hline \end{array} \otimes \begin{array}{|c|c|} \hline a & a \\ \hline b & \\ \hline \end{array} = & \begin{array}{|c|c|c|c|c|} \hline & & a & a & b \\ \hline & & & & \\ \hline \end{array} \oplus \begin{array}{|c|c|c|c|} \hline & & a & a \\ \hline & & b & \\ \hline \end{array} \oplus \begin{array}{|c|c|c|c|} \hline & & a & a \\ \hline & & & \\ \hline & & & b \\ \hline \end{array} \\
& \oplus \begin{array}{|c|c|c|c|} \hline & & a & b \\ \hline & & a & \\ \hline \end{array} \oplus \begin{array}{|c|c|c|c|} \hline & & a & \\ \hline & & a & b \\ \hline \end{array} \oplus \begin{array}{|c|c|c|c|} \hline & & a & \\ \hline & & a & \\ \hline & & & b \\ \hline \end{array} \\
& \oplus \begin{array}{|c|c|c|c|} \hline & & a & b \\ \hline & & & \\ \hline & & & a \\ \hline \end{array} \oplus \begin{array}{|c|c|c|c|} \hline & & a & \\ \hline & & b & \\ \hline & & a & \\ \hline \end{array} \oplus \begin{array}{|c|c|c|c|} \hline & & a & b \\ \hline & & a & \\ \hline & & a & \\ \hline \end{array} \oplus \begin{array}{|c|c|c|c|} \hline & & a & \\ \hline & & a & b \\ \hline \end{array}.
\end{aligned} \tag{5.5}$$



We now use the restriction of admissible (appropriate) sequences [146] to avoid double counting. The restriction to read these boxes is from right to left, top to bottom. The sequences of equation (5.5) would correspond to

$$\begin{array}{|c|c|} \hline & \\ \hline & \\ \hline \end{array} \otimes \begin{array}{|c|c|} \hline a & a \\ \hline b & \\ \hline \end{array} = baa \oplus aab \oplus aab \oplus baa \oplus aba \oplus aab \oplus baa \oplus aba \oplus baa \oplus aba. \quad (5.6)$$

Dropping *baa* which is an inadmissible sequence,

$$\begin{array}{|c|c|} \hline & \\ \hline & \\ \hline \end{array} \otimes \begin{array}{|c|c|} \hline a & a \\ \hline b & \\ \hline \end{array} = \begin{array}{|c|c|c|} \hline & a & a \\ \hline & b & \\ \hline \end{array} \oplus \begin{array}{|c|c|c|c|} \hline & & a & a \\ \hline & & & \\ \hline & & b & \\ \hline \end{array} \oplus \begin{array}{|c|c|c|} \hline & & a \\ \hline & a & b \\ \hline \end{array} \\ \oplus \begin{array}{|c|c|c|} \hline & & a \\ \hline & a & \\ \hline b & & \\ \hline \end{array} \oplus \begin{array}{|c|c|c|} \hline & & a \\ \hline & b & \\ \hline a & & \\ \hline \end{array} \oplus \begin{array}{|c|c|c|} \hline & & a \\ \hline & a & b \\ \hline \end{array} \quad (5.7) \\ = \underline{27} + \underline{10} + \underline{\bar{10}} + \underline{8} + \underline{8} + \underline{1} \\ = \underline{1} + 2(\underline{8}) + \underline{10} + \underline{\bar{10}} + \underline{27}$$

(5.7) shows the result for glueball consisting of two gluons. Thus two color-octet gluons can form a color singlet glueball. It means that if only one glueball is observed, the glueball must be composed of two gluons. Similarly, from the bound state of three or more gluons the corresponding representations can be found out.

## 5.3 Results

In Table 5.1 we show the possible number of color singlet glueballs corresponding to the maximum number of constituent gluons. The results are obtained for glueballs up to 7

constituent gluons. The only condition is that each of the glueballs are color singlets. We have denoted  $n$  multiplicity of  $\underline{m}$  dimensional irreducible representation of  $SU(3)_c$  as  $n(\underline{m})$ , ie for example  $3(\underline{10}) = \underline{10} + \underline{10} + \underline{10}$  and so on.

Table 5.1 Number of color singlets corresponding to the maximum number of constituent gluons.

Direct product	Direct sum	Number of color singlet glueballs
$8_c \times 8_c$	$\underline{1} + \underline{8} + \underline{8} + \underline{10} + \underline{10} + \underline{27}$	1
$8_c \times 8_c \times 8_c$	$2(\underline{1}) + 8(\underline{8}) + 4(\underline{10}) + 4(\underline{10}) + 6(\underline{27}) + 4(\underline{35}) + \underline{64}$	2
$8_c \times 8_c \times 8_c \times 8_c$	$8(\underline{1}) + 32(\underline{8}) + 22(\underline{10}) + 18(\underline{10}) + 33(\underline{27}) + 4(\underline{28}) + 30(\underline{35}) + 12(\underline{64}) + 6(\underline{81}) + \underline{125}$	8
$8_c \times 8_c \times 8_c \times 8_c \times 8_c$	$32(\underline{1}) + 145(\underline{8}) + 117(\underline{10}) + 83(\underline{10}) + 180(\underline{27}) + 40(\underline{28}) + 200(\underline{35}) + 94(\underline{64}) + 10(\underline{80}) + 72(\underline{81}) + 20(\underline{125}) + 8(\underline{154}) + \underline{216}$	32
$8_c \times 8_c \times 8_c \times 8_c \times 8_c \times 8_c$	$145(\underline{1}) + 702(\underline{8}) + 642(\underline{10}) + 408(\underline{10}) + 999(\underline{27}) + 322(\underline{28}) + 1260(\underline{35}) + 10(\underline{55}) + 660(\underline{64}) + 140(\underline{80}) + 630(\underline{81}) + 215(\underline{125}) + 140(\underline{154}) + 18(\underline{162}) + 30(\underline{216}) + 10(\underline{260}) + \underline{343}$	145
$8_c \times 8_c \times 8_c \times 8_c \times 8_c \times 8_c \times 8_c$	$702(\underline{1}) + 3598(\underline{8}) + 3603(\underline{10}) + 2109(\underline{10}) + 5670(\underline{27}) + 7840(\underline{35}) + 2352(\underline{28}) + 168(\underline{55}) + 4424(\underline{64}) + 1400(\underline{80}) + 4872(\underline{81}) + 1890(\underline{125}) + 1568(\underline{154}) + 336(\underline{162}) + 426(\underline{216}) + 239(\underline{260}) + 41(\underline{343}) + 28(\underline{280}) + 12(\underline{405}) + \underline{512} + \underline{273} + \underline{330}$	702

In Table 5.2, we show the correspondence between the observed number of glueballs and the possible number of constituent gluons in them. For example, if the number of detected glueballs is 31, the possible number of constituent gluons will be 2, 3, 4 (Table 5.2).

Table 5.2 Possible number of constituent gluons corresponding to the number of scalar glueballs observed.

Number of scalar glueballs observed	Possible number of constituent gluons
1	2
2-7	2,3
8-31	2,3,4
32-144	2,3,4,5
145-701	2,3,4,5,6
702	2,3,4,5,6,7

The above analysis demonstrates that the Young Tableau calculation gives the possibility to infer the maximum number of constituent gluons from any number of observed glueballs. Here we have confined the results for glueballs up to multiplicity of 702.

However, the predictions discussed above do not give any information about the relationship between the number of constituent gluons and the masses of the observed glueballs, since, in exact  $SU(3)_C$  symmetry, gluons are massless and the present work doesn't incorporate any dynamics.

## 5.4 Conclusion

In this chapter, we have shown how one can use Young Tableau to infer the number of constituent gluons from the multiplicity of low-lying glueballs. In lattice QCD calculation, low-lying  $C=+1$  glueballs are identified with two gluon states [43](or at least with hadrons in

which two gluon components are widely dominant). The group theoretical approach cannot make the distinction among the glueballs of different number of constituent gluons. The only constraint is that the glueballs must have total orbital momentum and total spins of the constituent gluons be separately 0 so that angular momentum does not have any role in its spectroscopy. The proposed simple constituent gluon counting rule will hopefully be useful for the glueballs to be searched in near future.

# 6

## Summary, limitation and future outlook

The work of the thesis is devoted to theoretical and phenomenological studies of heavy flavored pseudoscalar mesons in a QCD inspired quark model. In the model, the analytic expression for the non-relativistic Schrödinger wave functions for the Coulomb-plus-linear potential,  $V(r) = -\frac{4\alpha_s}{3r} + br$ , called Cornell potential are obtained. The first-order wave functions are obtained using Dalgarno's method of perturbation. Relativistic effects are then incorporated into the wave functions by using standard Dirac modification factor in a parameter-free way [82, 83]. The model is then used to calculate the masses, form factors, charge radii, RMS radii, decay constants of heavy flavored mesons, besides Isgur-Wise function and its derivatives, the convexity parameter and charge radius of heavy-light mesons are

studied. The results are compared with available experimental data and with the predictions of other models and also with the earlier work.

Certain improvement to the model has been incorporated in the present work compared to previous studies [63–66, 69–71, 78, 117–119]. First is based on the Quantum Mechanics principle that a scale factor ‘ $c$ ’ in the potential should not affect the wave function of the system even while applying the perturbation theory, the term ‘ $c$ ’ is considered to be zero in the Cornell potential. Another is depending on the perturbative piece of the Hamiltonian (confinement or linear) the effective radial separation between the quark and antiquark ‘ $r$ ’ is divided at the point  $r^P$ .

These modifications provide a satisfactory explanation of the quantities we obtain in our model.

In **Chapter 2**, we obtain the analytical form of the wave functions for the Cornell potential, considering both Coulomb potential as the parent and linear as the perturbation, and linear potential as parent and Coulomb as the perturbation. The strong coupling constant  $\alpha_s$ , we use the standard values of  $\bar{M}S$  scheme-  $\alpha_{\bar{M}S}(m_c) = 0.39$  and  $\alpha_{\bar{M}S}(m_b) = 0.22$  [94] at the charmonium and bottomonium mass scales respectively. The values of cut-off parameter  $r^P$  are calculated for both the mass scales. The additional cut-off  $r_0$  is used in the model basically due to the polynomial approximation of the series expansion used in the Dalgarno’s method of perturbation. The cut-off  $r_0$  is independent of the property of the Airy function.

The acquired wave functions are then used to calculate the masses, charge radii and RMS radii of various  $D$  and  $B$  mesons. The results for masses derived here are found to be in good agreement with the experimental data, especially for  $B$  mesons (Table 2.2). The results

for charge radii of mesons clearly shows an improvement over the earlier analysis of ref. [69] and [78] for  $B$  mesons. However, the RMS radii calculated in Chapter 1 for  $c\bar{c}$  and  $b\bar{b}$  are higher than those of other theoretical models compared (Table 2.6) .

In **Chapter 3**, we have reported the results of Isgur-Wise function calculating its slopes and curvatures. The Isgur-Wise function of the heavy-light mesons is studied in the infinite heavy quark mass limit and also for the finite mass corrections. From the study, it is seen that for the mesons where light quark/antiquark is not so light compared to the heavy quark/antiquark, the finite mass limit does show a very strong dependence on the spectator quark mass.

In **Chapter 4**, we study the leptonic decay constants of various  $D$  and  $B$  mesons. The decay constants of the mesons are calculated in coordinate space using Van-Royen-Weisskopf formula (4.1) and (4.2) with the regularized wave functions (4.6) and (4.7) at the origin using a short distance cut-off ( $r_c$ ) as defined in equation (4.5).

Our calculated results (Table 4.3) were found to be in agreement with the experimental data and other model values compared. In the chapter, we have also used a different formula (4.9) as given by Godfrey [127] to study decay constants of the mesons in momentum space. To use that formula we obtain the wave functions at the momentum space (4.10) and (4.11) by doing Fourier Transformation of wave functions (2.21) and (2.35) respectively. The Fourier Transformation of the cut-off  $r^P$  is also obtained as  $p^P$  in momentum space. Since the formula (4.9) is sufficient to incorporate relativistic effect for decay constant, therefore, to achieve the results we have considered  $\varepsilon = 0$  in the wave functions (4.10) and (4.11). The results obtained using (4.18) are found smaller than those of experimental data and other theoretical values (Table 4.4). The addition of the Dirac modification factor to the

wave function will further reduce the results. Moreover, it is to be noted that this relativistic formula (equation 4.9) in our semi-relativistic approach doesn't help to compare with the data available.

To summarize, we have outlined in chapters 2, 3 and 4 of the thesis an improved QCD quark model and reported several quantities of phenomenological importance in the meson sector.

Let us now discuss the limitation of this work presented in chapters 2, 3 and 4, which arise mainly because of the approximations we have used. In the model we have considered the cut-offs  $r^P$  and  $p^P$  in coordinate and momentum space respectively. Another important point of the analysis is the introduction of the additional cut-off  $r_0$  (or  $p_0$ ) used in the wave function (2.35). It is employed in the integration basically due to the polynomial approximation of the series expansion used in the Dalgarno's method of perturbation. It may be taken as the demerit of the perturbation technique we are using. A possible way to do calculations without these assumptions will be a part of the further study.

Further in this work, the full relativity could not be considered for heavy-light meson systems. Though the relativistic effect is introduced through the Dirac modification factor in this work, there should also have some other significant dynamical effects that have been studied in various relativistic treatments of the problem [113]. So this can be considered as one of the limitations of the present version of the work. Further study needed to take into account such limitation.

Besides the studies of heavy flavored mesons, in **Chapter 5**, we have studied the group theoretical tool of Young Tableau to find the possible number of constituents gluons in an



observed scalar glueball. The present work is based on the pure  $SU(3)_c$  symmetry of Young Tableau. The limitation of the work is that it could only predict the number of possible constituent gluons in a particular glueball multiplicity, not beyond it. The proper gluon dynamics is to be incorporated to obtain the masses of such multi-gluon systems. This aspect needs further study.

# References

- [1] K. G. Wilson, Phys. Rev. D **10**, 2445 (1974).
- [2] C. Patrignani et al. (Particle Data Group), Chin. Phys. C **40**, 100001 (2016).
- [3] G. P. Lepage and S. J. Brodsky, Phys. Rev. D **22**, 2157 (1980).
- [4] M. Neubert, Phys. Reports **245**, 259 (1994).
- [5] E. Jenkins, Nucl. Phys. B **412**, 181 (1994).
- [6] E. V. Shuryak, Nucl. Phys. B **198**, 83 (1982).
- [7] M. A. Shifman, A. I. Vainshtein and V. I. Zakharov, Nucl. Phys. B **147**, 385 (1979).
- [8] A. Manohar, H. Georgi, Nucl. Phys. B **234**, 189 (1984).
- [9] K. D. Born, et al., Phys. Rev. D **40**, 1653 (1989).
- [10] I. J. R. Aitchison and J. J. Dudek, Eur. Journ. of Phys. **23**, 605 (2002).
- [11] J. L. Richardson, Phys. Lett. B **82**, 272 (1979).
- [12] X. Song, Journ. Phys. G **17**, 49 (1991).
- [13] E. Eichten et al., Phys. Rev. D **21**, 313 (1980).
- [14] E. Eichten et al., Phys. Rev. Lett. **34**, 1276 (1976).
- [15] S. C. Chhajlany and D. A. Letov, Phys. Rev. A **44**, 4725 (1991).
- [16] A. K. Ghatak and S. Lokanathan, *Quantum Mechanics* (McGraw Hill, 2004).
- [17] F. M. Fernández, *Introduction to Perturbation Theory In Quantum Mechanics* (CRC Press, 2000).
- [18] A. Dalgarno, *Stationary Perturbation Theory in Quantum theory, I.Elements* (Academic, 1961).
- [19] J. L. Rosner, S. Stone, R. S. V. Water, arXiv: 1509.02220v2 [hep-ph] (2016).
- [20] P. Renton, *Interactions* (Cambridge University Press, 1990).
- [21] A. Pais, *Inward Bound* (Oxford University Press, 1986).
- [22] F. J. Gilman and R. L. Singleton, Phys. Rev. D **41**, 142 (1990).

- [23] K. Hagiwara, A. D. Martin and M. F. Wade, Nucl. Phys. B **327**, 569 (1989).
- [24] H. Georgi, Phys. Lett. B **240**, 447 (1990).
- [25] N. Isgur and M. B. Wise, Phys. Lett. B **232**, 113 (1989).
- [26] N. Isgur and M. B. Wise, Phys. Lett. B **237**, 527 (1990).
- [27] S. Nussinov and W. Wetzel, Phys. Rev. D **36**, 130 (1987).
- [28] M. B. Voloshin and M. A. Shifman, Sov. J. Nucl. Phys. **45**, 292 (1987).
- [29] M. B. Voloshin and M. A. Shifman, Sov. J. Nucl. Phys. **47**, 511 (1988).
- [30] H. D. Politzer and M. B. Wise, Phys. Lett. B **206**, 681 (1988).
- [31] H. D. Politzer and M. B. Wise, Phys. Lett. B **208**, 504 (1988).
- [32] E. V. Shuryak, Phys. Lett. B **93**, 134 (1980).
- [33] B. Grinstein, Nucl. Phys. B **339**, 253 (1990).
- [34] F. E. Close and A. Wambach, Nucl. Phys. B **412**, 169 (1994).
- [35] F. E. Close and A. Wambach, Phys. Lett. B **348**, 207 (1995).
- [36] J. M. Cornwall, Phys. Rev. D **26**, 1453 (1982).
- [37] J. M. Cornwall and A. Soni, Phys. Lett. **120B**, 431 (1983).
- [38] V. Mathieu, F. Buisseret and C. Semay, Phys. Rev. D **77**, 114022 (2008).
- [39] W. S. Hou and G. G. Wong, Phys. Rev. D **67**, 034003 (2003).
- [40] V. Mathieu, N. Kochelev and V. Vento, Int. Journ. Mod. Phys. E **18**, 1 (2009).
- [41] R. L. Jaffe and K. Johnson, Phys. Lett. B **60**, 201 (1976).
- [42] W. S. Hou and A. Soni, Phys. Rev. D **29**, 1 (1984).
- [43] U. Gastaldi, *Physics at LEAR with Low-Energy Cooled Antiprotons* (Springer, 1982).
- [44] E. Klempt, arXiv:hep-ph/0404270v1 (2004).
- [45] N. Isgur and J. Paton, Phys. Lett. B **124**, 247 (1983).
- [46] N. Isgur and J. Paton, Phys. Rev. D **31**, 2910 (1985).
- [47] L. S. Kisslinger and M.B. Johnson, Phys. Lett. B **523**, 127 (2001).
- [48] J. Sexton, A. Vaccarino and D. Weingarten, Phys. Rev. Lett. **75**, 4563 (1995).
- [49] D. Weingarten, Nucl. Phys. Proc. Suppl. **53**, 232 (1997).
- [50] J. Beringer, et al., (Particle Data Group) Phys. Rev. D **86**, 010001 (2012, 2013, 2014).

- [51] C. A. Meyer, arXiv:hep-ex/0308010v1 (2003).
- [52] M. Ablikim, et al., (BES Collaboration) Phys. Lett. B **607**, 243 (2005).
- [53] C. P. Singh, Journ. of scientific Research **37** (1987).
- [54] C. J. Morningstar and M. Peardon, Phys. Rev. D **60**, 034509 (1999).
- [55] A. Vaccarino and D. Weingarten, Phys. Rev. D **60**, 114501 (1999).
- [56] C. Liu, Nucl. Phys. Proc. Suppl. **94**, 255 (2001).
- [57] G. S. Bali and K. Schilling, Phys. Lett. B **309**, 378 (1993).
- [58] D. Bettoni, J. Phys. Conf. Ser. **9**, 309 (2005).
- [59] M. Chanowitz, Int. Journ. Mod. Phys. A **21**, 5535 (2006).
- [60] D. S. Carman, AIP Conf. Proc. **814**, 173 (2006).
- [61] B. Alessandro, et al., (ALICE Collaboration) Journ. Phys. G **32**, 1295 (2006).
- [62] N. Vandersickel, D. Dudal, H. Verschelde, in *Proceeding for the International Workshop on QCD Green's Functions, Confinement and Phenomenology*, PoS QCD-TNT **09**, 048 (2009).
- [63] D. K. Choudhury, et al., Pramana Journ. Phys. **44**, 519 (1995).
- [64] D. K. Choudhury, et al., Pramana Journ. Phys. **46**, 349 (1996).
- [65] D. K. Choudhury and N. S. Bordoloi, Mod. Phys. Lett. A **17**, 1909 (2002).
- [66] D. K. Choudhury and N. S. Bordoloi, Mod. Phys. Lett. A **26**, 443 (2009).
- [67] M. Peter, Phys. Rev. Lett. **78**, 602 (1997).
- [68] Y. Schroder, Phys. Lett. B **447**, 321 (1999).
- [69] B. J. Hazarika and D. K. Choudhury, Pramana Journ. Phys. **84**, 69 (2015).
- [70] K. K. Pathak, D. K. Choudhury, Pramana Journ. Phys. **79**, 1385 (2012).
- [71] S. Roy, D. K. Choudhury, Mod. Phys. Lett. A **27**, 1250110 (2012).
- [72] D. Ebert, R. N. Faustov and V. O. Galkin, Phys. Rev. D **79**, 114029 (2009).
- [73] M. Z. Yang, Eur. Journ. Phys. C **72**, 1880 (2012).
- [74] D. Scora and N. Isgur, Phys. Rev. D **52**, 2783 (1995).
- [75] H. M. Choi, et al., Phys. Rev. C **92**, 055203 (2015).
- [76] A. K. Grant and J. L. Rosner, arXiv:hep-ph/9211313 (1992).

- [77] W. Greiner, S. Schramm, E. Stein, D. A. Bromley, *Quantum Chromodynamics* (Springer, 2007).
- [78] N. S. Bordoloi, D. K. Choudhury, Ind. Journ. Phys. **82**, 779 (2008).
- [79] B. Liu, P. N. Shen and H. C. Chiang, Phys. Rev. C **55**, 3021 (1997).
- [80] F. Karsch, M. T. Mehr, H. Satz, Z Phys C **37**, 617 (1988).
- [81] A. De Rujula, H. Georgi and S. L. Glashow, Phys. Rev. D **12**, 3589 (1975).
- [82] J. J. Sakurai, *Advanced Quantum Mechanics* (Addison-Wiley Publishing Company, 1986).
- [83] C. Itzykson and J. Zuber, *Quantum Field Theory* (McGraw Hill, 1986).
- [84] Y. Ishikawa and K. Koc, Phys. Rev. A **50**, 4733 (1994).
- [85] M. Abramowitz and I. A. Stegun, *Handbook of Mathematical Functions* (National Bureau of Standards, 1964).
- [86] O. Vallee and M. Soares, *Airy Functions and Applications to Physics* (World Scientific, 2004).
- [87] A. K. Rai, B. Patel and P. C. Vinodkumar, Phys. Rev. C **78**, 055202 (2008).
- [88] D. P. Stanley, D. Robson, Phys. Rev. D **21**, 3180 (1980).
- [89] C. W. Hwang, Eur. Phys. Journ. C **23**, 585 (2002).
- [90] N. Akbar, B. Masud, S. Noor, Eur. Phys. Journ. A **47**, 124 (2011).
- [91] A. M. Yasser, G. S. Hassan, T. A. Nahool, Journ. of Mod. Phys. **5**, 1938 (2014).
- [92] A. K. Likhoded, A. V. Luchinsky and S. V. Poslavsky, Phys. Rev. D **91**, 114016 (2015).
- [93] S. Godfrey and N. Isgur, Phys. Rev. D **32**, 189 (1985).
- [94] D. E. Groom, et al., (Particle Data Group) Eur. Phys. Journ. C **15**, 1 (2000).
- [95] G S Bali, *Proceedings from Quark Confinement and Hadron Spectrum IV*, (World Scientific, Ed. W. Lucha, K M Maung), p. 209, arXiv:hep-ph/0010032v1 (2002).
- [96] W. I. Giersche and C. R. Munz, Phys. Rev. C **53**, 2554 (1996).
- [97] R. J. Lombard, J. Mares, Phys. Lett. B **472**, 150 (2000).
- [98] Dan Green, *Lectures in Particle Physics* (World Scientific notes in Physics) Vol. 55, page 31, ISBN: 981-02-1682-3.
- [99] A. G. Drutskoy, et al., Eur. Journ. Phys. A **49**, 7 (2013).
- [100] G. Bonvicini, et al., (CLEO Collaboration) Phys. Rev. D **89**, 072002 (2014).

- [101] Y. K. Hsiao, C Q Geng, Phys. Lett. B **757**, 47 (2016).
- [102] The ATLAS, CDF, CMS and DO Collaborations, arXiv:1403.4427v1 [hep-ex] (2014).
- [103] S. Godfrey, S. L. Olsen, Ann. Rev. Nucl. Part. Sci. **58**, 51 (2008).
- [104] J. Ping, et al., Phys. Lett. B **602**, 197 (2004).
- [105] H. Hassanabadi, S. Rahmani, S. Zarrinkamar, Phys. Rev. D **90**, 074024 (2014).
- [106] H. Hassanabadi, S. Rahmani, S. Zarrinkamar, Eur. Phys. Journ. C **74**, 3104 (2014).
- [107] B. Blossier, M. Wagner, O. Pene, Journ. of High Eenergy Phys. **06**, 022 (2009).
- [108] N. Isgur, D. Scora, B. Grinstein and M. B. Wise, Phys. Rev. D **39**, 799 (1989).
- [109] A. Le Yaounac, L. Oliver and J. C. Raynal, Phys. Rev. D **69**, 094022 (2004).
- [110] J. L. Rosner, Phys. Rev. D **42**, 3732 (1990).
- [111] T. Mannel, W. Roberts and Z. Ryzak, Phys. Lett. B **255**, 593 (1993).
- [112] M. Neubert, Phys Lett. B **264**, 455 (1991).
- [113] D. Ebert, R. N. Faustov and V. O. Galkin, Phys. Rev. D **75**, 074008 (2007).
- [114] Y. B. Dai, et al., Phys. Lett. B **387**, 379 (1996).
- [115] K. C. Bowler, et al., Nucl. Phys. B **637**, 293 (2002).
- [116] J. Bartlet, et al., Phys. Rev. Lett. **82**, 3746 (1999).
- [117] K. K. Pathak, D. K. Choudhury, *Int. Journ. of Mod. Phys. A* **28**, 1350097 (2013).
- [118] B. J. Hazarika, K. K. Pathak and D. K. Choudhury, Mod. Phys. Lett. A **26**, 1547 (2011).
- [119] B. J. Hazarika, D. K. Choudhury, Pramana Journ. of Phys., **78** (2012).
- [120] M. Beneke, G. Buchalla, M. Neubert and C. T. Sachrajda, Nucl. Phys. B **591**, 313 (2000).
- [121] H. N. Li, Phys. Rev. D **52**, 3958 (1995).
- [122] C. H. Chang and H. N. Li, Phys. Rev. D **55**, 5577 (1997).
- [123] Y. Y. Keum, H. N. Li and A. I. Sanda, Phys. Lett. B **504**, 6 (2001).
- [124] R. V. Royen and V. F. Weisskopf, Nuovo Cimento A **50**, 617 (1967).
- [125] E. Braaten and S. Fleming, Phys. Rev. D **52**, 181 (1995).
- [126] K. K. Pathak, D. K. Choudhury, Chin. Phys. Lett. **28**, 10 (2011).
- [127] S. Godfrey, Phys. Rev. D **33**, 5 (1986).

- [128] S Leitaο, et al., Phys. Rev. D **90**, 096003 (2014).
- [129] D. Asner, et al., (Heavy Flavor Averaging Group), arXiv: 1010.1589 (2010).
- [130] B. I. Eisenstein, et al., (CLEO Collaboration) Phys. Rev. D **78**, 052003 (2008).
- [131] D. Ebert, R. N. Faustov and V. O. Galkin, Phys. Lett. B **635**, 93 (2006).
- [132] D. Ebert, R. N. Faustov and V. O. Galkin, Phys. Rev. D **67**, 014027 (2003).
- [133] F. Schwabl, *Quantum Mechanics* (Narosa Publishing House, 1992).
- [134] K. M. Ecklund, et. al., (CLEO Collaboration) Phys. Rev. Lett. **100**, 161801 (2008).
- [135] J. P. Alexander, et al., (CLEO Collaboration) Phys. Rev. D **79**, 052001 (2009).
- [136] K. Abe, et al., (Belle Collaboration) Phys. Rev. Lett. **100**, 241801 (2008).
- [137] P. del Amo Sanchez, et al., (BABAR Collaboration) Phys. Rev. D **82**, 091103 (2010).
- [138] R. A. Briere, (BES III Collaboration) arXiv:1308.1121v1[hep-ex] (2013).
- [139] F. Close, *New developments in hadron spectroscopy, lecture presented at the summer school on particle physics*, ICTP, Trieste (2005).
- [140] W. Ochs, Nucl. Phys. Proc. Suppl. **174**, 146 (2007).
- [141] N. Boulanger, F. Buisseret, V. Mathieu and C. Semay, Eur. Journ. Phys. A **38**, 317 (2008).
- [142] J. G. Messchendorp, (PANDA Collaboration) ECONF C070910, 123 (2007).
- [143] A. Young "On quantitative substitutional analysis", Proceedings of the London Mathematical society, Ser. 1, 33 (1): 97-145, doi: 10.1112/plms/s1-33.1.97.
- [144] B. E. Sagan, *The Symmetric Group* (Springer, 2001).
- [145] A. Yong, Notices Amer. Math. Soc **54**, 240 (2007).
- [146] M. Beckmann, L. Hannover, S. Löffler and T. Wien, *Young Tableaux* (2007).
- [147] H. F. Jones, *Groups, Representations and Physics* (CRC Press, 1998).



# Wave function for Coulomb potential $(-\frac{4\alpha_s}{3r})$ as parent and linear potential $(br)$ as perturbation

The first-order perturbed eigenfunction  $\psi^{(1)}$  and first-order eigenenergy  $W^{(1)}$  using quantum mechanical perturbation theory (Dalgarno's method) can be obtained using the relation (2.10),



$$(H_0 - W^{(0)})\psi^{(1)} = (W^{(1)} - H')\psi^{(0)}. \quad (\text{A.1})$$

For Cornell potential (2.8), we consider

$$H_0 = -\frac{\nabla^2}{2\mu} - \frac{4\alpha_s}{3r}, \quad (\text{A.2})$$

(taking  $\hbar^2 = 1$ ) and

$$H' = br. \quad (\text{A.3})$$

Putting

$$A = \frac{4\alpha_s}{3}, \quad (\text{A.4})$$

we obtain

$$H_0 = -\frac{\nabla^2}{2\mu} - \frac{A}{r}, \quad (\text{A.5})$$

$$W^{(0)} = E = \frac{\mu A^2}{2} \quad (\text{A.6})$$

and

$$\psi^{(0)}(r) = \frac{1}{\sqrt{\pi a_0^3}} e^{-\frac{r}{a_0}}, \quad (\text{A.7})$$

where  $\psi^{(0)}$  is the unperturbed wave function in the zero<sup>th</sup> order of perturbation and  $a_0$  is given by equation (2.18).

Equation (A.1),

$$\Rightarrow \left( -\frac{\nabla^2}{2\mu} - \frac{A}{r} - E \right) \psi^{(1)} = (W^{(1)} - br) \frac{1}{\sqrt{\pi a_0^3}} e^{-\frac{r}{a_0}}$$

$$\begin{aligned}
&\Rightarrow \left( \nabla^2 + \frac{2\mu A}{r} - \mu^2 A^2 \right) \psi^{(1)} = (br - W^{(1)}) \frac{2\mu}{\sqrt{\pi a_0^3}} e^{-\frac{r}{a_0}} \\
&\Rightarrow \left( \nabla^2 + \frac{2}{a_0 r} - \frac{1}{a_0^2} \right) \psi^{(1)} = (br - W^{(1)}) \frac{2\mu}{\sqrt{\pi a_0^3}} e^{-\frac{r}{a_0}}. \tag{A.8}
\end{aligned}$$

Let

$$\psi^{(1)} = (br)R(r), \tag{A.9}$$

then

$$(A.8) \Rightarrow \left( \frac{d^2}{dr^2} + \frac{2}{r} \frac{d}{dr} + \frac{2}{a_0 r} - \frac{1}{a_0^2} \right) (br)R(r) = D(br - W^{(1)})e^{-\frac{r}{a_0}}, \tag{A.10}$$

where we put

$$D = \frac{2\mu}{\sqrt{\pi a_0^3}}. \tag{A.11}$$

Now

$$\frac{d}{dr} (brR(r)) = bR(r) + br \frac{dR}{dr}, \tag{A.12}$$

$$\frac{d^2}{dr^2} (brR(r)) = 2b \frac{dR}{dr} + br \frac{d^2 R}{dr^2} \tag{A.13}$$

Using (A.12) and (A.13) in (A.10) we obtain

$$\begin{aligned}
&br \frac{d^2 R}{dr^2} + 2b \frac{dR}{dr} + \frac{2}{r} bR(r) + \frac{2}{r} br \frac{dR}{dr} + \frac{2}{a_0 r} brR(r) - \frac{1}{a_0^2} brR(r) \\
&\quad = D(br - W^{(1)})e^{-\frac{r}{a_0}}. \tag{A.14}
\end{aligned}$$

Putting

$$R(r) = F(r)e^{-\frac{r}{a_0}}, \tag{A.15}$$

$$\frac{dR}{dr} = F'(r)e^{-\frac{r}{a_0}} - \frac{1}{a_0}F(r)e^{-\frac{r}{a_0}}, \quad (\text{A.16})$$

$$\frac{d^2R}{dr^2} = F''(r)e^{-\frac{r}{a_0}} - \frac{2}{a_0}F'(r)e^{-\frac{r}{a_0}} + \frac{1}{a_0^2}F(r)e^{-\frac{r}{a_0}}, \quad (\text{A.17})$$

$$\begin{aligned} (\text{A.14}) \Rightarrow br \left\{ F''(r) - \frac{2}{a_0}F'(r) + \frac{1}{a_0^2}F(r) \right\} + 2b \left\{ F'(r) - \frac{1}{a_0}F(r) \right\} + \frac{2b}{r}F(r) \\ + 2bF'(r) - \frac{2b}{a_0}F(r) + \frac{2b}{a_0}F(r) - \frac{1}{a_0^2}brF(r) = D(br - W^{(1)}) \end{aligned}$$

$$\Rightarrow brF''(r) + \left\{ 4b - \frac{2b}{a_0}r \right\} F'(r) + \left\{ \frac{2b}{r} - \frac{2b}{a_0} \right\} F(r) = D(br - W^{(1)}). \quad (\text{A.18})$$

Let

$$F(r) = \sum_{n=0}^{\infty} A_n r^n, \quad (\text{A.19})$$

then

$$F'(r) = \sum_{n=0}^{\infty} nA_n r^{n-1} \quad (\text{A.20})$$

and

$$F''(r) = \sum_{n=0}^{\infty} n(n-1)A_n r^{n-2}. \quad (\text{A.21})$$

$$\begin{aligned} (\text{A.18}) \Rightarrow br \sum_{n=0}^{\infty} n(n-1)A_n r^{n-2} + \left\{ 4b - \frac{2b}{a_0}r \right\} \sum_{n=0}^{\infty} nA_n r^{n-1} + \left\{ \frac{2b}{r} - \frac{2b}{a_0} \right\} \sum_{n=0}^{\infty} A_n r^n \\ = D(br - W^{(1)}) \end{aligned}$$

$$\begin{aligned}
&\Rightarrow \left\{ b \sum_{n=0}^{\infty} n(n-1)A_n + 4b \sum_{n=0}^{\infty} nA_n + 2b \sum_{n=0}^{\infty} A_n \right\} r^{n-1} - \left\{ \frac{2b}{a_0} \sum_{n=0}^{\infty} nA_n + \frac{2b}{a_0} \sum_{n=0}^{\infty} A_n \right\} r^n \\
&\quad = D(br - W^{(1)}).
\end{aligned}
\tag{A.22}$$

Equating the co-efficients of  $r^{-1}$  on both sides of the above identity (A.22)

$$2bA_0 = 0,$$

since  $b \neq 0$ , therefore

$$\Rightarrow A_0 = 0. \tag{A.23}$$

Equating the co-efficients of  $r^0$  on both sides of the identity (A.22),

$$\begin{aligned}
&4bA_1 + 2bA_1 - \frac{2b}{a_0}A_0 = -DW^{(1)} \\
&\Rightarrow A_1 = -\frac{DW^{(1)}}{6b}.
\end{aligned}
\tag{A.24}$$

Equating the co-efficients of  $r^1$  on both sides of the identity (A.22),

$$2bA_2 + 8bA_2 + 2bA_2 - \frac{2b}{a_0}A_1 - \frac{2b}{a_0}A_1 = Db.$$

Using (A.24),

$$A_2 = \frac{D}{12} - \frac{DW^{(1)}}{18ba_0}. \tag{A.25}$$

Equating the co-efficients of  $r^2$  on both sides of the identity (A.22),

$$6bA_3 + 12bA_3 + 2bA_3 - \frac{4b}{a_0}A_2 - \frac{2b}{a_0}A_2 = 0. \quad (\text{A.26})$$

Using (A.25),

$$A_3 = \frac{D}{40a_0} - \frac{DW^{(1)}}{60ba_0^2}. \quad (\text{A.27})$$

Equating the co-efficients of  $r^3$  on both sides of the identity (A.22),

$$12bA_4 + 16bA_4 + 2bA_4 - \frac{2b}{a_0}3A_3 - \frac{2b}{a_0}A_3 = 0.$$

Using (A.27),

$$A_4 = \frac{D}{150a_0^2} - \frac{DW^{(1)}}{225ba_0^3}. \quad (\text{A.28})$$

From (A.19)

$$F(r) = A_0r^0 + A_1r^1 + A_2r^2 + A_3r^3 + A_4r^4 + \dots \quad (\text{A.29})$$

Now from (A.9), (A.15) and (A.29),

$$\psi^{(1)}(r) = brF(r)e^{-\frac{r}{a_0}} \quad (\text{A.30})$$

$$= br(A_0r^0 + A_1r^1 + A_2r^2 + A_3r^3 + A_4r^4 + \dots)e^{-\frac{r}{a_0}}$$

$$= \left\{ A_0(br) + A_1(br^2) + A_2(br^3) + A_3(br^4) + A_4(br^5) + \dots \right\} e^{-\frac{r}{a_0}}. \quad (\text{A.31})$$

Now applying (A.23), (A.24), (A.25), (A.27), (A.28) to (A.31),

$$\begin{aligned}\psi^{(1)}(r) = & \left[ -\frac{DW}{6b}(br^2) + \left\{ \frac{D}{6} \left( \frac{1}{2} - \frac{W}{3ba_0} \right) \right\} (br^3) + \left\{ \frac{D}{20a_0} \left( \frac{1}{2} - \frac{W}{3ba_0} \right) \right\} (br^4) \right. \\ & \left. + \left\{ \frac{D}{75a_0^2} \left( \frac{1}{2} - \frac{W}{3ba_0} \right) \right\} (br^5) \right] e^{-\frac{r}{a_0}}.\end{aligned}\tag{A.32}$$

Again from (2.13)

$$\begin{aligned}W^{(1)} &= \int \psi_{100}^* H' \psi_{100} d\tau \\ &= \frac{1}{\pi a_0^3} \int_0^\infty (br)r^2 e^{-\frac{2r}{a_0}} dr \int_0^\pi \sin\theta d\theta \int_0^{2\pi} d\phi \\ &= \frac{4\pi}{\pi a_0^3} \int_0^\infty (br^3) e^{-\frac{2r}{a_0}} dr \\ &= \frac{4}{a_0^3} \left[ b \frac{6a_0^4}{16} \right] \\ &= \frac{3}{2} ba_0.\end{aligned}\tag{A.33}$$

Hence

$$\frac{1}{2} - \frac{W}{3ba_0} = 0.\tag{A.34}$$

Therefore, (A.32) reduces to

$$\psi^{(1)}(r) = \left[ -\frac{DW}{6b}(br^2) \right] e^{-\frac{r}{a_0}}$$

$$= -\frac{1}{2\sqrt{\pi a_0^3}} \mu b a_0 r^2 e^{-\frac{r}{a_0}}. \quad (\text{A.35})$$

The total wave function is thus

$$\psi^{total} = \psi^{(0)} + \psi^{(1)}$$

$$= \frac{1}{\sqrt{\pi a_0^3}} \left[ 1 - \frac{1}{2} \mu b a_0 r^2 \right] e^{-\frac{r}{a_0}}. \quad (\text{A.36})$$

Considering relativistic correction factor the equation (A.36) becomes

$$\psi^{total}(r) = \frac{N}{\sqrt{\pi a_0^3}} \left[ 1 - \frac{1}{2} \mu b a_0 r^2 \right] \left( \frac{r}{a_0} \right)^{-\varepsilon} e^{-\frac{r}{a_0}}. \quad (\text{A.37})$$

# B

Wave function for linear potential ( $br$ ) as  
parent and Coulomb potential ( $-\frac{4\alpha_s}{3r}$ ) as  
perturbation

For the Cornell potential (2.8), we consider

$$H_0 = -\frac{\nabla^2}{2\mu} + br \tag{B.1}$$



and

$$H' = -\frac{4\alpha_s}{3r}. \quad (\text{B.2})$$

To find the unperturbed wave function corresponding to  $H_0$ , we employ the radial Schrödinger's equation for potential  $br$  for ground state,

$$-\frac{1}{2\mu} \left[ \left( \frac{d^2}{dr^2} + \frac{2}{r} \frac{d}{dr} \right) + br \right] R(r) = ER(r), \quad (\text{B.3})$$

where  $R(r)$  is the radial wave function. We introduce  $u(r) = rR(r)$  and the dimensionless variable

$$\rho(r) = (2\mu b)^{\frac{1}{3}} r - \left( \frac{2\mu}{b^2} \right)^{\frac{1}{3}} E. \quad (\text{B.4})$$

The equation (B.3) then reduces to

$$\frac{d^2 u}{d\rho^2} - \rho u = 0. \quad (\text{B.5})$$

The solution of this second order homogeneous differential equation contains linear combination of two types of Airy's functions  $Ai[r]$  and  $Bi[r]$ .

The nature of the Airy's function reveals that

$$Ai[r] \rightarrow 0 \text{ and } Bi[r] \rightarrow \infty \text{ as } r \rightarrow \infty.$$

So, it is reasonable to reject the  $Bi[r]$  part of the solution.

The unperturbed wave function for ground state is

$$\psi^{(0)}(r) = \frac{N_0}{r} Ai[\rho_1 r + \rho_0], \quad (\text{B.6})$$

where  $N_0$  is the normalization constant and  $\rho_1 = (2\mu b)^{1/3}$ .

$\rho_0$  is the zero of the Airy function, such that  $Ai[\rho_0] = 0$ .

$\rho_0$  has the explicit form as mentioned in equation (2.29).

The first order perturbed eigen function  $\psi^{(1)}$  is obtained using relation (A.1).

Then taking  $\hbar^2 = 1$ , equation (A.1),

$$\Rightarrow \left( -\frac{\hbar^2}{2\mu} \nabla^2 + br - E \right) \psi^{(1)} = \left( W^{(1)} + \frac{4\alpha_s}{3r} \right) \psi^{(0)}(r). \quad (\text{B.7})$$

In terms of the radial wave function the above equation can be expressed as

$$\left[ \left( \frac{d^2}{dr^2} + \frac{2}{r} \frac{d}{dr} \right) - 2\mu(br - E) \right] R(r) = -2\mu \left( W^{(1)} + \frac{4\alpha_s}{3r} \right) \frac{1}{r} Ai[\rho]. \quad (\text{B.8})$$

Let

$$R(r) = \frac{1}{r} F(r) Ai[\rho] = \frac{1}{r} F(r) Ai[\rho_1 r + \rho_0], \quad (\text{B.9})$$

so that

$$\frac{dR}{dr} = -\frac{1}{r^2} F(r) Ai[\rho] + \frac{1}{r} F'(r) Ai[\rho] + \frac{\rho_1}{r} F(r) Ai'[\rho], \quad (\text{B.10})$$

$$\begin{aligned} \frac{d^2 R}{dr^2} = & \frac{2}{r^3} F(r) Ai[\rho] - \frac{2}{r^2} F'(r) Ai[\rho] - \frac{2\rho}{r^2} F(r) Ai'[\rho] + \frac{1}{r} F''(r) Ai[\rho] + \\ & \frac{2\rho_1}{r} F'(r) Ai'[\rho] + \frac{\rho_1^2}{r} F(r) Ai''[\rho]. \end{aligned} \quad (\text{B.11})$$

Now we introduce the identity

$$Ai'[\rho] = \frac{dAi(\rho)}{dr} = Z(\rho)Ai(\rho), \quad (\text{B.12})$$

so that

$$Ai''(\rho) = Z^2(\rho)Ai(\rho) + Z'(\rho)Ai(\rho). \quad (\text{B.13})$$

Then the equation (B.8) becomes

$$\begin{aligned} F''(r) + 2\rho_1 F'(r)Z(\rho) + \rho_1^2 [Z^2(\rho) + Z'(\rho)]F(r) - 2\mu(br - E)F(r) \\ = -\frac{4\alpha_s}{3} \frac{2\mu}{r} - 2\mu W^{(1)}. \end{aligned} \quad (\text{B.14})$$

Assuming

$$Z(\rho) = \frac{k_1(r)}{r}$$

and

$$Z^2(\rho) + Z'(\rho) = \frac{k_2(r)}{r^2},$$

$$(B.14) \Rightarrow F''(r) + 2\rho_1 F'(r) \frac{k_1(r)}{r} + \rho_1^2 F(r) \frac{k_2(r)}{r^2} - 2\mu(br - E)F(r) = -\frac{4\alpha_s}{3} \frac{2\mu}{r} - 2\mu W^{(1)}. \quad (\text{B.15})$$

Now using (A.19), (A.20) and (A.21), the above equation (B.15) becomes

$$\begin{aligned} n(n-1) \sum_n A_n r^{n-2} + 2\rho_1 l \sum_n A_n r^{n-1} \frac{k_1}{r} + \rho_1^2 \sum_n A_n r^n \frac{k_2}{r^2} - 2\mu(br - E) \sum_n A_n r^n \\ = -\frac{4\alpha_s}{3} \frac{2\mu}{r} - 2\mu W^{(1)} \end{aligned} \quad (\text{B.16})$$

$$\begin{aligned} \Rightarrow \left[ n(n-1) \sum_n A_n + 2\rho_1 n \sum_n A_n k_1 + \rho_1^2 \sum_n A_n k_2 \right] r^{n-2} - 2\mu b \sum_n A_n r^{n+1} + \\ 2\mu E \sum_n A_n r^n = -\frac{4\alpha_s}{3} \frac{2\mu}{r} - 2\mu W^{(1)}. \end{aligned} \quad (\text{B.17})$$

Now equating the co-efficients of  $r^{-2}$  from the above equation (B.17),

$$\rho_1^2 A_0 k_2 = 0$$

$$\Rightarrow A_0 = 0. \quad (\text{B.18})$$

Equating the co-efficients of  $r^{-1}$  of (B.17),

$$2\rho_1 A_1 k_1 + \rho_1^2 A_1 k_2 = -2\mu \frac{4\alpha_s}{3},$$

$$\Rightarrow A_1 = \frac{-2\mu \frac{4\alpha_s}{3}}{2\rho_1 k_1 + \rho_1^2 k_2}. \quad (\text{B.19})$$

Equating the co-efficients of  $r^0$  of (B.17),

$$2A_2 + 4\rho_1 A_2 k_1 + \rho_1^2 A_2 k_2 + 2\mu E A_0 = -2\mu W^{(1)}$$

$$\Rightarrow A_2 = \frac{-2\mu W^{(1)}}{2 + 4\rho_1 k_1 + \rho_1^2 k_2}. \quad (\text{B.20})$$

Equating the co-efficients of  $r^1$  of (B.17),

$$6A_3 + 6\rho_1 A_3 k_1 + \rho_1^2 A_3 k_2 - 2\mu b A_0 + 2\mu E A_1 = 0$$

$$\Rightarrow A_3 = \frac{-2\mu EA_1}{6 + 6\rho_1 k_1 + \rho_1^2 k_2}. \quad (\text{B.21})$$

Equating the co-efficients of  $r^2$  of (B.17),

$$12A_4 + 8\rho_1 A_4 k_1 + \rho_1^2 A_4 k_2 - 2\mu b A_1 + 2\mu E A_2 = 0$$

$$\Rightarrow A_4 = \frac{-2\mu E A_2 + 2\mu b A_1}{12 + 8\rho_1 k_1 + \rho_1^2 k_2}. \quad (\text{B.22})$$

Equating the co-efficients of  $r^3$  of (B.17),

$$20A_5 + 10\rho_1 A_5 k_1 + \rho_1^2 A_5 k_2 - 2\mu b A_2 + 2\mu E A_3 = 0$$

$$\Rightarrow A_5 = \frac{-2\mu E A_3 + 2\mu b A_2}{20 + 10\rho_1 k_1 + \rho_1^2 k_2}. \quad (\text{B.23})$$

Equating the co-efficients of  $r^4$  of (B.17),

$$30A_6 + 12\rho_1 A_6 k_1 + \rho_1^2 A_6 k_2 - 2\mu b A_3 + 2\mu E A_4 = 0$$

$$\Rightarrow A_6 = \frac{-2\mu E A_4 + 2\mu b A_3}{30 + 12\rho_1 k_1 + \rho_1^2 k_2}. \quad (\text{B.24})$$

Equating the co-efficients of  $r^5$  of (B.17),

$$42A_7 + 14\rho_1 A_7 k_1 + \rho_1^2 A_7 k_2 - 2\mu b A_4 + 2\mu E A_5 = 0$$

$$\Rightarrow A_7 = \frac{-2\mu E A_5 + 2\mu b A_4}{42 + 14\rho_1 k_1 + \rho_1^2 k_2}. \quad (\text{B.25})$$

and so on.

Using (A.29), the perturbed wave function will be

$$\psi^{(1)}(r) = \frac{1}{r} [A_0 r^0 + A_1 r^1 + A_2 r^2 + A_3 r^3 + A_4 r^4 + A_5 r^5 + A_6 r^6 + A_7 r^7 + \dots] Ai[\rho_1 r + \rho_0]. \quad (\text{B.26})$$

Now the total wave function with relativistic correction factor is

$$\psi^{total}(r) = \frac{N'}{r} [1 + A_0 r^0 + A_1 r^1 + A_2 r^2 + A_3 r^3 + A_4 r^4 + A_5 r^5 + A_6 r^6 + A_7 r^7 + \dots] Ai[\rho_1 r + \rho_0] \left( \frac{r}{a_0} \right)^{-\epsilon}. \quad (\text{B.27})$$

The co-efficients  $A_0, A_1, A_2, A_3, \dots$  are appearing from the series solution of Schrödinger equation using the Dalgarno's method of perturbation.

# C

## Continuity of the wave functions $\psi_I(r)$ and $\psi_{II}(r)$ at $r^P$

To check the continuity of the wave functions, we first plot the wave function ' $\psi_I(r)$  vs  $r$ ' in the range  $0 < r < r^P$  and then the wave function ' $\psi_{II}(r)$  vs  $r$ ' in the range  $r^P < r < r^0$  as shown in figures C.1 and C.2 respectively.

A plot of complete wave function ' $\psi_I(r) + \psi_{II}(r)$  vs  $r$ ' is drawn in fig. C.3 to check the continuity of the wave function at the point ' $r^P$ '.

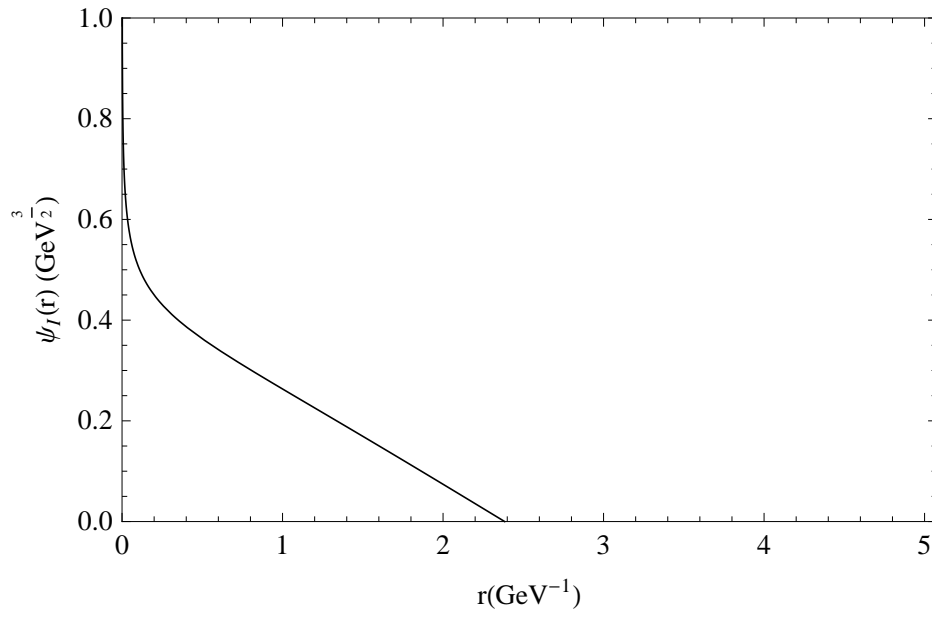


Fig. C.1 The wave function  $\psi_I(r)$  for  $D(c\bar{u}/c\bar{d})$  meson.

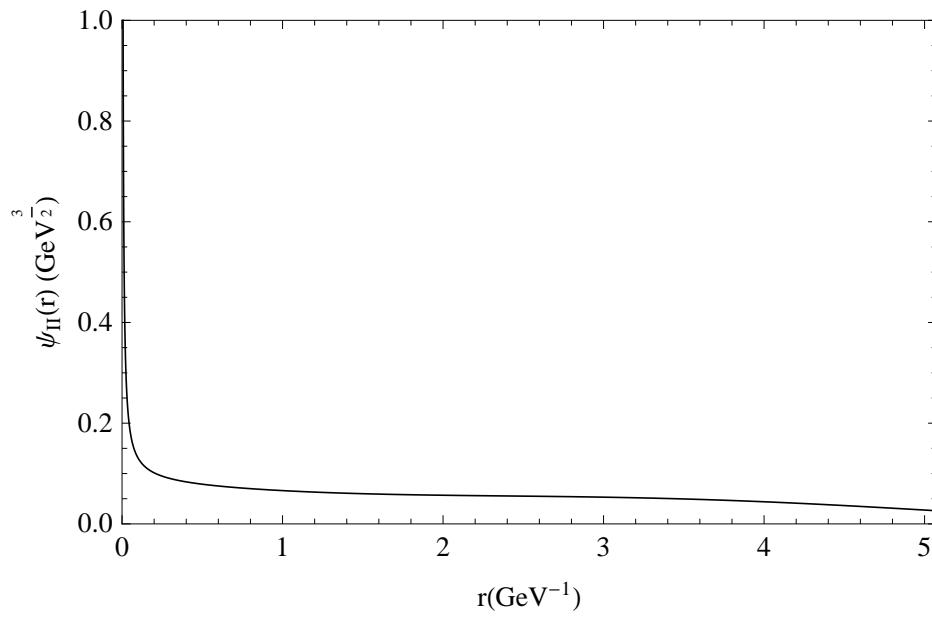


Fig. C.2 The wave function  $\psi_{II}(r)$  for  $D(c\bar{u}/c\bar{d})$  meson.

From the fig. C.3, it is evident that there is no break or mismatch of the wave functions  $\psi_I(r)$  and  $\psi_{II}(r)$  at the point  $r^P$ .



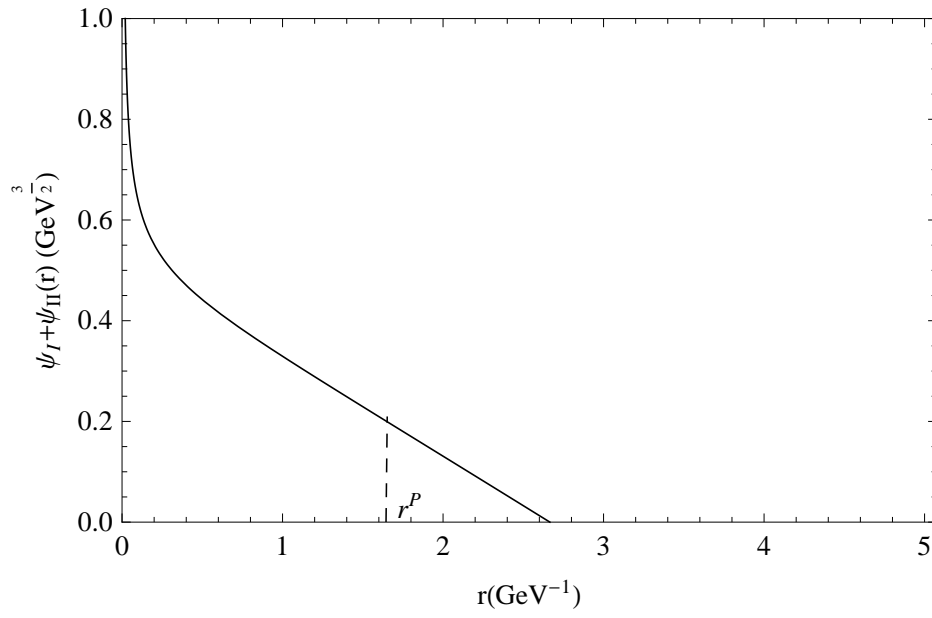


Fig. C.3 The complete wave function  $\psi_I(r) + \psi_{II}(r)$  for  $D(c\bar{u}/c\bar{d})$  meson.

# D

Mass of  $D(c\bar{u}/c\bar{d})$  meson using formula  
(2.37) considering various co-efficients of  
equation (B.27)

From Table D.1, it can be inferred that the with increase of the cut-off  $r_0$  the mass of the meson increases slightly at the beginning, then becomes stable with the increase of  $r_0$ . Similarly, the change is not so significant with the increase of the number of terms of the wave function

Table D.1 Mass of  $D(c\bar{u}/c\bar{d})$  meson in  $GeV$  with different order of the terms of wave function (B.27) and with the different values of upper cut-off  $r_0$ .

$r_0$ ( $GeV^{-1}$ )	With Eqn.(B.6)	upto $O(r^1)$	upto $O(r^2)$	upto $O(r^3)$	upto $O(r^4)$	upto $O(r^5)$	upto $O(r^6)$	upto $O(r^7)$
5.076	2.253	2.308	2.313	2.311	2.438	2.256	2.211	2.322
10	2.260	2.368	2.460	2.461	2.604	2.512	2.570	2.547
100	2.260	2.369	2.461	2.463	2.641	2.542	2.623	2.756
Infinity	2.260	2.369	2.461	2.463	2.641	2.542	2.623	2.756

(B.27).

Now, considering the wave function (B.27) upto  $O(r^7)$  we check the behavior of the normalization constant with different  $r_0$ ,

$$N' = \left( \int_{r^p}^{r_0} 4\pi \left[ 1 + A_0 r^0 + A_1(r)r + A_2(r)r^2 + A_3(r)r^3 + A_4(r)r^4 + A_5 r^5 + A_6 r^6 + A_7 r^7 \right]^2 (A_i[\rho_1 r + \rho_0])^2 \left( \frac{r}{a_0} \right)^{-2\epsilon} dr \right)^{-\frac{1}{2}}. \quad (D.1)$$

Table D.2 Normalization constant with different upper cut-off  $r_0$ .

$r_0$ ( $GeV^{-1}$ )	5.076	8	10	14	18	25	50	100	1000	Infinity
$N'$	0.0143	0.0081	0.0076	0.0060	0.0059	0.0059	0.0059	0.0059	0.0059	0.0059

The graphical representation of Table D.2 is shown in Fig. D.1.

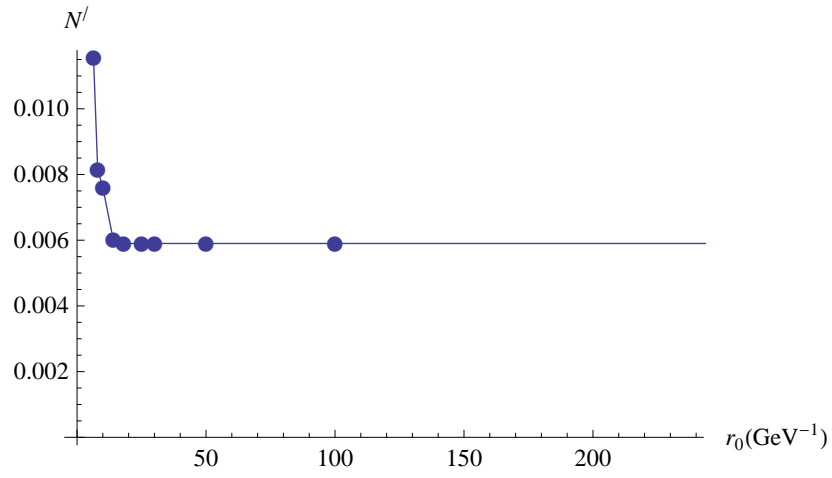


Fig. D.1 Normalization constant (D.1) with different  $r_0$ .

From Fig. D.1, it is clear that the Normalization constant of the wave function B.27 converges with the increase of  $r_0$  and becomes stable after a particular value of  $r_0 \leq 18 \text{GeV}^{-1}$ .

# E

Form factor  $F(Q^2)_I$  with wave function

(2.21)

$$F(Q^2) |_I = \sum_{i=1}^2 \frac{e_i}{Q_i} \int_0^{r^P} 4\pi r |\psi_I(r)|^2 \sin(Q_i r) dr \quad (\text{E.1})$$

Using equation (2.21) in equation (E.1) and integrating over  $r$ ,

$$\begin{aligned} F(Q^2) |_I = N^2 \sum_{i=1}^2 \frac{e_i}{Q_i} & \left[ \frac{2^{2\varepsilon}}{a_0} (\gamma(2-2\varepsilon, r^P)) \sin((2-2\varepsilon) \cdot \theta_i) \left(1 + \frac{a_0^2 Q_i^2}{4}\right)^{\varepsilon-1} \right. \\ & + \frac{a_0^5}{2^{6-2\varepsilon}} \mu^2 b^2 (\gamma(6-2\varepsilon, r^P)) \sin((6-2\varepsilon) \cdot \theta_i) \left(1 + \frac{a_0^2 Q_i^2}{4}\right)^{\varepsilon-3} \\ & \left. - \frac{a_0^2}{2^{2-2\varepsilon}} \mu b (\gamma(4-2\varepsilon, r^P)) \sin((4-2\varepsilon) \cdot \theta_i) \left(1 + \frac{a_0^2 Q_i^2}{4}\right)^{\varepsilon-2} \right], \end{aligned} \quad (\text{E.2})$$

where

$$\theta_i = \sin^{-1} \left[ \frac{Q_i}{\left(Q_i^2 + \frac{4}{a_0^2}\right)^{\frac{1}{2}}} \right], \quad (\text{E.3})$$

where only the first term of the following series is considered

$$\sin^{-1}(x) \approx x + \frac{x^3}{6} + \frac{3x^5}{40}, \quad (\text{E.4})$$

with

$$x = \frac{Q_i}{\left(Q_i^2 + \frac{4}{a_0^2}\right)^{\frac{1}{2}}} \quad (\text{E.5})$$

which is true for very low  $Q^2$ .

We split the *sine* function of equation (E.2) using

$$\sin y = y - \frac{y^3}{3!} + \frac{y^5}{5!}. \quad (\text{E.6})$$

Now equation (E.2) becomes

$$\begin{aligned} F(Q^2) |_{I=0} = N^2 \sum_{i=1}^2 \frac{e_i}{Q_i} \left[ \frac{2^{2\varepsilon}}{a_0} (\gamma(2-2\varepsilon, r^P)) \left( (2-2\varepsilon)\theta_i - \frac{(2-2\varepsilon)^3}{3!} \theta_i^3 + \frac{(2-2\varepsilon)^5}{5!} \theta_i^5 \right) \left( 1 + \frac{a_0^2 Q_i^2}{4} \right)^{\varepsilon-1} \right. \\ \left. + \frac{a_0^5}{2^{6-2\varepsilon}} \mu^2 b^2 (\gamma(6-2\varepsilon, r^P)) \left( (6-2\varepsilon)\theta_i - \frac{(6-2\varepsilon)^3}{3!} \theta_i^3 + \frac{(6-2\varepsilon)^5}{5!} \theta_i^5 \right) \left( 1 + \frac{a_0^2 Q_i^2}{4} \right)^{\varepsilon-3} \right. \\ \left. - \frac{a_0^2}{2^{2-2\varepsilon}} \mu b (\gamma(4-2\varepsilon, r^P)) \left( (4-2\varepsilon)\theta_i - \frac{(4-2\varepsilon)^3}{3!} \theta_i^3 + \frac{(4-2\varepsilon)^5}{5!} \theta_i^5 \right) \left( 1 + \frac{a_0^2 Q_i^2}{4} \right)^{\varepsilon-2} \right]. \quad (\text{E.7}) \end{aligned}$$

Using (E.2) and (E.5) in equation (E.7),

$$\begin{aligned} F(Q^2) |_{I=0} = N^2 \sum_{i=1}^2 e_i \left[ \frac{2^{2\varepsilon}}{a_0} (\gamma(2-2\varepsilon, r^P)) \left( (2-2\varepsilon)X_i - \frac{(2-2\varepsilon)^3}{3!} Q_i^2 X_i^3 + \frac{(2-2\varepsilon)^5}{5!} Q_i^4 X_i^5 \right) \left( 1 + \frac{a_0^2 Q_i^2}{4} \right)^{\varepsilon-1} \right. \\ \left. + \frac{a_0^5}{2^{6-2\varepsilon}} \mu^2 b^2 (\gamma(6-2\varepsilon, r^P)) \left( (6-2\varepsilon)X_i - \frac{(6-2\varepsilon)^3}{3!} Q_i^2 X_i^3 + \frac{(6-2\varepsilon)^5}{5!} Q_i^4 X_i^5 \right) \left( 1 + \frac{a_0^2 Q_i^2}{4} \right)^{\varepsilon-3} \right. \\ \left. - \frac{a_0^2}{2^{2-2\varepsilon}} \mu b (\gamma(4-2\varepsilon, r^P)) \left( (4-2\varepsilon)X_i - \frac{(4-2\varepsilon)^3}{3!} Q_i^2 X_i^3 + \frac{(4-2\varepsilon)^5}{5!} Q_i^4 X_i^5 \right) \left( 1 + \frac{a_0^2 Q_i^2}{4} \right)^{\varepsilon-2} \right], \quad (\text{E.8}) \end{aligned}$$

where

$$X_i = \left( Q_i^2 + \frac{4}{a_0^2} \right)^{-\frac{1}{2}}. \quad (\text{E.9})$$

At low  $Q^2$  limit, equation (E.8) reduces to equation (2.46) and with  $\varepsilon = 0$  to (2.49).

F

Form factor  $F(Q^2)_H$  with wave function  
(2.35)

$$F(Q^2)_H = \sum_{i=1}^2 \frac{e_i}{Q_i} \int_{r^p}^{r_0} 4\pi r |\psi_H(r)|^2 \sin(Q_i r) dr \tag{F.1}$$



At low  $Q^2$  limit equation (F.1) gives

$$\begin{aligned}
 F(Q^2) |_{II} = 4\pi N^2 a_0^{2\varepsilon} \sum_{i=1}^2 e_i \left[ \frac{(a_1 - b_1 \rho_0)^2 (\gamma(-2\varepsilon, r_0) - \gamma(-2\varepsilon, r^P)) \sin((-2\varepsilon)\phi_i)}{(Q_i^2)^{\frac{1-2\varepsilon}{2}}} \right. \\
 + \frac{(b_1 \rho_1)^2 (\gamma(2-2\varepsilon, r_0) - \gamma(2-2\varepsilon, r^P)) \sin((2-2\varepsilon)\phi_i)}{(Q_i^2)^{\frac{3-2\varepsilon}{2}}} \\
 - \frac{2b_1 \rho_1 (a_1 - b_1 \rho_0) (\gamma(1-2\varepsilon, r_0) - \gamma(1-2\varepsilon, r^P)) \sin((1-2\varepsilon)\phi_i)}{(Q_i^2)^{\frac{2-2\varepsilon}{2}}} \\
 - \frac{16}{3} \frac{(a_1 - b_1 \rho_0)^2 \mu \alpha_s (\gamma(3-2\varepsilon, r_0) - \gamma(3-2\varepsilon, r^P)) \sin((3-2\varepsilon)\phi_i)}{(\rho_1 k)^2 (Q_i^2)^{\frac{4-2\varepsilon}{2}}} \\
 + \frac{16}{3} \frac{(a_1 - b_1 \rho_0)^2 \mu \alpha_s 2\sqrt{2\rho_1} (\gamma(4-2\varepsilon, r_0) - \gamma(4-2\varepsilon, r^P)) \sin((4-2\varepsilon)\phi_i)}{(\rho_1 k)^3 (Q_i^2)^{\frac{5-2\varepsilon}{2}}} \\
 - \frac{16}{3} \frac{(b_1 \rho_1)^2 \mu \alpha_s (\gamma(5-2\varepsilon, r_0) - \gamma(5-2\varepsilon, r^P)) \sin((5-2\varepsilon)\phi_i)}{(\rho_1 k)^2 (Q_i^2)^{\frac{6-2\varepsilon}{2}}} \\
 + \frac{16}{3} \frac{(b_1 \rho_1)^2 \mu \alpha_s 2\sqrt{2\rho_1} (\gamma(6-2\varepsilon, r_0) - \gamma(6-2\varepsilon, r^P)) \sin((6-2\varepsilon)\phi_i)}{(\rho_1 k)^3 (Q_i^2)^{\frac{7-2\varepsilon}{2}}} \\
 + \frac{32}{3} \frac{b_1 \rho_1 (a_1 - b_1 \rho_0) \mu \alpha_s (\gamma(4-2\varepsilon, r_0) - \gamma(4-2\varepsilon, r^P)) \sin((4-2\varepsilon)\phi_i)}{(\rho_1 k)^2 (Q_i^2)^{\frac{5-2\varepsilon}{2}}} \\
 - \frac{32}{3} \frac{b_1 \rho_1 (a_1 - b_1 \rho_0) 2\sqrt{2\rho_1} \mu \alpha_s (\gamma(5-2\varepsilon, r_0) - \gamma(5-2\varepsilon, r^P)) \sin((5-2\varepsilon)\phi_i)}{(\rho_1 k)^3 (Q_i^2)^{\frac{6-2\varepsilon}{2}}} \\
 - \frac{8}{3} \frac{(a_1 - b_1 \rho_0)^2 \mu \alpha_s (\gamma(4-2\varepsilon, r_0) - \gamma(4-2\varepsilon, r^P)) \sin((4-2\varepsilon)\phi_i)}{(\rho_1 k)^2 (Q_i^2)^{\frac{5-2\varepsilon}{2}}} \\
 + \frac{8}{3} \frac{(a_1 - b_1 \rho_0)^2 \mu \alpha_s 2\sqrt{2\rho_1} (\gamma(5-2\varepsilon, r_0) - \gamma(5-2\varepsilon, r^P)) \sin((5-2\varepsilon)\phi_i)}{(\rho_1 k)^3 (Q_i^2)^{\frac{6-2\varepsilon}{2}}} \\
 + (\frac{8\mu\alpha_s}{3})^2 \frac{(b_1 \rho_1)^2 (\gamma(8-2\varepsilon, r_0) - \gamma(8-2\varepsilon, r^P)) \sin((8-2\varepsilon)\phi_i)}{(\rho_1 k)^4 (Q_i^2)^{\frac{9-2\varepsilon}{2}}} \\
 + (\frac{8\mu\alpha_s}{3})^2 \frac{8\rho_1 (b_1 \rho_1)^2 (\gamma(10-2\varepsilon, r_0) - \gamma(10-2\varepsilon, r^P)) \sin((10-2\varepsilon)\phi_i)}{(\rho_1 k)^6 (Q_i^2)^{\frac{11-2\varepsilon}{2}}} \\
 - (\frac{8\mu\alpha_s}{3})^2 \frac{(b_1 \rho_1)^2 4\sqrt{2\rho_1} (\gamma(9-2\varepsilon, r_0) - \gamma(9-2\varepsilon, r^P)) \sin((9-2\varepsilon)\phi_i)}{(\rho_1 k)^5 (Q_i^2)^{\frac{10-2\varepsilon}{2}}} \\
 - (\frac{8\mu\alpha_s}{3})^2 \frac{2b_1 \rho_1 (a_1 - b_1 \rho_0) (\gamma(7-2\varepsilon, r_0) - \gamma(7-2\varepsilon, r^P)) \sin((7-2\varepsilon)\phi_i)}{(\rho_1 k)^4 (Q_i^2)^{\frac{8-2\varepsilon}{2}}} \\
 - (\frac{8\mu\alpha_s}{3})^2 \frac{2b_1 \rho_1 (a_1 - b_1 \rho_0) 8\rho_1 (\gamma(9-2\varepsilon, r_0) - \gamma(9-2\varepsilon, r^P)) \sin((9-2\varepsilon)\phi_i)}{(\rho_1 k)^6 (Q_i^2)^{\frac{10-2\varepsilon}{2}}} \\
 \left. + (\frac{8\mu\alpha_s}{3})^2 \frac{4b_1 \rho_1 (a_1 - b_1 \rho_0) 2\sqrt{2\rho_1} (\gamma(8-2\varepsilon, r_0) - \gamma(8-2\varepsilon, r^P)) \sin((8-2\varepsilon)\phi_i)}{(\rho_1 k)^5 (Q_i^2)^{\frac{9-2\varepsilon}{2}}} \right],
 \end{aligned} \tag{F.2}$$

where

$$\phi_i = \sin^{-1}(1),$$

$$a_1 = 0.355028,$$

$$\begin{aligned}
b_1 &= 0.258819, \\
b &= 0.183 \text{ GeV}^2, \\
\rho_0 &= -\frac{3}{4} 3^{\frac{1}{3}} \pi^{\frac{2}{3}}, \\
\rho_1 &= 0.715309 \mu^{\frac{1}{3}} \\
\text{and } k &= 1.33586 \mu^{\frac{1}{3}}.
\end{aligned}$$

Putting these values in equation (F.2) and using approximations (E.4) and (E.6), the equation (F.2) reduces to

$$\begin{aligned}
F(Q^2) |_{H=4\pi N'^2 a_0^2} \sum_{i=1}^2 e_i & \left[ 0.913(\gamma(-2\varepsilon, r_0) - \gamma(-2\varepsilon, r^P))(-2\varepsilon) \frac{1}{(Q_i^2)^{\frac{1-2\varepsilon}{2}}} \right. \\
& - 0.353\mu^{\frac{1}{3}}(\gamma(1-2\varepsilon, r_0) - \gamma(1-2\varepsilon, r^P))(1-2\varepsilon) \frac{1}{(Q_i^2)^{\frac{2-2\varepsilon}{2}}} \\
& + 0.0342\mu^{\frac{2}{3}}(\gamma(2-2\varepsilon, r_0) - \gamma(2-2\varepsilon, r^P))(2-2\varepsilon) \frac{1}{(Q_i^2)^{\frac{3-2\varepsilon}{2}}} \\
& - 5.33\mu\alpha_s(\gamma(3-2\varepsilon, r_0) - \gamma(3-2\varepsilon, r^P))(3-2\varepsilon) \frac{1}{(Q_i^2)^{\frac{4-2\varepsilon}{2}}} \\
& + (13.35\mu^{\frac{7}{6}} + 2.06\mu^{\frac{4}{3}} - 2.66\mu)\alpha_s(\gamma(4-2\varepsilon, r_0) - \gamma(4-2\varepsilon, r^P))(4-2\varepsilon) \frac{1}{(Q_i^2)^{\frac{5-2\varepsilon}{2}}} \\
& + (6.675\mu^{\frac{7}{6}} - 5.17\mu^{\frac{3}{2}} - 0.2\mu^{\frac{5}{3}})\alpha_s(\gamma(5-2\varepsilon, r_0) - \gamma(5-2\varepsilon, r^P))(5-2\varepsilon) \frac{1}{(Q_i^2)^{\frac{6-2\varepsilon}{2}}} \\
& + 0.501\mu^{\frac{11}{6}}\alpha_s(\gamma(6-2\varepsilon, r_0) - \gamma(6-2\varepsilon, r^P))(6-2\varepsilon) \frac{1}{(Q_i^2)^{\frac{7-2\varepsilon}{2}}} \\
& - 3.017\mu^{\frac{7}{3}}\alpha_s^2(\gamma(7-2\varepsilon, r_0) - \gamma(7-2\varepsilon, r^P))(7-2\varepsilon) \frac{1}{(Q_i^2)^{\frac{8-2\varepsilon}{2}}} \\
& + (0.292\mu^{\frac{8}{3}} + 15.1\mu^{\frac{5}{2}})\alpha_s^2(\gamma(8-2\varepsilon, r_0) - \gamma(8-2\varepsilon, r^P))(8-2\varepsilon) \frac{1}{(Q_i^2)^{\frac{9-2\varepsilon}{2}}} \\
& - (1.463\mu^{\frac{17}{6}} + 18.91\mu^{\frac{8}{3}})\alpha_s^2(\gamma(9-2\varepsilon, r_0) - \gamma(9-2\varepsilon, r^P))(9-2\varepsilon) \frac{1}{(Q_i^2)^{\frac{10-2\varepsilon}{2}}} \\
& \left. + 1.83\mu^3\alpha_s^2(\gamma(10-2\varepsilon, r_0) - \gamma(10-2\varepsilon, r^P))(10-2\varepsilon) \frac{1}{(Q_i^2)^{\frac{11-2\varepsilon}{2}}} \right]. \tag{F.3}
\end{aligned}$$

$$\begin{aligned}
F(Q^2) |_{II} = 4\pi N'^2 a_0^{2\varepsilon} \sum_{i=1}^2 e_i \left[ F_1 \frac{1}{(Q_i^2)^{\frac{1-2\varepsilon}{2}}} + F_2 \frac{1}{(Q_i^2)^{\frac{2-2\varepsilon}{2}}} + F_3 \frac{1}{(Q_i^2)^{\frac{3-2\varepsilon}{2}}} + F_4 \frac{1}{(Q_i^2)^{\frac{4-2\varepsilon}{2}}} \right. \\
+ F_5 \frac{1}{(Q_i^2)^{\frac{5-2\varepsilon}{2}}} + F_6 \frac{1}{(Q_i^2)^{\frac{6-2\varepsilon}{2}}} + F_7 \frac{1}{(Q_i^2)^{\frac{7-2\varepsilon}{2}}} + F_8 \frac{1}{(Q_i^2)^{\frac{8-2\varepsilon}{2}}} \\
\left. + F_9 \frac{1}{(Q_i^2)^{\frac{9-2\varepsilon}{2}}} + F_{10} \frac{1}{(Q_i^2)^{\frac{10-2\varepsilon}{2}}} + F_{11} \frac{1}{(Q_i^2)^{\frac{11-2\varepsilon}{2}}} \right], \quad (F.4)
\end{aligned}$$

where

$$\begin{aligned}
F_1 &= 0.913(\gamma(-2\varepsilon, r_0) - \gamma(-2\varepsilon, r^P))(-2\varepsilon), \\
F_2 &= -0.353\mu^{\frac{1}{3}}(\gamma(1-2\varepsilon, r_0) - \gamma(1-2\varepsilon, r^P))(1-2\varepsilon), \\
F_3 &= 0.0342\mu^{\frac{2}{3}}(\gamma(2-2\varepsilon, r_0) - \gamma(2-2\varepsilon, r^P))(2-2\varepsilon), \\
F_4 &= -5.33\mu\alpha_s(\gamma(3-2\varepsilon, r_0) - \gamma(3-2\varepsilon, r^P))(3-2\varepsilon), \\
F_5 &= (13.35\mu^{\frac{7}{6}} + 2.06\mu^{\frac{4}{3}} - 2.66\mu)\alpha_s(\gamma(4-2\varepsilon, r_0) - \gamma(4-2\varepsilon, r^P))(4-2\varepsilon), \\
F_6 &= (6.675\mu^{\frac{7}{6}} - 5.17\mu^{\frac{3}{2}} - 0.2\mu^{\frac{5}{3}})\alpha_s(\gamma(5-2\varepsilon, r_0) - \gamma(5-2\varepsilon, r^P))(5-2\varepsilon), \\
F_7 &= 0.501\mu^{\frac{11}{6}}\alpha_s(\gamma(6-2\varepsilon, r_0) - \gamma(6-2\varepsilon, r^P))(6-2\varepsilon), \\
F_8 &= -3.017\mu^{\frac{7}{3}}\alpha_s^2(\gamma(7-2\varepsilon, r_0) - \gamma(7-2\varepsilon, r^P))(7-2\varepsilon), \\
F_9 &= (0.292\mu^{\frac{8}{3}} + 15.1\mu^{\frac{5}{3}})\alpha_s^2(\gamma(8-2\varepsilon, r_0) - \gamma(8-2\varepsilon, r^P))(8-2\varepsilon), \\
F_{10} &= -(1.463\mu^{\frac{17}{6}} + 18.91\mu^{\frac{8}{3}})\alpha_s^2(\gamma(9-2\varepsilon, r_0) - \gamma(9-2\varepsilon, r^P))(9-2\varepsilon), \\
F_{11} &= 1.83\mu^3\alpha_s^2(\gamma(10-2\varepsilon, r_0) - \gamma(10-2\varepsilon, r^P))(10-2\varepsilon). \quad (F.5)
\end{aligned}$$

We can express equation (F.4) as defined in (2.48),

$$F(Q^2) |_{II} = 4\pi N'^2 a_0^{2\varepsilon} \sum_{i=1}^2 e_i \left[ \sum_{k=1}^{11} F_k \frac{1}{(Q_i^2)^{\frac{k-2\varepsilon}{2}}} \right]. \quad (F.6)$$

With  $\varepsilon = 0$ , the equation (F.6) reduces to (2.50).

$$F(Q^2) |_{II} = 4\pi N'^2 \sum_{i=1}^2 e_i \left[ \sum_{k=2}^{11} F'_k \frac{1}{(Q_i^2)^{\frac{k}{2}}} \right] \quad (F.7)$$

where

$$\begin{aligned}
F'_2 &= -0.353\mu^{\frac{1}{3}}(\gamma(1, r_0) - \gamma(1, r^P)), \\
F'_3 &= 2 \times 0.0342\mu^{\frac{2}{3}}(\gamma(2, r_0) - \gamma(2, r^P)), \\
F'_4 &= -3 \times 5.33\mu\alpha_s(\gamma(3, r_0) - \gamma(3, r^P)), \\
F'_5 &= 4 \times (13.35\mu^{\frac{7}{6}} + 2.06\mu^{\frac{4}{3}} - 2.66\mu)\alpha_s(\gamma(4, r_0) - \gamma(4, r^P)), \\
F'_6 &= 5 \times (6.675\mu^{\frac{7}{6}} - 5.17\mu^{\frac{3}{2}} - 0.2\mu^{\frac{5}{3}})\alpha_s(\gamma(5, r_0) - \gamma(5, r^P)), \\
F'_7 &= 6 \times 0.501\mu^{\frac{11}{6}}\alpha_s(\gamma(6, r_0) - \gamma(6, r^P)), \\
F'_8 &= -7 \times 3.017\mu^{\frac{7}{3}}\alpha_s^2(\gamma(7, r_0) - \gamma(7, r^P)), \\
F'_9 &= 8 \times (0.292\mu^{\frac{8}{3}} + 15.1\mu^{\frac{5}{2}})\alpha_s^2(\gamma(8, r_0) - \gamma(8, r^P)), \\
F'_{10} &= -9 \times (1.463\mu^{\frac{17}{6}} + 18.91\mu^{\frac{8}{3}})\alpha_s^2(\gamma(9, r_0) - \gamma(9, r^P)), \\
F'_{11} &= 10 \times 1.83\mu^3\alpha_s^2(\gamma(10, r_0) - \gamma(10, r^P)).
\end{aligned} \tag{F.8}$$

In obtaining (2.46), (2.48), (2.49) and (2.50) we have used the integration<sup>1</sup>,

$$\int_0^\infty x^{p-1} e^{-ax} \sin(mx) dx = \frac{\Gamma(p) \sin(p\theta)}{(a^2 + m^2)^{\frac{p}{2}}}. \tag{F.9}$$

The Incomplete Gamma Function used in obtaining (2.48) and (2.50) is

$$\int_u^v t^{s-1} e^{-t} dt = \gamma(s, v) - \gamma(s, u). \tag{F.10}$$

---

<sup>1</sup>I. S. Gradshteyn, I. M. Ryzhik, *Table of Integrals, Series and Products* (Elsevier, 2007).

G

## Derivation of equation (4.1) from equation (4.9)

From equation (4.9), we get

$$f_P = \sqrt{\frac{12}{M_P}} \int \frac{d^3 p}{(2\pi)^{\frac{3}{2}}} \left( \frac{E_i + m_i}{2E_i} \right)^{\frac{1}{2}} \left( \frac{E_j + m_j}{2E_j} \right)^{\frac{1}{2}} \left( 1 + \lambda_P \frac{p^2}{[E_i + m_i][E_j + m_j]} \right) \psi(p). \quad (\text{G.1})$$

We know from the relativistic formula of energy,

$$E^2 = p^2 c^2 + m^2 c^4. \quad (\text{G.2})$$

In the natural unit,  $c = 1$ ,

$$E = \sqrt{p^2 + m^2}. \quad (\text{G.3})$$

In the non-relativistic limit  $m^2 \gg p^2$ ,

$$E = \sqrt{m^2} = m. \quad (\text{G.4})$$

Now replacing  $E_i = m_i$  and  $E_j = m_j$  and  $\lambda_P = -1$  for the pseudoscalar meson in equation (G.1),

$$f_P = \sqrt{\frac{12}{M_P}} \int \frac{d^3 p}{(2\pi)^{\frac{3}{2}}} \left( \frac{m_i + m_i}{2m_i} \right)^{\frac{1}{2}} \left( \frac{m_j + m_j}{2m_j} \right)^{\frac{1}{2}} \left( 1 + \lambda_P \frac{p^2}{[m_i + m_i][m_j + m_j]} \right) \psi(p). \quad (\text{G.5})$$

Neglecting the last term in the non-relativistic limit  $\frac{p^2}{m^2} \rightarrow 0$ , we get

$$f_P = \sqrt{\frac{12}{M_P}} \int \frac{d^3 p}{(2\pi)^{\frac{3}{2}}} \psi(p). \quad (\text{G.6})$$

Again, from the Fourier transform

$$\psi(r) = \frac{1}{(2\pi)^{\frac{3}{2}}} \int \psi(p) e^{ipr} d^3 p. \quad (\text{G.7})$$

Putting  $r = 0$  in (G.7),

$$(2\pi)^{\frac{3}{2}} \psi(0) = \int \psi(p) d^3 p. \quad (\text{G.8})$$

Hence from equations (G.6) and (G.8), we obtain equation (4.1),

$$f_P = \sqrt{\frac{12}{M_P} |\psi(0)|^2}. \quad (\text{G.9})$$

# H

The wave function (4.10) in momentum  
space

$$\psi_I(p)^{total} = \frac{2N\sqrt{2}a_0^{\frac{3}{2}}\gamma(2, r^P)}{\pi(1 + a_0^2 p^2)^{\frac{3}{2}}} \left[ 1 - \frac{12\mu b a_0^3}{2(1 + a_0^2 p^2)} \right], \quad (\text{H.1})$$

where  $N$  is the normalization constant.

In obtaining (H.1), we have used Incomplete Gamma function

$$\int_0^{r^P} t^{s-1} e^{-t} dt = \gamma(s, r^P). \quad (\text{H.2})$$





## The wave function (4.11) in momentum space

$$\psi_{II}(p)^{total} = N' [(a_1 - b_1 \rho_0)(T_1 + T_2 + T_3 + T_4 + T_5) - b_1 \rho_1(T_6 + T_7 + T_8 + T_9 + T_{10})], \quad (\text{I.1})$$

where  $N'$  is the normalization constant and the co-efficients  $T_1, T_2, T_3, \dots, T_{10}$  are

$$T_1 = -\frac{32}{3} \sqrt{\frac{2}{\pi}} \frac{\mu \alpha_s}{(\rho_1 k)^2} \frac{(\gamma(4, r_0) - \gamma(4, r^P))}{p^5} \left(1 - \frac{2\sqrt{10}\rho_1}{\rho_1 k p}\right), \quad (\text{I.2})$$

$$T_2 = -\sqrt{\frac{2}{\pi}} \frac{10\mu W^1}{(\rho_1 k)^2} \frac{(\gamma(5, r_0) - \gamma(5, r^P))}{p^6} \left(1 - \frac{12\sqrt{(2+4\rho_1)}}{\rho_1 k p}\right), \quad (\text{I.3})$$

$$T_3 = \sqrt{\frac{2}{\pi}} \frac{128\mu^2 \alpha_s W^0}{3(\rho_1 k)^4} \frac{(\gamma(8, r_0) - \gamma(8, r^P))}{p^9} \left[1 - \left(\frac{18\sqrt{(6+6\rho_1)} + 18\sqrt{2\rho_1}}{\rho_1 k p}\right) + \frac{360\sqrt{12\rho_1(1+\rho_1)}}{(\rho_1 k p)^2}\right], \quad (\text{I.4})$$

$$T_4 = \sqrt{\frac{2}{\pi}} \frac{36\mu^2 W^0 W^1}{(\rho_1 k)^4} \frac{(\gamma(9, r_0) - \gamma(9, r^P))}{p^{10}} \left[1 - \left(\frac{40\sqrt{(3+2\rho_1)} + 20\sqrt{(2+4\rho_1)}}{\rho_1 k p}\right) + \frac{880\sqrt{(3+2\rho_1)(2+4\rho_1)}}{(\rho_1 k p)^2}\right], \quad (\text{I.5})$$

$$T_5 = -\frac{144}{3} \sqrt{\frac{2}{\pi}} \frac{\mu^2 b \alpha_s}{(\rho_1 k)^4} \frac{(\gamma(9, r_0) - \gamma(9, r^P))}{p^{10}} \left[1 - \left(\frac{20\sqrt{2\rho_1} + 20\sqrt{(12+8\rho_1)}}{\rho_1 k p}\right) + \frac{440\sqrt{2\rho_1(12+8\rho_1)}}{(\rho_1 k p)^2}\right], \quad (\text{I.6})$$

$$T_6 = -\frac{40}{3} \sqrt{\frac{2}{\pi}} \frac{\mu \alpha_s}{(\rho_1 k)^2} \frac{(\gamma(5, r_0) - \gamma(5, r^P))}{p^6} \left(1 - \frac{12\sqrt{2\rho_1}}{\rho_1 k p}\right), \quad (\text{I.7})$$

$$T_7 = -\sqrt{\frac{2}{\pi}} \frac{12\mu W^1}{(\rho_1 k)^2} \frac{(\gamma(6, r_0) - \gamma(6, r^P))}{p^7} \left(1 - \frac{14\sqrt{(2+4\rho_1)}}{\rho_1 k p}\right), \quad (\text{I.8})$$

$$T_8 = \sqrt{\frac{2}{\pi}} \frac{144\mu^2 \alpha_s W^0}{3(\rho_1 k)^4} \frac{(\gamma(9, r_0) - \gamma(9, r^P))}{p^{10}} \left[1 - \left(\frac{20\sqrt{(6+6\rho_1)} + 20\sqrt{2\rho_1}}{\rho_1 k p}\right) + \frac{440\sqrt{12\rho_1(1+\rho_1)}}{(\rho_1 k p)^2}\right], \quad (\text{I.9})$$

$$T_9 = \sqrt{\frac{2}{\pi}} \frac{40\mu^2 W^0 W^1}{(\rho_1 k)^4} \frac{(\gamma(10, r_0) - \gamma(10, r^P))}{p^{11}} \left[1 - \left(\frac{44\sqrt{(3+2\rho_1)} + 22\sqrt{(2+4\rho_1)}}{\rho_1 k p}\right) + \frac{1056\sqrt{(3+2\rho_1)(2+4\rho_1)}}{(\rho_1 k p)^2}\right], \quad (\text{I.10})$$

$$T_{10} = -\frac{160}{3} \sqrt{\frac{2}{\pi}} \frac{\mu^2 b \alpha_s}{(\rho_1 k)^4} \frac{(\gamma(10, r_0) - \gamma(10, r^P))}{p^{11}} \left[1 - \left(\frac{22\sqrt{2\rho_1} + 22\sqrt{(12+8\rho_1)}}{\rho_1 k p}\right) + \frac{528\sqrt{2\rho_1(12+8\rho_1)}}{(\rho_1 k p)^2}\right]. \quad (\text{I.11})$$

The Incomplete Gamma function as shown in equation (I.12) is used in obtaining the co-efficients  $T_1, T_2, T_3, \dots, T_{10}$ ,

$$\int_u^v t^{s-1} e^{-t} dt = \gamma(s, v) - \gamma(s, u). \quad (\text{I.12})$$

In obtaining (H.1) and (I.1) we have used the integration as defined in equation (F.9).